

On estimating the effective sample size of phylogenetic trees in an autocorrelated chain

Jonathan Klawitter^{1,*}, Lars Berling^{2,4}, Jordan Douglas^{1,3},
Dong Xie¹, and Alexei J. Drummond¹

¹ University of Auckland, Aotearoa New Zealand

² Simon Fraser University, Canada

³ Research School of Biology, Australian National University, Australia

⁴ University of Canterbury, Aotearoa New Zealand

* [jo.klawitter\[at\]gmail.com](mailto:jo.klawitter[at]gmail.com)

Abstract. Estimating the effective sample size (ESS) is fundamental in Bayesian phylogenetic inference to properly account for autocorrelation in MCMC samples. While methods for continuous parameters are well established, the discrete and high-dimensional nature of treespace poses substantial challenges. Here, we compare existing tree ESS estimators with novel approaches that leverage tractable tree distributions, specifically Conditional Clade Distributions (CCDs), as well as a new probabilistic estimator based on clade frequency differences between independent chains. Using simulated chains with known ESS bounds, we assess estimator accuracy and evaluate their stability and robustness on simulated and real datasets. We further examine how multimodality in posterior distributions and poor mixing can substantially affect ESS estimates, highlighting the need for careful interpretation. Our CCD-based estimators perform comparably to existing approaches, with two methods showing lower variance by averaging across multiple estimates. In contrast, the probabilistic estimator and two previously recommended methods incur prohibitive computational costs for long chains. Together, these results provide guidance for reliable and efficient tree ESS estimation in complex phylogenetic analyses.

1 Introduction

Bayesian inference with a Markov chain Monte Carlo (MCMC) algorithm is one of the main inference paradigms in phylogenetics [6, 24, 39, 42]. MCMC algorithms explore the parameter space by proposing changes to the current state (such as tree topology modifications or parameter value adjustments) and accepting or rejecting these proposals based on their likelihood and prior probability. The objective is to construct a Markov chain that effectively converges to the posterior distribution of phylogenetic trees along with associated parameters, such as substitution and clock rates. This posterior distribution spans the entire space of possible trees (the *treespace*) and their parameters. In practice, however, we can only approximate this posterior through a finite sequence of samples collected during the MCMC run.

A key challenge of MCMC is autocorrelation: consecutive samples are typically dependent, which reduces the *effective sample size (ESS)* and lowers the precision of posterior estimates [14, 38, 47]. This dependence is quantified by the *autocorrelation time (ACT)*, which measures the average number of iterations needed to obtain effectively independent samples. For a chain of length N , the ESS (N_{Eff}) is inversely related to the ACT (τ) by the equation $N_{\text{Eff}} = N/\tau$. Thus, a higher ACT directly translates to a lower ESS, requiring more iterations to achieve reliable posterior estimates. This challenge is particularly acute in phylogenetics, where MCMC must navigate the complex, high-dimensional, and non-Euclidean phylogenetic treespace using local tree rearrangement operations [1, 5, 7].

Understanding the ESS is crucial for properly accounting for autocorrelation in downstream analyses and assessing the quality of posterior estimates. The ESS quantifies how many independent samples would provide the same statistical precision as the autocorrelated MCMC samples. A low ESS relative to the total number of draws indicates that the chain is moving slowly through the parameter space, signalling that more samples are needed for accurate estimates. See Magee et al. [35] for an in-depth study of the relation between the ESS of phylogenetic trees and the Monte Carlo error. Monitoring ESS is therefore essential for assessing MCMC efficiency and determining whether sufficient effectively independent samples have been collected. Since MCMC in phylogenetics explores multiple parameter spaces with varying efficiency, the ESS must be calculated separately for each parameter. In the field of phylogenetic MCMC, a common rule of thumb suggests a minimum ESS of 200 for all important parameters, including the posterior density and likelihood. Magee et al. [35] and Fabreti and Höhna [16] advocate for higher thresholds of 500 and 625, respectively.

Reliable ESS estimation provides several critical benefits for phylogenetic MCMC analyses. First, a low ESS often indicates that an MCMC chain should be run for additional iterations. While a large ESS does not guarantee convergence, it serves as a valuable diagnostic for assessing convergence when used alongside other lines of evidence, as discussed by Berling, Bouckaert, and Gavryushkin [3]. Reliable ESS estimation is thus an essential post-processing step for interpreting and ensuring the robustness of MCMC results. Second, ESS and ACT values quantify sampling efficiency, enabling researchers to compare different MCMC algorithms, evaluate the effectiveness of proposal mechanisms, and optimize tuning parameters. Third, the ESS is fundamental for computing Monte Carlo standard errors, which quantify the precision of posterior estimates due to finite sampling [16, 35]. Finally, in Bayesian model averaging [48] and model selection approaches such as AIC and BIC, the ESS can be used to adjust effective sample sizes or serve as weights to prevent overestimation of model support [26].

We tackle the challenging problem of estimating the ESS for samples of phylogenetic tree topologies (i.e., without branch lengths). The fundamental difficulty stems from the discrete, high-dimensional nature of treespace, which lacks the metric properties of Euclidean spaces and therefore cannot accommodate existing ESS estimation methods designed for continuous parameters.

Related Work. To estimate the ESS for samples of phylogenetic tree topologies, previous approaches have mapped the sampled trees to traces of real-valued parameters, enabling the application of existing ESS estimators developed for continuous variables [14]. Lanfear, Hua, and Warren [32] introduced the tree ESS estimator `pseudoESS`, which computes the distance from each sampled tree to a set of randomly selected reference (focal) trees from the sample, derives ESS estimates from these distance traces, and reports the median value along with summary statistics. They proposed plotting these distances as tree topology traces and in addition also propose jump distances which visualize tree distances between pairs of trees at increasing sampling intervals. In a related vein, the RNNI distance [7] to a fixed tree estimate (UPGMA and neighbour joining) is used to address gene tree topology convergence in the StarBeast3 multispecies coalescent program [9]. Fabreti and Höhna [16] took a different approach, converting (unrooted) trees into binary traces that indicate the presence or absence of specific splits (or clades for rooted trees). Magee et al. [35] adapted the initial positive sequence estimation method—a popular ESS estimator for Euclidean variables—for use with trees by approximating the covariance structure through a tree metric. They named their method `frechetCorrelationESS` to reflect its use of the Fréchet mean and variance. Lanfear et al. [32] also proposed a similar approach, `approximateESS`, which employs a more heuristic approach to estimating ACT and ESS. In a comparative study, Magee et al. [35] evaluated the accuracy of these and additional ESS estimators using simulated chains. Their evaluation was based on comparing estimated values to known Monte Carlo sampling errors, using simulated chains that replicate key characteristics of real phylogenetic posterior tree samples.

Contribution. In this paper, we present new methods for estimating the effective sample size of phylogenetic tree topologies, a refined evaluation framework based on simulated chains with known ESS bounds, and a case study examining the effect of multimodality on tree ESS estimation.

We contribute two distinct methodological approaches. First, we extend the class of tree-to-trace mappings by leveraging *Conditional Clade Distributions (CCD)* [4, 23, 33]. We map each sampled tree to (i) its posterior log probability, (ii) its Robinson-Foulds (RF) distance to the CCD MAP tree (point estimate) [4], and (iii) its mean RF distance to the full posterior tree distribution, computed using a new efficient algorithm that avoids focal tree selection. Second, we propose a probabilistic estimator based on observed clade frequencies across multiple independent MCMC chains, which operates independently of distance metrics, autocorrelation time, and tuning parameters. While this approach is theoretically appealing, it ultimately proves less accurate and more computationally demanding than existing approaches.

Additionally, we refine the evaluation methodology using simulated MCMC chains with known lower bounds on the ESS. Inspired by Fabreti and Höhna [16] and Magee et al. [35], we generate i.i.d. tree samples from CCDs fitted to real posterior distributions [4], then apply controlled perturbations ranging from sim-

ple repetition to structured transitions in RNNI treespace [7] to simulate realistic autocorrelation patterns.

2 Methods

We begin by briefly recalling CCDs and introducing a new algorithm for computing the expected RF distance. We then present both existing and new tree ESS estimators, followed by the evaluation framework used to test them. Finally, we outline the real datasets used in our experiments, both for direct analysis and for simulated chains, and explain our approach for assessing their modality. We assume throughout that all phylogenetic trees are rooted and binary (fully resolved).

2.1 Conditional Clade Distributions

A *conditional clade distribution (CCD)* is a distribution of phylogenetic trees (topologies) on the same taxa that parametrises treespace. A CCD is based on a *CCD graph*, which is bipartite graph on clades and clade splits. The CCD graph contains all trees that can be combined by these elements. The probability of picking a child clade split of a clade, called the *conditional clade probability*, yields probabilities on trees (and for other elements) [33]. Depending on the exact CCD[i] model [4, 27, 52], independence of clades (CCD0) or clade splits (CCD1) or pairs of clade splits (CCD2) is assumed. See Berling et al. [4] for more details on CCDs and examples. When a CCD is constructed based on an MCMC sample, both to form the CCD graph and populate its parameters, a CCD essentially smooths the Monte Carlo probability of the (in practice often sparse) sample to a larger treespace. This allows it to provide a better estimate of the posterior distribution for non-trivial instances [4]. Originally developed by Höhna and Drummond [23] and Larget [33], CCDs have found application in species tree–gene tree reconciliation [44], the efficient computation of the phylogenetic entropy [34], detecting rogue taxa [28], and computing credible sets [29]. Furthermore, similar tree distributions and parameter population methods have been investigated [27, 52, 53].

Here we use that a CCD D allows us to perform the following tasks efficiently:

- (i) sample a tree from D ,
- (ii) compute the probability $\Pr(T)$ of a tree T in D ,
- (iii) compute the probability $\Pr(C)$ of a clade C appearing in any tree in D ,
and
- (iv) find the tree with maximum probability in D , the *CCD MAP tree* of D .

As a summary tree, the CCD MAP tree outperforms the popular MCC tree in terms of accuracy and precision and performs at least as well as the greedy consensus tree while further guaranteeing being fully resolved [2, 4].

Expected RF Distance. Recall that for two trees T and T' , their *Robinson-Foulds (RF) distance* $d_{\text{RF}}(T, T')$ equals the symmetric distance of their clade sets $\mathcal{C}(T)$ and $\mathcal{C}(T')$, that is, the number of clades in $\mathcal{C}(T) \setminus \mathcal{C}(T')$ plus the number of clades in $\mathcal{C}(T') \setminus \mathcal{C}(T)$. For fully resolved trees, these two terms are equal and we thus use only one as RF distance.

Let D be a CCD and let T be a phylogenetic tree on the same taxon set as D . We want to define an RF distance between T and D . To this end, we compute, for each tree $R \in D$, the RF distance of T and R and weigh it by the probability of R . We call this the *expected RF distance* of T to D , denoted by $\text{ERF}(T, D)$:

$$\text{ERF}(T, D) = \mathbb{E}_{R \in D}[\text{d}_{\text{RF}}(T, R)] = \sum_{R \in D} \text{Pr}(R) \text{d}_{\text{RF}}(T, R) \quad (1)$$

The expected RF distance $\text{ERF}(T, D)$ can be computed efficiently with the CCD graph. Let C be a clade in D . Note that if $C \in \mathcal{C}(T)$, then C does not contribute to $\text{ERF}(T, D)$ regardless of what tree it is part of. Otherwise—i.e., if $C \notin \mathcal{C}(T)$ —note that C contributes with $\text{Pr}(R)$ to $\text{ERF}(T, D)$ for every tree $R \in D$ that C appears in (i.e., $C \in \mathcal{C}(R)$). Fortunately, these contributions of C sum up exactly to $\text{Pr}(C)$. Hence, we can compute $\text{ERF}(T, D)$ without iterating over all trees in D by instead iterating over all clades in D :

$$\text{ERF}(T, D) = \sum_{\substack{C \in \mathcal{C}(D) \\ C \notin \mathcal{C}(T)}} \text{Pr}(C) \quad (2)$$

We can compute $\text{Pr}(C)$ collectively for all C and the sum in Eq. (2) both in linear time in the size of D .

2.2 Tree ESS Estimators

The sequence of values of a specific parameter in the sample is known as the *trace*. Estimating the ESS and/or the ACT of a trace is a challenging statistical problem and so several different approaches have been developed, each addressing the impact of autocorrelation differently. Fabreti and Höhna [16] compared the three commonly used ESS estimation implementations used in phylogenetics: **Tracer** (an initial positive sequence estimator [15, 38, 45]), **coda** (a spectral density estimator [17, 20, 37]), and **MCMCSE** (a batch means estimator [11, 12]). In summary, they found that the initial positive sequence estimator of **Tracer** behaved most robust for small and large ACT, with consistent slight underestimation though no overestimation, which both other methods showed. We thus rely on **Tracer**'s method.

We start with the ESS estimators that map the trace of trees to a trace of values in an Euclidean space. We then discuss how Magee et al. [35] adapted the initial positive sequence estimator, before describing our new probabilistic approach.

Mapping Trees. Let $\mathcal{T} = \langle T_1, \dots, T_N \rangle$ be a trace of trees. Our first set of estimators map each tree T_j , $j \in \{1, \dots, N\}$, to a value (set of values), for which we can then use **Tracer** to obtain an ESS estimate. For those mappings utilizing a CCD, we tested both the CCD0 and CCD1 model; for $i \in \{0, 1\}$, let D_i be the CCD[i] on \mathcal{T} .

In non-trivial phylogenetic problems, most or even all trees in an MCMC chain are distinct and hence the Monte Carlo probability is not reliable (as each different topology gets probability $1/N$). However, CCDs offer a more accurate and refined probability of a tree T_j [4, 34]. Our first estimator logPi , $i \in \{0, 1\}$, utilizes the probability $\text{Pr}_i(T_j)$ given by D_i with a log transformation, since the variance can be span many orders of magnitude:

logPi Map T_j to $-\log \text{Pr}_i(T_j)$.

Note that this estimator does not require a choice of tree distance or focal trees.

The next set of estimators relate T_j to the posterior distribution based on a tree distance, in particular the RF distance. Lanfear et al. [32] also considered the path distance [41] and we tested the RNNI distance. We observed that greater variability between estimator approaches than between tree distance measures. Accordingly, since our focus is on the ESS of (unranked) tree topologies, we restrict the analysis to the RF distance.

Lanfear et al. [32] suggested with their method **pseudoESS** to map each T_j to its distance to a *focal* tree, repeating this several times, say $m = 100$, and then reporting the median estimated ESS. Since we use the RF distance, we call this method **pseudoMedianRF**. We also introduce an estimator that uses the CCD i MAP tree as focal tree. Instead of having to choose focal trees, we suggest using the relation to the whole distribution by using the expected RF distance.

pseudoMedianRF Map T_j to a vector of RF distances to 100 (or less, if $N < 100$) random focal trees of \mathcal{T} , estimate the ESS for each focal tree, and report the median.

mapRF i Map T_j to $d_{\text{RF}}(T_j, T)$ with T being the MAP tree of D_i .

expRF i Map T_j to $\text{ERF}(T_j, D_i)$, the expected RF distance of T_j to D_i (with the algorithm in Section 2.1).

There exist several other estimators that use distance-based mappings, though none showed an overall better performance than **pseudoMedianRF** (see Magee et al. [35, SM]).

Another estimator using mappings is by Fabreti and Höhna [16], who suggested to use binary vectors of clade presence and absence:

cladeInd For each clade C in \mathcal{T} , create a trace with entry j set to $\mathbf{1}_{C \in T_j}$, i.e., 1 if C is in T_j and 0 otherwise. Estimate the ESS for each trace and report the mean.

Adaptation to Trees. Magee et al. [35] used the RF distance with Fréchet generalizations of mean and variance. They applied these to adapt both the initial positive sequence and the batch means estimators, and also proposed further ad hoc approaches. Here we focus only on the former.

fréchetIPSE Adapt the initial positive sequence estimator (IPSE) to trees by estimating covariance and correlations via Fréchet means and variances using squared RF distances.

In their experiments, Magee et al. [35, SM] also included another new estimator **foldedRankmedoidESS** and the ad hoc estimator **approximateESS** by Lanfear et al. [32]. Based on their experiments, they recommend the use of **pseudoMedianRF** and **fréchetIPSE**. It is worth noting that Lanfear et al.’s **approximateESS** and **foldedRankmedoidESS** performed nearly as good. Nonetheless, we included only **fréchetIPSE** in our list of evaluated estimators.

A downside of **fréchetIPSE** is that it computes all pairwise distances of trees in the chain. (**foldedRankmedoidESS** and **approximateESS** share this downside.) In practice, this can take a considerable amount of time and, if the full distance matrix is stored, also space⁵. We ran preliminary experiments to see whether using random subsamples of trees suffice to estimate Fréchet variance and mean, but found that in some instances this lead to the algorithm not converging. We thus did not further pursue this potential method to speed up **fréchetIPSE** for long chains. Hence, in our main experiments, we gave **fréchetIPSE** a time limit of five minutes. We further report on running times for different chain sizes.

Expected Difference of Clade Frequencies. When assessing convergence across multiple independent MCMC runs in phylogenetics, a key challenge is determining whether observed differences in clade frequencies between chains reflect genuine non-convergence or merely sampling variation. Fabreti and Höhna [16] addressed this through their *Expected Difference of Split Frequencies (EDSF)* method. They demonstrated that the expected difference in split frequencies between two converged chains depends critically on both the true split frequency and the effective sample size. By modeling split presence/absence as binomial draws, they derived the theoretical distribution of frequency differences and used the 95th percentile as a convergence threshold. Crucially, their approach assumes that a reliable ESS estimate is already available from other methods, which is then used to determine appropriate thresholds for each split.

Building on this foundation, we propose a complementary approach that inverts the logic: rather than assuming a known ESS to test convergence, we directly estimate the ESS from observed clade frequencies across multiple independent chains. Our method requires no prior ESS estimates, no distance metrics, and no explicit autocorrelation time calculations. Instead, we model the relationship between raw MCMC samples and effectively independent samples through a probabilistic framework. We call this approach *Expected Difference of Clade Frequencies (EDCF)*. We present this method in full as the derivation is non-trivial and the negative result is informative; we discuss its limitations in [Section 4](#).

⁵ Concerning the space usage of **fréchetIPSE**, we improved the implementation by Magee et al. by not storing the whole distance matrix. Instead we directly compute all values derived from the distance matrix either directly or offsets between consecutive values (for different lags).

Model. Suppose we have m independent MCMC chains of phylogenetic trees where chain i has ℓ_i samples. Let K_i denote the number of times a clade was observed in chain i . We model the sampling process hierarchically: there exists an unknown parameter R with $0 < R \leq 1$ representing the proportion of samples that are effectively independent. The *effective* number of observations of a clade in chain i is $\lfloor RK_i \rfloor$, and we assume these effective counts are binomially distributed:

$$\lfloor RK_i \rfloor \sim \text{Binomial}(n = \lfloor R\ell_i \rfloor, p = C), \quad (3)$$

$$\text{where } C \sim \text{Beta}(\alpha = a, \beta = b), \quad (4)$$

Here, C represents the true posterior probability of the clade, which is itself modeled with a Beta prior. This hierarchical structure allows us to integrate over our uncertainty about true clade probabilities while estimating the autocorrelation factor R .

The probability model gives the following:

$$\Pr(\lfloor RK_i \rfloor | C) = \binom{\lfloor R\ell_i \rfloor}{\lfloor RK_i \rfloor} C^{\lfloor RK_i \rfloor} (1 - C)^{\lfloor R\ell_i \rfloor - \lfloor RK_i \rfloor} \quad (5)$$

$$\Pr(C) = \frac{C^{a-1} (1 - C)^{b-1}}{B(a, b)} \quad (6)$$

This strategy is depicted in Fig. 1 for a fixed ESS.

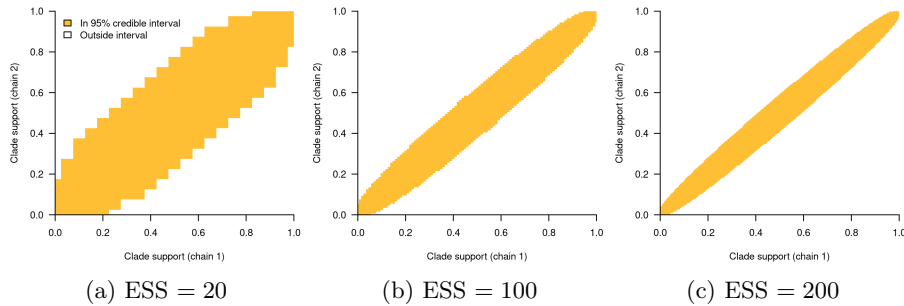


Fig. 1: Each panel shows the 95% credible intervals in clade support probabilities under the EDCF strategy, given a fixed ESS. Larger ESSes give smaller sampling errors across the $m = 2$ independent chains. This sampling error can be used to estimate the ESS using both maximum likelihood and Bayesian inference approaches.

Likelihood for Two Chains. Consider the case of two independent chains ($m = 2$). By integrating out clade probability C and accounting for the combinatorial

relationship between a count K_i and a rounded fraction of that count $\lfloor RK_i \rfloor$, we obtain the joint probability of K_1 and K_2 :

$$\begin{aligned} \Pr(K_1, K_2 | R) &= \int_0^1 \frac{\Pr(\lfloor RK_1 \rfloor | C)}{\mathcal{N}(K_1, R)} \frac{\Pr(\lfloor RK_2 \rfloor | C)}{\mathcal{N}(K_2, R)} \Pr(C) dC \\ &= \left(\frac{\lfloor R\ell_1 \rfloor}{\lfloor RK_1 \rfloor} \right) \left(\frac{\lfloor R\ell_2 \rfloor}{\lfloor RK_2 \rfloor} \right) \frac{B(f_1, f_2)}{\mathcal{N}(K_1, R) \mathcal{N}(K_2, R) B(a, b)}, \end{aligned} \quad (7)$$

$$\text{where } f_1 = \lfloor RK_1 \rfloor + \lfloor RK_2 \rfloor + a,$$

$$f_2 = \lfloor RL_1 \rfloor + \lfloor RL_2 \rfloor - \lfloor RK_1 \rfloor - \lfloor RK_2 \rfloor + b,$$

$$\text{and } B(x, y) = \int_0^1 q^{x-1} (1-q)^{y-1} dq = \frac{\Gamma(x) \Gamma(y)}{\Gamma(x+y)} \text{ is the beta function.}$$

The combinatorial term $\mathcal{N}(k, r)$ accounts for the discrete nature of the floor operation, counting the total number of integers z such that $\lfloor zr \rfloor = \lfloor kr \rfloor$, for $0 < r \leq 1$. That is, find the number of values in $z \in \mathbb{Z}$ such that $x \leq zr < x+1$, where $x = \lfloor kr \rfloor$. This count can be directly solved as:

$$\mathcal{N}(k, r) = \left\lfloor \frac{x+1}{r} \right\rfloor - \left\lceil \frac{x}{r} \right\rceil + \begin{cases} 0 & \text{if } \frac{x+1}{r} \in \mathbb{Z} \\ 1 & \text{if } \frac{x+1}{r} \notin \mathbb{Z} \end{cases} \quad \text{where } x = \lfloor kr \rfloor \quad (8)$$

Then, given two vectors of n_c clade frequencies $(\vec{K}_1) = (K_{1,1}, \dots, K_{1,n_c})$ and $(\vec{K}_2) = (K_{2,1}, \dots, K_{2,n_c})$, and assuming independence between observations, we evaluate the joint likelihood. To avoid the intractably large space of unobserved clades, we condition on observing each clade at least once across both chains, i.e., $K_{(1,j)} + K_{(2,j)} > 0$:

$$\begin{aligned} L(\vec{K}_1, \vec{K}_2 | R) &= \Pr(\vec{K}_1, \vec{K}_2 | R, \vec{K}_1 > 0 \wedge \vec{K}_2 > 0) \\ &= \prod_{j=1}^{n_c} \frac{\Pr(K_{1,j}, K_{2,j} | R)}{1 - \Pr(K_1 = 0, K_2 = 0 | R)}. \end{aligned} \quad (9)$$

A key limitation in this comes from the assumption of independence between clade counts (when in reality we know that clades share hierarchical relationships with each other).

ESS Estimation. The effective sample size is computed using $N_{\text{EFF}} = R(\ell_1 + \ell_2 + \dots + \ell_m)$. This represents the number of effectively independent samples across all chains, interpreted as the number of independent draws from the posterior needed to achieve the same sampling precision as the m autocorrelated chains. Importantly, this ESS estimate depends only on observed clade frequencies and requires no distance metrics or explicit autocorrelation calculations.

We estimate R either through maximum likelihood of $L(\vec{K}_1, \vec{K}_2 | R)$ or through Bayesian inference with posterior:

$$\Pr(R | \vec{K}_1, \vec{K}_2) \propto L(\vec{K}_1, \vec{K}_2 | R) \Pr(R) \quad (10)$$

For Bayesian inference, we perform MCMC using a single unidimensional proposal on R – the interval operator in BEAST 2 [6], with a step size sampled from a Bactrian kernel [49]. We set $a = b = 1$, corresponding to a uniform prior distribution of clade support probabilities. This approach estimates not just the mean N_{Eff} but its full posterior distribution, enabling conservative convergence assessment by ensuring that the 95% credible interval of N_{Eff} exceeds recommended thresholds. The tree ESS across chains is thus estimated by running a comparatively computationally inexpensive auxiliary MCMC on R , ensuring this auxiliary chain itself achieves an ESS over 500.

We refer to the tree ESS estimator using maximum likelihood as EDCF-ML and the one using Bayesian MCMC as EDCF-B (B for Bayesian).

2.3 Evaluation Datasets

We evaluate the accuracy and robustness of the tree ESS estimators on both simulated and empirical data sets, building on ideas from Lanfear et al. [32], Magee et al. [35], and Fabreti and Höhna [16]. For our simulated chains, we aim to establish ground truth by constructing chains with known, controllable ESS values and to ensure samples reflect realistic posterior distributions.

Lanfear et al. [32] generated samples of 1000 trees on 50 taxa by performing a fixed number of subtree prune & regraft (SPR) moves [5, 21] between subsequent samples, with the number of moves ranging from 1 to 50. Increasing the number of SPR moves reduces correlation between consecutive samples and therefore raises the ESS estimate. This relationship was recovered by their ESS estimators. However, this approach has two limitations: the true ESS remains unknown, preventing assessment of estimator accuracy, and the samples are generated through a random walk over the entire treespace rather than from a concentrated posterior distribution.

Magee et al. [35] improved the realism of simulated samples by using the 95% credible set from an inferred posterior tree sample as a *reference distribution*. They simulated MCMC chains within this distribution using nearest neighbor interchange (NNI) moves. They then applied each tested tree ESS estimator. For each simulated chain and estimator, they drew as many i.i.d. samples from the reference distribution as the estimated ESS, then compared both samples (simulated chain and i.i.d. sample) by estimating clade probabilities, tree probabilities, and majority rule consensus trees. By comparing the standard error of these estimates across many replicates, they evaluated whether the estimated ESS correctly predicted the precision of posterior estimates. While we build on their simulation approach, it is limited by restricting sampling to the discrete set of trees in the original MCMC sample, which itself represents only a sparse sample from the true posterior.

Fabreti and Höhna [16] developed a more general evaluation framework that also considered Metropolis-coupled MCMC with chain swapping and adaptive MCMC algorithms. For their baseline evaluation, they generated samples of length N with *known* ESS N_{Eff} by using N_{Eff} many i.i.d. samples from a posterior distribution and repeating each roughly ACT $\tau = N/N_{\text{Eff}}$ many times. While this

repetition is quite artificial, it may mimic scenarios with concentrated posteriors or low MCMC acceptance rates. Testing with the ESS ranging from 100 to 1000 and ACT from 1 to 1000, they found that the initial positive sequence estimator (as used by **Tracer**) is the most robust method with only slight but consistent underestimation; CODA and MCMCSE were less robust and in particular for higher ACT also overestimating the ESS. Following their recommendation and as already mentioned above, we use **Tracer** for the trace based estimators.

Building on these approaches, we now describe our evaluation datasets and simulation procedures. We first detail the real datasets and testing procedures, then explain our chain simulation methodology.

Real Datasets. We use the datasets DS1–11, which are popular for benchmarking computational phylogenetic software [10, 31]; see Table 1 for details. For each dataset, we ran a BEAST 2 MCMC chain with a length of 10 million iterations, using a sampling interval of 100 and discarding a pre-burnin of 500 000 trees, resulting in a final sample of 100 000 trees per chain. We ran two independent analyses for each dataset. The remaining MCMC setup follows the one in Berling et al. [3] and the BEAST 2 XML files can be accessed through the ASM package⁶. For the experiments in Section 3.3, we used the same setup for DS1–11 but increased the sampling rate to oversample on purpose.

Since multimodal posteriors can challenge both MCMC mixing and ESS estimation, we assessed the modality of each tree posterior. We used a subsample of 1000 trees from each dataset, computed all pairwise RNNI distances, and applied multidimensional scaling (MDS). The number of clusters reported in Table 1 are based on visual assessment of the resulting MDS plots, which are available in the Supplementary Material E. We further report in Table 1 the mean RNNI distance between consecutive draws from a CCD0 based on each dataset (sample size 1000).

Robustness and Stability Testing on Real Datasets. While the real datasets do not provide ground truth for ESS values, we used them to assess estimator robustness and stability through two complementary tests.

Robustness to partitioning. We used chains of 10 000 tree samples from each dataset and partitioned each into k equally-sized fragments for $k \in \{1, 2, \dots, 10\}$. We then applied each tree ESS estimator to every fragment and summed the resulting estimates. A robust estimator should yield similar total ESS values regardless of how the chain is fragmented, resulting in low variance across different values of k . However, as we demonstrate below, poor mixing and multimodality can substantially affect this stability.

Stability under oversampling. We ran MCMC analyses with intentional oversampling by reducing the sampling interval from 100 to 10 iterations while main-

⁶ GitHub ASM package github.com/rbouckaert/asm

⁷ The *phylogenetic entropy* of a tree distribution D is defined as the sum of $-\Pr(T) \log \Pr(T)$ over all trees of D , here computed with a CCD1 [28].

Table 1: Datasets used for our experiments with n the number of taxa, H the phylogenetic entropy⁷, the mean RNNI distance given with standard deviation, and a visual assessment of multimodality using RNNI-based MDS (see Supplementary Material E).

Dataset	n	H	mean RNNI dist.	# Modes	Reference
DS1	27	5.7	8.75 ± 4.00	2	[19]
DS2	29	5.2	4.74 ± 2.52	4	[13]
DS3	36	5.1	3.90 ± 1.91	2	[50]
DS4	41	5.7	7.46 ± 4.16	2	[22]
DS5	50	26.4	42.33 ± 10.69	1	[31]
DS6	50	12.8	30.19 ± 11.11	2	[54]
DS7	59	10.5	8.41 ± 2.78	1	[51]
DS8	64	16.1	27.91 ± 9.78	1	[40]
DS9	67	37.7	71.17 ± 11.38	1	[25]
DS10	67	15.0	32.31 ± 12.93	2	[43]
DS11	71	46.7	123.28 ± 15.68	1	[30]

taining all other parameters, yielding chains of 1000 trees with higher autocorrelation. We estimated tree ESS on the full chain and on systematically thinned versions (retaining every 2nd, 4th, 8th, and 16th tree) to assess whether estimators remain stable under different levels of thinning.

Accuracy Evaluation on Simulated Chains. Building on ideas from Fabreti and Höhna [16] and Magee et al. [35], we simulate chains with known bounds on ESS and ACT. We first construct a CCD1 based on the posterior tree sample from the real dataset DS1–11 as reference distribution. We sample $k = 1000$ independent trees from the CCD, which establishes our maximum tested ESS value; let T_i denote the i th sampled tree for $i \in \{1, \dots, k\}$. If the target ACT is $\tau = 1$, then the independent samples form the chain directly. For $\tau > 1$, we introduce autocorrelation by filling the gaps between independent samples using one of the following methods:

Simple Repetition. Repeat each tree T_i exactly τ times before proceeding to T_{i+1} .

Noisy Repetition. For each $i \in \{1, \dots, k\}$, sample τ_i from a normal distribution with mean τ and variance such that 90% of values lie within $[0.75\tau, 1.25\tau]$, rounding to the nearest integer. Build the chain by repeating each tree T_i exactly τ_i times.

Shortest RNNI Path. As in noisy repetition, first sample τ_i for each $i \in \{1, \dots, k\}$. To mimic MCMC movement through treespace, compute the shortest RNNI path P_i from T_i to T_{i+1} (with indices taken modulo k). Fill the chain between T_i and T_{i+1} with $\tau_i - 1$ trees sampled uniformly at random from P_i . We call this an *RNNI chain*.

Accuracy of estimators. To evaluate estimators at a target ESS of $k' < k$, we truncate the simulated chain after tree $T_{k'}$. For repetition chains, the tree ESS is exactly k' , proving ground truth. For RNNI chains, the ESS is at least k' , since the random sampling along paths may introduce some additional independence; the number of independent samples k' thus constitutes a lower bound. How tight this bound is depends on the mean RNNI distance between independent samples in the reference distribution: small mean distances lead to more repeated trees along paths, making the true ESS closer to k' , particularly at small ACT values. We report average RNNI distances for our datasets in [Table 1](#).

Realism of simulated chains. To assess how well our simulated chains mimic true MCMC chains, we compare the autocorrelation sequences ρ_k at different lags using Tracer: The ACT can be expressed as the sum of autocorrelation over increasing lags,

$$\tau = 1 + 2 \sum_{k=1}^{\infty} \rho_k, \quad (11)$$

which forms the basis of the initial positive sequence estimator. We call the autocorrelation sequence truncated at the first negative value, following the stopping criterion of the initial positive sequence estimator, the *autocorrelation signature* of that trace.

Finally, we note a computational consideration: computing shortest RNNI paths can be done in polynomial time [7], whereas computing shortest NNI paths is NP-hard. For RNNI path computation, we must specify rankings for each tree T_i , which we derive from common ancestor heights of clades, as our CCD model does not explicitly represent vertex heights or rankings.

Simulated Datasets. In addition to the real datasets, we include the `Yule50` datasets from Berling et al. [4] that serve as a controlled baseline with well-behaved posterior distributions. These datasets were simulated using `LinguaPhylo` [10] under a Yule model with 50 taxa. For each dataset, we ran two independent MCMC replicates in `BEAST 2` [6], sampling 10 000 trees after burn-in. The inference used a birth-death prior with a log-normal distribution (mean 3.21, s.d. 0.3 in log space) and a HKY+G substitution model [18]. The shape parameter for the gamma distribution of site rates was modelled using a log-normal distribution (mean -1.0 , s.d. 0.5 in log space). The transition/transversion rate ratio (κ) also followed a log-normal distribution (mean 1.0, s.d. 1.25 in log space). The nucleotide base frequencies were independently simulated for each replicate from a Dirichlet distribution with a concentration parameter array of [5.0, 5.0, 5.0, 5.0]. The length of the sequence alignments was 300 sites and the mutation rate was fixed at 1.0, so that divergence ages were in units of substitutions per site.

3 Results

We first assess our chain simulation methods by comparing their autocorrelation structure to that of real MCMC chains. We then evaluate estimator accuracy

on simulated chains with known ESS, validate stability with respect to over-sampling and robustness under partitioning, and finally examine the effects of multimodality.

We consider the following ESS estimators: the trace-based estimators `logP`, `pseudoMedianRF`, `mapRF`, `expRF`, and `cladeInd`, the Fréchet variance-based `fréchetIPSE`, and the new probabilistic methods `EDCF-ML` and `MCMC`.

Throughout this section, we focus on two datasets, DS3 and DS4, as representative contrasting cases: both exhibit bimodality (cf. Table 1), but DS4 additionally suffers from poor mixing between modes, which substantially affects ESS estimation (on the real but not the simulated chains). In Section 3.5, we identify a possible explanation for the observed differences in estimator performance between these two datasets. Summary results across all datasets are presented alongside and additional plots in the Supplementary Material.

3.1 Simulated Chains

To assess how closely our simulated chains mimic the autocorrelation structure of real MCMC chains, we analyzed the autocorrelation signatures of selected traces.

First, we selected a sub-chain from an MCMC chain by finding the smallest multiple of 1000 samples that would have its ESS estimate at least 200. For the simulated chains, we use the subsample of trees that contains 200 i.i.d. trees from the CCD and a target ACT of 25. As our main reference, we used the posterior trace of the MCMC chains and for all simulated chains we considered the expected RF distance and `logP1` traces. The results for DS3 are shown in Fig. 2 and of the others in the Supplementary Material A.

Considering first the autocorrelation signatures from the real reference MCMC chains, we observe that these chains exhibit substantial variation and irregular fluctuations across lags. Simple repetition chains produce autocorrelation signatures consisting of flat line segments with sharp breakpoints at the target ACT value. Noisy repetition chains smooth these transitions slightly but still show clear linear segments and visible breakpoints. RNNI chains reduce the prominence of breakpoints and introduce more variable behaviour across lags, though breakpoints remain visible. Overall, while none of our simulation methods fully replicate real MCMC behaviour, RNNI chains represent a clear improvement, with autocorrelation signatures that more closely resemble those of real chains.

3.2 Accuracy

For each of the eleven datasets, DS1–11, we used the two independent replicates to obtain CCDs as reference distribution. Then for each pair of reference distributions and for all target ACTs 1, 2, 5, 10, 25, 50, 75, and 100, we simulated two simple and two noisy repetition chains as well as two RNNI chains. So for each dataset, each target ACT, and each simulation method, we obtained four simulated chains. Because of computational limitations we were only able to compute the accuracy on simulated RNNI chains for up to an ACT value of 25.

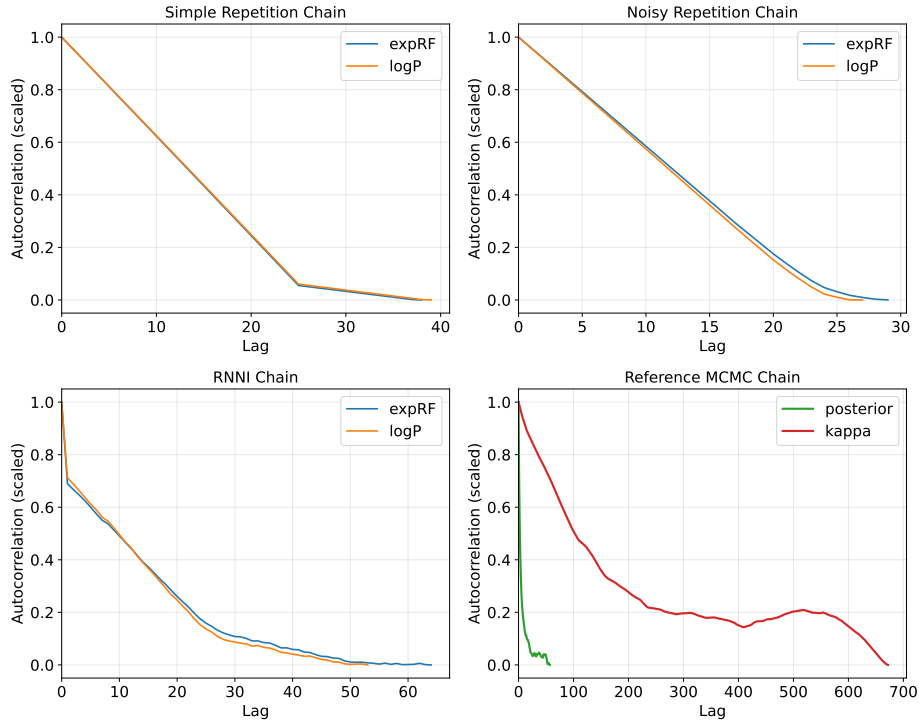
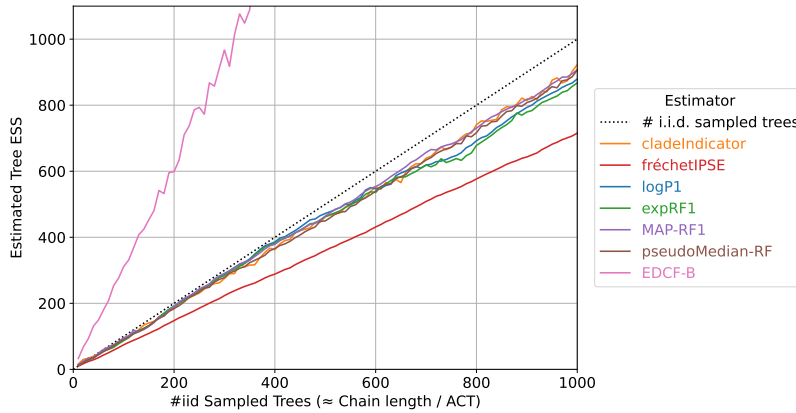


Fig. 2: Scaled autocorrelation signatures for DS3 of the $\log P$ and expRF traces for the three chain simulation methods with a target $\text{ACT}=25$, and the posterior and κ (transition/transversion rate ratio) traces for the corresponding MCMC chain.

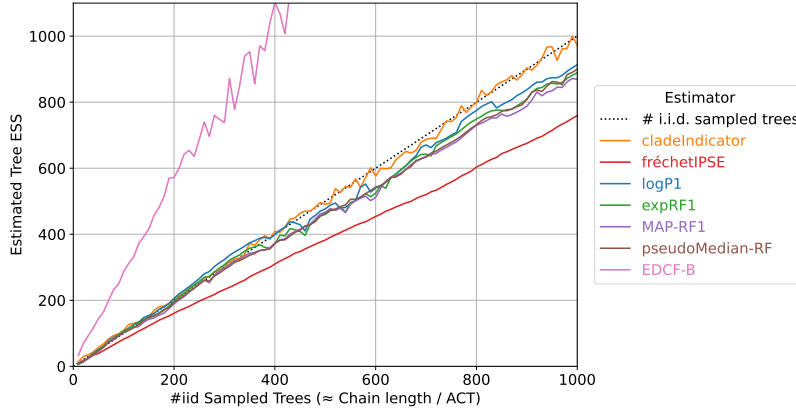
Due to our simulation procedure, we have a known lower bound on the true ESS in these simulated chains given by the number of independent samples. This allows us to assess the accuracy of different estimators by comparing this bound with the estimated ESS values, as shown in Fig. 3. We observe that all estimators except EDCF lie close to the diagonal, which represents the expected number of independently sampled trees. For DS3, all estimators (except EDCF) underestimate the ESS, with fréchetIPSE exhibiting the strongest underestimation but with low variance. A similar pattern is observed for the DS4 simulated chains, where the cladeInd estimator is closest to the diagonal.

In addition to these absolute estimates, we examine the relative estimates in Fig. 4, defined as the ratio between the estimated ESS and the lower bound (i.e., number of independent samples). Here, we omit the EDCF estimator to facilitate comparison among the remaining methods. Again, fréchetIPSE shows a consistent underestimation, while the other estimators exhibit greater variability, with no single method consistently outperforming the others in terms of proximity to the expected value.

We want to point out again that the diagonal (or, in the case of the relative evaluation, the zero line) represents a lower bound on the ESS. As mentioned previously, the RNNI simulation process may generate additional trees that effectively act as independent samples. However, we do not expect this process to introduce a large number of new effectively independent samples when the RNNI distance is small. In the case of the two datasets presented here, the average RNNI distance is below 10, and we therefore expect the true number of effectively independent samples to remain close to the diagonal. Consequently, the overestimation observed for the EDCF method may only partially be attributed to a higher true ESS and more likely represents true overestimation.



(a) DS3



(b) DS4

Fig. 3: Estimated tree ESS for DS3 and DS4 on simulated RNNI chains with an underlying ACT of 5 across different chain lengths and different ESS estimators. Estimator accuracy is measured as the deviation from the diagonal (lower true ESS bound); summary results of this accuracy evaluation are shown in Fig. 5.

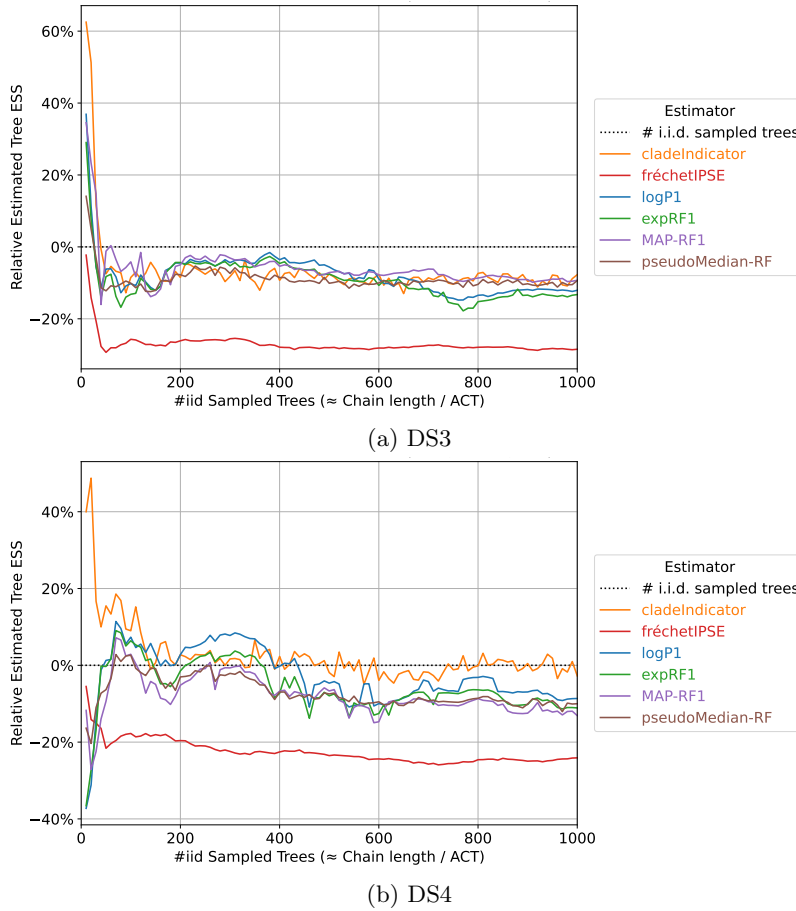


Fig. 4: Relative estimated tree ESS for DS3 and DS4, showing the same data as Fig. 3 but normalised by the expected lower bound. The EDCF estimator is omitted due to its comparatively high values.

Summarizing Robustness Accuracy. Using our simulated chains, for which the true ESS (or at least a lower bound) is known, we can directly assess the accuracy of different ESS estimators. To concisely summarize these evaluations, we employ the *mean relative error (MRE)*, which quantifies the deviation of the estimated ESS values from the expected ESS (lower bound). Formally, for each dataset and ACT value, we compute

$$\text{MRE} = \frac{1}{n} \sum_{i=1}^n \frac{(Y_i - \hat{Y}_i)}{\hat{Y}_i}$$

where Y_i denotes the ESS estimated by a given method and \hat{Y}_i is the corresponding expected ESS.

Conceptually, this approach is equivalent to a linear regression between estimated and expected ESS values, as displayed in Fig. 3. An MRE of zero indicates that an estimator matches the expected lower bound on average, while a positive MRE signals overestimation and a negative MRE indicates underestimation. Because the expected ESS value \hat{Y}_i ranges from 10 to 1000, we use the relative error to compress the evaluation for all datasets and expected ESS values given a fixed ACT value. Overall, we would expect a well-performing estimator to have an MRE close to zero (or slightly below, as the initial positive sequence estimator method consistently underestimates [16]), reflecting accurate or slightly lower estimates of the ESS.

Across the eleven real datasets, we observe that the estimated ESS generally increases with larger ACT values (Fig. 5). Besides EDCF consistently overestimating, `cladeInd` provides the next highest estimates, along with the `logP1` and `exprF1` estimators. Note that these show substantial overlap of their interquartile ranges. The `mapRF1` and `pseudoMedianRF` estimators produce very similar estimates across all ACT values, while the `fréchetIPSE` consistently yields the lowest ESS estimates, albeit with a high consistency across ACT values.

To establish a baseline for estimator performance, we further evaluate accuracy on simulated Yule datasets, which we assume to represent well-behaved posterior distributions without multimodality or mixing issues (Fig. 6). In this setting we use the noisy chain simulation method with ACT values ranging from 2 to 100. Most estimators produce similar ESS values, although `exprF`, `logP1`, and `mapRF1` exhibit the largest variability. Once again, `cladeInd` provides highly consistent estimates across all ACT values. Due to its high computational cost, `fréchetIPSE` is only reported for ACT values between 2 and 10.

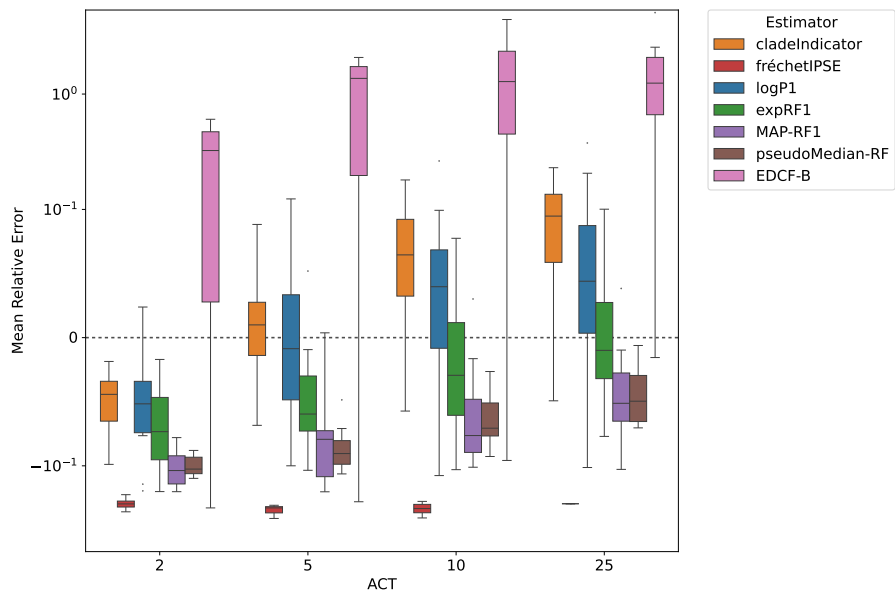


Fig. 5: Summary of estimator accuracy on simulated RNNI chains for all eleven datasets. Performance is quantified using the relative mean error, taking into account the known ESS bound. Results are reported up to an ACT of 25 due to computational limitations.

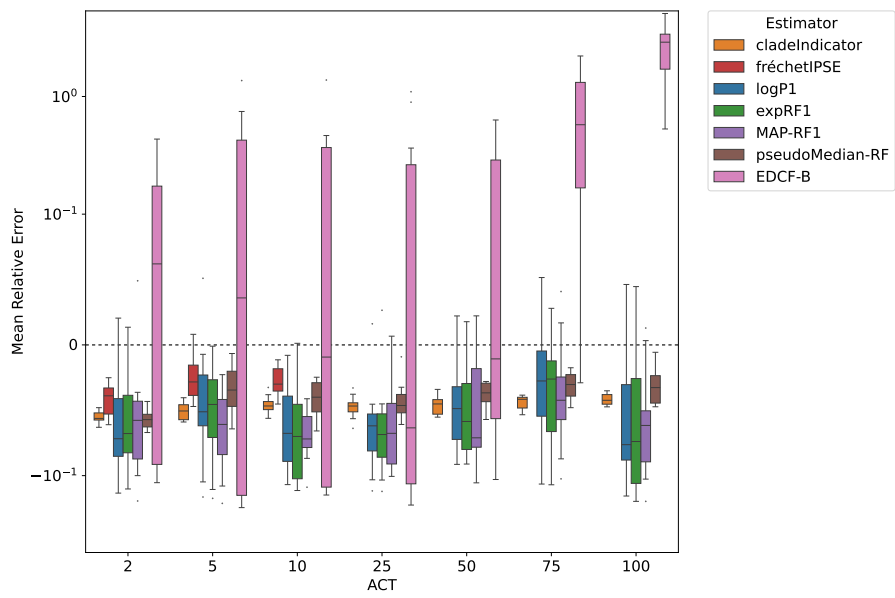


Fig. 6: Summary of the estimator accuracy on the simulated noisy repetition chains for all 10 Yule datasets.

3.3 Stability

To evaluate the stability of the different tree ESS estimators, we investigate the variance of the estimates under different thinning intervals. If an MCMC is over-sampled, its output contains large amounts of autocorrelated (i.e., non independent) trees. Consequently, ESS estimates should remain stable across thinning intervals until thinning begins to remove effectively independent samples.

In Fig. 7, we present the raw ESS estimates for DS3 and DS4 under different thinning intervals, namely 0, 2, 4, 8, and 16 when starting with the oversampled chain (cf. Section 2.3). The plots for the all datasets and with more estimators shown can be found in Supplementary Material C. All estimators appear to be very stable under oversampling, with the only outlier in terms of stability being the EDCF methods (only EDCF-B shown here). As expected, the other estimators yield slightly lower but very similar estimates at higher thinning intervals.

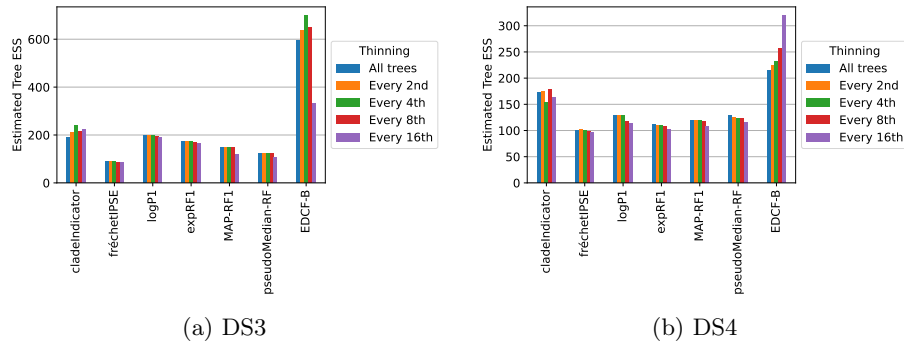


Fig. 7: Tree ESS estimates for different thinning intervals of oversampled datasets as per our stability experiment.

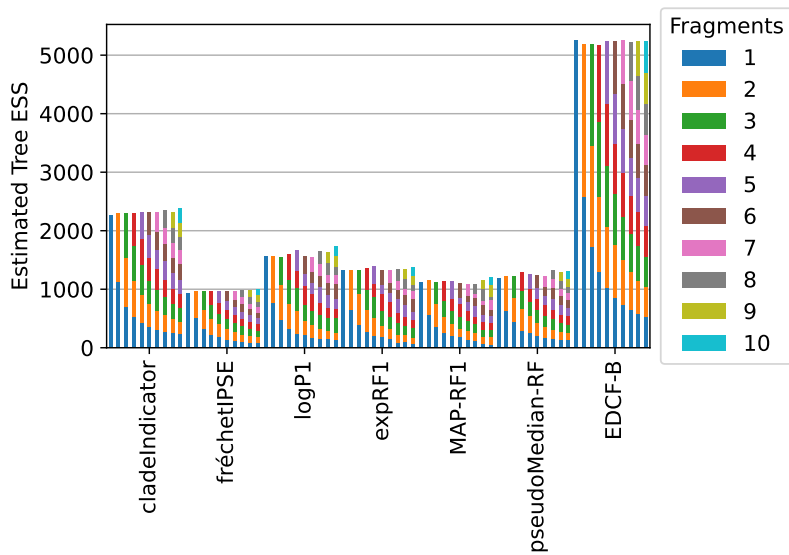
3.4 Robustness

Here we assess how well the different ESS estimators satisfy an additivity property by evaluating their behaviour under varying numbers of fragmented sub-chains. For a well-behaved estimator, we expect low variance in the total ESS across different numbers of fragments, such that the sum of the ESS estimates remain approximately constant. Substantial deviations from this behaviour may indicate issues such as poor mixing, multimodality in the underlying distribution, or inadequate removal of burn-in. This approach has previously been used in the context of convergence assessment [3].

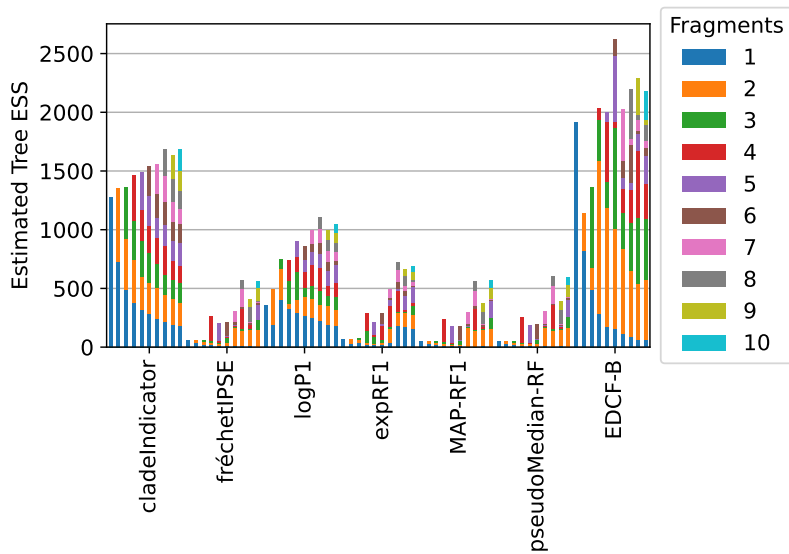
For this evaluation we used chains of 10 000 trees from each dataset and partitioned each into k equally sized fragments, for $k \in \{1, 2, \dots, 10\}$. For each k , we estimate the ESS for all fragments and then combined these estimates into a single value. In this part of the paper, we present the results for DS3

and DS4, Fig. 8, and the remaining datasets are available in the Supplementary Material D. For DS3 we observe a very stable sum of total ESS over all different fragments for all estimators. However, for DS4 we find high variability among all estimators with a tendency for higher sums of ESS estimates with more fragments, independent of the specific estimator.

From the perspective of the estimators, these results indicate that, with the exception of EDCF, all methods behave robustly under chain fragmentation when the underlying posterior distribution is well behaved, as in the case of DS3. In such settings, splitting the chain does not substantially affect the total ESS, suggesting that these estimators are internally consistent with respect to additivity. Conversely, when the posterior exhibits poor mixing or multimodality (see Section 3.5), as in DS4, all estimators show similar instability, with increasing fragmentation leading to inflated ESS estimates. This suggests that the observed lack of robustness is primarily driven by properties of the underlying tree distribution rather than by deficiencies of individual estimators. Consequently, additivity-based diagnostics are better interpreted as tools for detecting mixing and convergence issues in MCMC tree samples, rather than as a means of distinguishing between ESS estimators.



(a) DS3



(b) DS4

Fig. 8: Robustness of ESS estimators under different chain fragmentations. The two datasets exhibit markedly different behaviour, while no estimator shows a consistently distinct trend.

Summarizing Robustness Evaluation. To concisely summarise the robustness analysis, we report a table containing summary statistics of the additivity across different chain fragmentations. Columns correspond to datasets and rows to ESS estimators. Each table entry reports the mean and standard deviation of the absolute pairwise differences in the total ESS obtained from different numbers of fragments. Specifically, for each estimator and dataset, we compute the summed ESS values S_k for fragmentations into $k \in \{1, \dots, 10\}$ equally sized subsets, and then consider all $\binom{10}{2}$ absolute differences $|S_i - S_j|$ for $i < j$. The reported mean and standard deviation are normalised by the maximum observed summed ESS for the corresponding dataset and estimator. Here we restrict the table to a subset of estimators and complete tables can be found in the Supplementary Material D.1. These values quantify how stable the total ESS remains under different numbers of fragments. In the context of the previous stacked histograms, these statistics indicate how the total heights of the bars vary for each estimator.

In Table 2, we present these summary statistics for the eleven datasets. The table is colour-coded to indicate what we consider good behaviour in green (mean and standard deviation below 0.05), slightly worse performance in yellow (values between 0.05 and 0.1), and poor behaviour in red (values above 0.1). It is evident from the table that datasets 2, 3, and 7 exhibit well-behaved additivity across all estimators. In contrast, the remaining datasets mostly show values larger than 0.1, indicating substantial variation in the summed ESS across different fragmentations.

To verify that these results are driven by the underlying datasets rather than by the estimators themselves, we present the same summary table for the 10 simulated Yule datasets in Table 3. As in the accuracy analysis, this experiment serves as a baseline, since these datasets are assumed to represent well-behaved tree distributions without multimodality or mixing issues. Here we observe that all 10 datasets predominantly yield values below 0.05, with only the EDCF estimator exhibiting more pronounced variability.

Overall, the robustness analysis indicates that fragmentation primarily exposes characteristics of the posterior distribution and the underlying sampling behaviour, rather than systematic differences among estimators. These insights underscore the value of additivity-based diagnostics for identifying convergence and mixing issues in tree MCMC samples, setting the stage for a more detailed investigation in the next section.

Table 2: Robustness of ESS estimates across the datasets DS1–11 (10,000 trees), with lower values indicating more robust performance.

	1	2	3	4	5	6	7	8	9	10	11
LogP1	0.21 ± 0.16	0.06 ± 0.04	0.04 ± 0.03	0.26 ± 0.18	0.14 ± 0.09	0.18 ± 0.13	0.05 ± 0.04	0.19 ± 0.12	0.19 ± 0.13	0.15 ± 0.11	0.17 ± 0.12
cladeIndicator	0.18 ± 0.12	0.02 ± 0.02	0.02 ± 0.01	0.10 ± 0.06	0.09 ± 0.06	0.09 ± 0.06	0.01 ± 0.01	0.08 ± 0.05	0.08 ± 0.05	0.10 ± 0.06	0.02 ± 0.02
fréchetIPSE	0.27 ± 0.19	0.03 ± 0.02	0.02 ± 0.02	0.40 ± 0.27	0.09 ± 0.06	0.31 ± 0.28	0.05 ± 0.04	0.05 ± 0.04	0.09 ± 0.06	0.29 ± 0.19	0.05 ± 0.03
expRF1	0.19 ± 0.13	0.06 ± 0.04	0.02 ± 0.01	0.43 ± 0.29	0.16 ± 0.11	0.30 ± 0.29	0.04 ± 0.03	0.20 ± 0.13	0.23 ± 0.15	0.26 ± 0.17	0.27 ± 0.20
MAP-RF1	0.18 ± 0.12	0.06 ± 0.04	0.03 ± 0.02	0.41 ± 0.28	0.12 ± 0.08	0.35 ± 0.31	0.05 ± 0.03	0.12 ± 0.09	0.16 ± 0.11	0.33 ± 0.21	0.18 ± 0.13
pseudoMedian-RF	0.28 ± 0.20	0.03 ± 0.02	0.04 ± 0.03	0.41 ± 0.28	0.08 ± 0.05	0.33 ± 0.30	0.04 ± 0.03	0.07 ± 0.04	0.11 ± 0.07	0.32 ± 0.21	0.03 ± 0.02
EDCF-Bayesian	0.24 ± 0.24	0.03 ± 0.02	0.01 ± 0.00	0.18 ± 0.14	0.07 ± 0.06	0.26 ± 0.24	0.22 ± 0.15	0.15 ± 0.11	0.03 ± 0.02	0.28 ± 0.18	0.05 ± 0.03

Table 3: Robustness of ESS estimates across 10 Yule datasets (10,000 trees), with lower values indicating more robust performance.

	1	2	3	4	5	6	7	8	9	10
LogP1	0.04 ± 0.03	0.02 ± 0.01	0.02 ± 0.01	0.01 ± 0.01	0.02 ± 0.02	0.04 ± 0.03	0.02 ± 0.01	0.01 ± 0.01	0.04 ± 0.02	0.01 ± 0.01
cladeIndicator	0.00 ± 0.00	0.01 ± 0.00	0.01 ± 0.01	0.00 ± 0.00	0.00 ± 0.00	0.01 ± 0.01	0.01 ± 0.00	0.00 ± 0.00	0.00 ± 0.00	0.01 ± 0.00
fréchetIPSE	0.00 ± 0.00	0.00 ± 0.00	0.00 ± 0.00	0.00 ± 0.00	0.02 ± 0.01	0.00 ± 0.00	0.00 ± 0.00	0.00 ± 0.00	0.00 ± 0.00	0.01 ± 0.00
expRF1	0.02 ± 0.01	0.01 ± 0.01	0.02 ± 0.01	0.01 ± 0.01	0.02 ± 0.02	0.04 ± 0.04	0.03 ± 0.02	0.01 ± 0.00	0.02 ± 0.02	0.01 ± 0.01
MAP-RF1	0.02 ± 0.01	0.01 ± 0.01	0.02 ± 0.02	0.04 ± 0.02	0.03 ± 0.02	0.02 ± 0.02	0.04 ± 0.03	0.02 ± 0.02	0.02 ± 0.01	0.02 ± 0.01
pseudoMedian-RF	0.01 ± 0.01	0.01 ± 0.01	0.01 ± 0.01	0.01 ± 0.01	0.01 ± 0.01	0.01 ± 0.01	0.01 ± 0.00	0.01 ± 0.01	0.01 ± 0.01	0.01 ± 0.01
EDCF-Bayesian	0.01 ± 0.01	0.06 ± 0.06	0.03 ± 0.04	0.09 ± 0.16	0.02 ± 0.02	0.03 ± 0.03	0.00 ± 0.00	0.11 ± 0.13	0.00 ± 0.00	0.10 ± 0.07

3.5 Multimodality, Poor Mixing, and ESS

To visualise and explore multimodality in the posterior tree sets, we first sub-sampled each dataset to 1000 trees to reduce computational cost while preserving representative diversity. These 1000 trees were sampled from the last 10 000 trees of each chain, keeping every 10th tree. Pairwise RNNI tree distances were then computed, and a 2-dimensional embedding was generated using t-distributed Stochastic Neighbour Embedding (t-SNE) [46], which emphasises local structure in high-dimensional spaces. To complement the visualisation, we applied spectral clustering to the affinity matrices derived from the pairwise tree distances, using a heat kernel transformation to convert distances into affinities [36]. Both t-SNE and spectral clustering were implemented using scikit-learn [36]. Visualisations combining the MDS embedding with the identified clusters were used for qualitative assessment of multimodality and mixing, with further details and individual dataset plots provided in the Supplementary Material E and more trace plots are provided in the Supplementary Material F.

Multimodality was assessed by visually inspecting the MDS plots. Poor mixing between modes, where chains remain in one mode for an extended period before transitioning to another, can lead to lower ESS estimates. Conversely, when multiple modes are present but the chain mixes well across them (see Fig. 9), ESS estimates tend to be more consistent and robust to chain fragmentation. These mixing issues are particularly evident in DS4 (see Fig. 10) and are reflected in both the robustness and accuracy analyses. In the robustness evaluation, the dataset itself appears to drive the observed instability in ESS estimates across chain fragmentation. In the accuracy assessment, poor mixing contributes to increase variability in the estimates for DS4 relative to DS3 (see Fig. 4), although the overall bias of the estimators is less affected. The MDS visualizations provide an intuitive explanation for the observed differences in ESS behaviour across datasets.

4 Discussion

We evaluated both new and existing estimators for the effective sample size (ESS) of tree topologies in MCMC samples, using a testing framework that combined simulated chains with empirical datasets. For the simulations, we integrated ideas

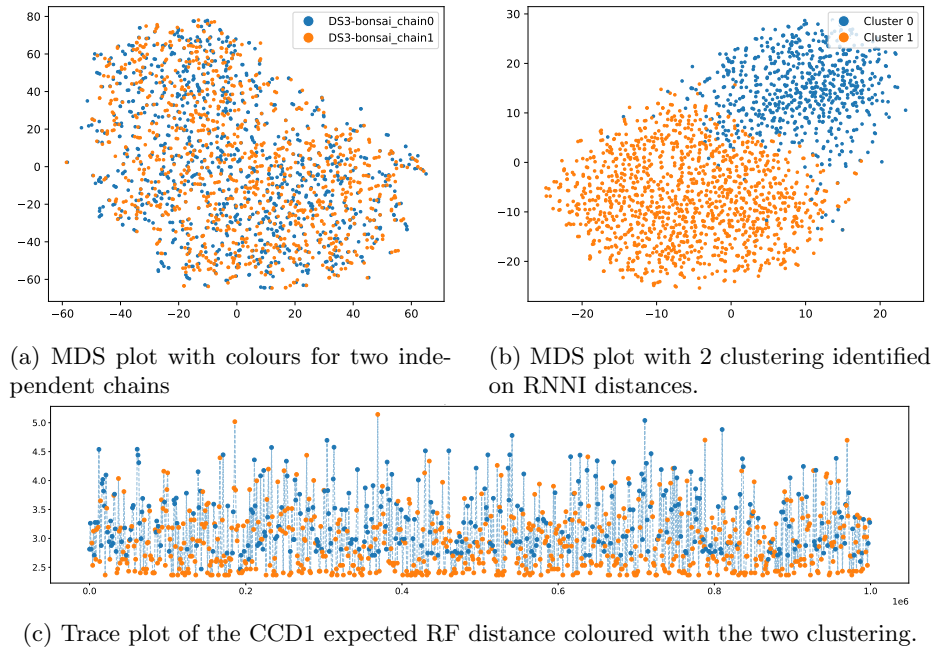


Fig. 9: MDS embedding and spectral clustering of two independent chains for DS3. The two identified clusters/modes correspond well with the MDS coordinates. Trace plots show no apparent mixing issues between the modes.

from previous approaches with the versatility of CCDs: chains were simulated by sampling from a CCD fitted to the posterior tree distribution, providing access to the true ESS (or at least a lower bound). To control the autocorrelation time, we extended these chains by connecting consecutive independent samples through random trees drawn from shortest RNNI paths between them.

Overall, we did not observe extreme differences in accuracy between most estimators, with the notable exception of the newly introduced probabilistic method (EDCF), which substantially overestimated ESS in most settings. Methods that map trees to numerical traces and subsequently apply the initial positive sequence estimator (as implemented in Tracer) yielded similar results across datasets. Consistent with the findings of Fabreti and Höhna [16] for the initial positive sequence estimator, these methods tended to slightly underestimate the ESS. The two methods that average over multiple traces, `cladeInd` and `pseudoMedianRF`, displayed lower variance and more stable accuracy, and are therefore our recommended estimators.

While `fréchetIPSE` performed comparably well in terms of accuracy and robustness, it requires the computation of pairwise distances between all trees, which becomes prohibitively expensive for long chains. In practice, we were forced to impose time limits in our experiments. Similar limitations apply to

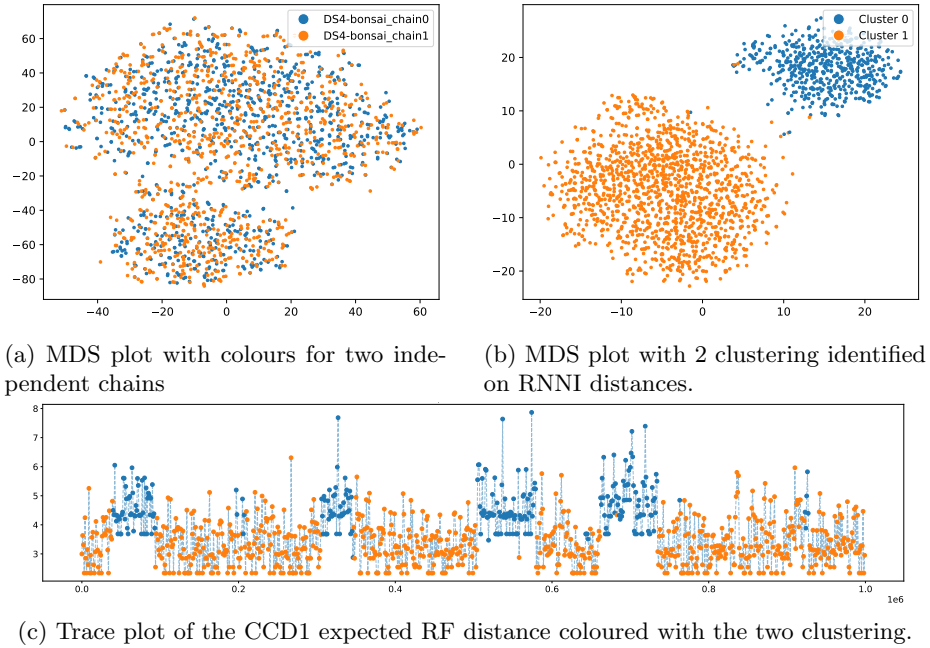


Fig. 10: MDS embedding and spectral clustering of two independent chains for DS4. The clustering aligns with the MDS coordinates. Trace plots reveal poor mixing between modes, explaining the robustness problems observed across ESS estimators.

`approximateESS` and EDCF. Although thinning could in principle mitigate these computational costs, our preliminary experiments indicated that estimator behaviour was not stable under thinning. We therefore recommend the simpler and faster estimators, which achieve comparable performance without substantial computational overhead.

The motivation behind EDCF was to leverage a probabilistic model of clade observations for ESS estimation. By construction, these estimates are independent of both tree order and distance metrics. This approach was recently applied to estimate the sampling error on clade counts from two independent MCMC chains, under the assumption of a fixed ESS [8]. Here we extended this strategy by estimating the ESS directly from observed clade frequencies, noting that clade frequencies have previously been used for convergence assessment. Although initial results were encouraging, the method lacks the accuracy and robustness of existing approaches, which likely results from the incorrect assumption of clade count independence. While further tuning of the model and parameters may improve performance, the strong behaviour of existing and other novel methods, combined with the computational demands of this estimator, suggests that the practical utility of such refinements is limited.

Our new trace-based methods, which map trees to numerical sequences via CCD log probabilities (`logP`), distances to the CCD MAP tree (`mapRF`), or expected RF distances with respect to the CCD (`expRF`), perform competitively with `pseudoMedianRF`, albeit with higher variance. While these may not be the first choice for a final ESS estimate, they offer distinct conceptual advantages. For instance, `logP` is independent of any explicit tree distance metric. Using the CCD MAP tree provides a fixed and reproducible reference point, which may be valuable for tree distance trace plots [32] and for ensuring comparability across analyses.

Overall, our practical recommendation for tree-based ESS estimation is to use `cladeInd` by Fabreti and Höhna [16] or `pseudoMedianRF` (implemented as `pseudoESS`) by Lanfear et al. [32].

We also introduced a new algorithm for efficiently computing the expected RF distance of a tree to a CCD. This quantity represents the expected distance between a given tree and a randomly drawn tree from the CCD distribution. We expect this algorithm to be useful beyond its role in the `expRF` estimator as it provides a principled way of measuring distances between individual trees and entire tree distributions. Extending this approach to other tree distance measures represents a promising direction for future work.

Finally, we briefly discuss the role of ESS for convergence assessment in practical phylogenetic analyses. Estimating tree ESS across multiple chains provides a valuable diagnostic of convergence: a high combined ESS suggests that chains are sampling from similar distributions, and therefore likely approximating the target stationary distribution. Conversely, a low combined ESS indicates that chains may not yet have explored sufficiently similar regions of treespace, signalling a lack of convergence. While this strategy has been applied previously [3], it is important to emphasize that a high ESS alone does not guarantee convergence to the correct target distribution. Independent checks, such as visual inspection of parameter traces and posterior distributions or the use of diagnostics like the Gelman–Rubin diagnostic, remain essential. Ultimately, the ESS should be interpreted as a measure of how many effectively independent samples have been obtained, and does not provide a proof of convergence in any case.

Some tree-based ESS estimators can be computed online during the MCMC run and are therefore candidates for inclusion in automated convergence testing frameworks, such as the ASM package. This is straightforward for `cladeInd`, and it is also feasible to maintain a CCD during MCMC in order to compute log-probability or RF-based traces online.

Finally, we observed that multimodality in the posterior distribution can substantially affect ESS estimates, particularly when mixing between modes is poor. When multiple well-separated modes are present, for example as indicated by MDS combined with clustering or by visual inspection of topology trace plots, we recommend considering ESS estimates both within individual modes and for transitions between modes. High ESS values for each component provide stronger evidence of adequate mixing than a single global ESS estimate, which may be misleading when transitions between modes are rare. We emphasize that meth-

ods such as MDS and clustering provide only coarse and potentially unreliable views of multimodality in treespace, with results that can depend strongly on the underlying choice of tree distance metric. Developing more principled and scalable approaches for detecting and characterizing multimodal posterior tree distributions remains an important direction for future work.

5 Conclusion

We have extended the toolkit for phylogenetic MCMC diagnostics by introducing CCD-based ESS estimators and a probabilistic approach based on clade frequencies, while providing a systematic comparison with existing methods. Our evaluation framework, combining simulated chains with known ESS bounds and robustness testing on real datasets, offers a general template for future method development. While computational constraints limit some approaches for large-scale analyses, methods such as `cladeInd` and `pseudoMedianRF` provide reliable and efficient ESS estimation for tree topologies. Together with the new expected RF distance algorithm, these contributions facilitate more rigorous assessment of phylogenetic inference quality and more efficient use of computational resources.

More broadly, our results highlight that effective sample size estimation for phylogenetic trees is a fundamentally challenging problem. Distinguishing between insufficient sampling within a single mode and poor mixing across multiple modes therefore requires careful interpretation of ESS values across chains. Methods that can be computed during MCMC runs further enable integration into automated convergence assessment frameworks, such as the ASM package [3], providing real-time diagnostics for practitioners. As phylogenetic analyses continue to grow in scale and complexity, robust ESS estimation for tree topologies remains fundamental to ensuring the validity of posterior inference.

Availability

Our trace-based tree ESS estimates are available to use via the `TreeStat2` package⁸ and `Tracer` [38]. The code for the EDCF methods, `fréchetIPSE`, and `approximateESS` are available in their own repository⁹. Lanfear et al. [32] also provide their tree ESS estimators `pseudoMedianRF` and `approximateESS` as well as methods for trace and jump distances plots in their R package `RWTY` (R We There Yet?)¹⁰. Magee et al. [35] also provide `fréchetIPSE` (and others) in their R package `treess`¹¹. The algorithm to compute the expected RF distance of a tree to a CCD is available in the `CCD` package/repository¹². For the RNNI based computations we utilized the `tetres` Python package¹³.

⁸ GitHub `TreeStat2` package github.com/alexeid/TreeStat2

⁹ GitHub `TreeESSEExtra` repository github.com/CompEvol/TreeESSEExtra

¹⁰ GitHub `RWTY` package github.com/danlwarren/RWTY/

¹¹ GitHub `treess` package github.com/afmagee/treess/

¹² GitHub `CCD` package github.com/CompEvol/CCD

¹³ GitHub `tetres` package github.com/bioDS/tetres

Acknowledgements

JK, JD, and AJD were partially supported by the Beyond Prediction Data Science Research Programme (MBIE grant UOAX1932).

References

1. Benjamin L. Allen and Mike Steel. Subtree Transfer Operations and Their Induced Metrics on Evolutionary Trees. *Annals of Combinatorics*, 5(1):1–15, 2001. doi:10.1007/s00026-001-8006-8.
2. Guy Baele, Luiz M Carvalho, Marius Brusselmanns, Gytis Dudas, Xiang Ji, John T McCrone, Philippe Lemey, Marc A Suchard, and Andrew Rambaut. HIPSTR: highest independent posterior subtree reconstruction in TreeAnnotator X. *Bioinformatics*, 41(10):btaf488, 2025. doi:10.1093/bioinformatics/btaf488.
3. Lars Berling, Remco Bouckaert, and Alex Gavryushkin. An automated convergence diagnostic for phylogenetic MCMC analyses. *IEEE/ACM Transactions on Computational Biology and Bioinformatics*, pages 1–13, 2024. doi:10.1109/TCBB.2024.3457875.
4. Lars Berling, Jonathan Klawitter, Remco Bouckaert, Dong Xie, Alex Gavryushkin, and Alexei J Drummond. Accurate bayesian phylogenetic point estimation using a tree distribution parameterized by clade probabilities. *PLOS Computational Biology*, 21(2):e1012789, 2025. doi:10.1371/journal.pcbi.1012789.
5. Magnus Bordewich and Charles Semple. On the Computational Complexity of the Rooted Subtree Prune and Regraft Distance. *Annals of Combinatorics*, 8(4):409–423, 2005. doi:10.1007/s00026-004-0229-z.
6. Remco Bouckaert, Timothy G Vaughan, Joëlle Barido-Sottani, Sebastián Duchêne, Mathieu Fourment, Alexandra Gavryushkina, Joseph Heled, Graham Jones, Denise Kühnert, Nicola De Maio, et al. BEAST 2.5: An advanced software platform for Bayesian evolutionary analysis. *PLoS Computational Biology*, 15(4):e1006650, 2019. doi:10.1371/journal.pcbi.1006650.
7. Lena Collienne and Alex Gavryushkin. Computing nearest neighbour interchange distances between ranked phylogenetic trees. *Journal of Mathematical Biology*, 82(1):8, 2021. doi:10.1007/s00285-021-01567-5.
8. Jordan Douglas, Remco Bouckaert, Simon C Harris, Charles W Carter Jr, and Peter R Wills. Evolution is coupled with branching across many granularities of life. *Proceedings of the Royal Society B: Biological Sciences*, 292(2047), 2025. doi:10.1098/rspb.2025.0182.
9. Jordan Douglas, Cinthy L Jiménez-Silva, and Remco Bouckaert. StarBeast3: adaptive parallelized Bayesian inference under the multispecies coalescent. *Systematic Biology*, 71(4):901–916, 2022. doi:10.1093/sysbio/syac010.
10. Alexei J Drummond, Kylie Chen, Fábio K Mendes, and Dong Xie. LinguaPhylo: a probabilistic model specification language for reproducible phylogenetic analyses. *PLOS Computational Biology*, 19(7):e1011226, 2023. doi:10.1371/journal.pcbi.1011226.
11. James M. Flegal, John Hughes, Dootika Vats, Ning Dai, Kushagra Gupta, and Uttiya Maji. *mcmcse: Monte Carlo Standard Errors for MCMC*. Riverside, CA, and Kanpur, India, 2021. R package version 1.5-0.
12. James M. Flegal and Galin L. Jones. Batch means and spectral variance estimators in Markov chain Monte Carlo. *The Annals of Statistics*, 38(2):1034–1070, 2010. doi:10.1214/09-A05735.

13. James R. Garey, Thomas J. Near, Michael R. Nonnemacher, and Steven A. Nadler. Molecular evidence for Acanthocephala as a subtaxon of Rotifera. *Journal of Molecular Evolution*, 43(3):287–292, 1996. doi:10.1007/BF02338837.
14. Andrew Gelman, John B Carlin, Hal S Stern, and Donald B Rubin. *Bayesian Data Analysis*. Chapman and Hall/CRC, 1995.
15. Charles J Geyer. Introduction to Markov Chain Monte Carlo. In Steve Brooks, Andrew Gelman, Galin Jones, and Xiao-Li Meng, editors, *Handbook of Markov Chain Monte Carlo*, pages 3–48, 2011.
16. Luiza Guimarães Fabreti and Sebastian Höhna. Convergence assessment for Bayesian phylogenetic analysis using MCMC simulation. *Methods in Ecology and Evolution*, 13(1):77–90, 2022. doi:10.1111/2041-210X.13727.
17. James D. Hamilton. *TIME SERIES ANALYSIS*. Princeton University Press, 1994.
18. Masami Hasegawa, Hirohisa Kishino, and Taka-aki Yano. Dating of the human-ape splitting by a molecular clock of mitochondrial DNA. *Journal of molecular evolution*, 22:160–174, 1985. doi:10.1007/BF02101694.
19. S B Hedges, K D Moberg, and L R Maxson. Tetrapod phylogeny inferred from 18S and 28S ribosomal RNA sequences and a review of the evidence for amniote relationships. *Molecular Biology and Evolution*, 7(6):607–633, 1990. doi:10.1093/oxfordjournals.molbev.a040628.
20. Philip Heidelberger and Peter D. Welch. A spectral method for confidence interval generation and run length control in simulations. *Communications of the ACM*, 24(4):233–245, 1981. doi:10.1145/358598.358630.
21. Jotun Hein. Reconstructing evolution of sequences subject to recombination using parsimony. *Mathematical Biosciences*, 98(2):185–200, 1990. doi:10.1016/0025-5564(90)90123-G.
22. Daniel A. Henk, Alex Weir, and Meredith Blackwell. Laboulbeniopsis termitarius, an ectoparasite of termites newly recognized as a member of the Laboulbeniomyces. *Mycologia*, 95(4):561–564, 2003. doi:10.1080/15572536.2004.11833059.
23. Sebastian Höhna and Alexei J. Drummond. Guided tree topology proposals for Bayesian phylogenetic inference. *Systematic Biology*, 61(1):1–11, 2012. doi:10.1093/sysbio/syr074.
24. Sebastian Höhna, Michael J. Landis, Tracy A. Heath, Bastien Boussau, Nicolas Lartillot, Brian R. Moore, John P. Huelsenbeck, and Fredrik Ronquist. RevBayes: Bayesian phylogenetic inference using graphical models and an interactive model-specification language. *Systematic Biology*, 65(4):726–736, 2016. doi:10.1093/sysbio/syw021.
25. Amanda L. Ingram and Jeff J. Doyle. Is eragrostis (poaceae) monophyletic? insights from nuclear and plastid sequence data. *Systematic Botany*, 29(3):545–552, 2004. doi:10.1600/0363644041744392.
26. M. J. Bayarri James Berger and L. R. Pericchi. The effective sample size. *Econometric Reviews*, 33(1-4):197–217, 2014. doi:10.1080/07474938.2013.807157.
27. Seong-Hwan Jun, Hassan Nasif, Chris Jennings-Shaffer, David H. Rich, Anna Kooperberg, Mathieu Fourment, Cheng Zhang, Marc A. Suchard, and Frederick A. Matsen. A topology-marginal composite likelihood via a generalized phylogenetic pruning algorithm. *Algorithms for Molecular Biology*, 18(10), 2023. doi:10.1186/s13015-023-00235-1.
28. Jonathan Klavitter, Remco Bouckaert, and Alexei J. Drummond. Skeletons in the forest: Using entropy-based rogue detection on Bayesian phylogenetic tree distributions. *bioRxiv*, 2024. doi:10.1101/2024.09.25.615070.

29. Jonathan Klawitter and Alexei J. Drummond. Credible sets of phylogenetic tree topology distributions, 2025. [arXiv:2505.14532](https://arxiv.org/abs/2505.14532), [doi:10.48550/arXiv.2505.14532](https://doi.org/10.48550/arXiv.2505.14532).
30. Scott Kroken and John W. Taylor. Phylogenetic species, reproductive mode, and specificity of the green alga trebouxia forming lichens with the fungal genus letharia. *The Bryologist*, 103(4):645–660, 2000.
31. Clemens Lakner, Paul Van Der Mark, John P Huelsenbeck, Bret Larget, and Fredrik Ronquist. Efficiency of Markov chain Monte Carlo tree proposals in Bayesian phylogenetics. *Systematic Biology*, 57(1):86–103, 2008. [doi:10.1080/10635150801886156](https://doi.org/10.1080/10635150801886156).
32. Robert Lanfear, Xia Hua, and Dan L. Warren. Estimating the Effective Sample Size of Tree Topologies from Bayesian Phylogenetic Analyses. *Genome Biology and Evolution*, 8(8):2319–2332, 2016. [doi:10.1093/gbe/evw171](https://doi.org/10.1093/gbe/evw171).
33. Bret Larget. The estimation of tree posterior probabilities using conditional clade probability distributions. *Systematic Biology*, 62(4):501–511, 2013. [doi:10.1093/sysbio/syt014](https://doi.org/10.1093/sysbio/syt014).
34. Paul O. Lewis, Ming-Hui Chen, Lynn Kuo, Louise A. Lewis, Karolina Fučíková, Suman Neupane, Yu-Bo Wang, and Daoyuan Shi. Estimating Bayesian phylogenetic information content. *Systematic Biology*, 65(6):1009–1023, 2016. [doi:10.1093/sysbio/syw042](https://doi.org/10.1093/sysbio/syw042).
35. Andrew Magee, Michael Karcher, Frederick A Matsen IV, and Volodymyr M Minin. How trustworthy is your tree? Bayesian phylogenetic effective sample size through the lens of Monte Carlo error. *Bayesian Analysis*, 1(1):1–29, 2023. [doi:10.1214/22-BA1339](https://doi.org/10.1214/22-BA1339).
36. F. Pedregosa, G. Varoquaux, A. Gramfort, V. Michel, B. Thirion, O. Grisel, M. Blondel, P. Prettenhofer, R. Weiss, V. Dubourg, J. Vanderplas, A. Passos, D. Cournapeau, M. Brucher, M. Perrot, and E. Duchesnay. Scikit-learn: Machine learning in Python. *Journal of Machine Learning Research*, 12:2825–2830, 2011.
37. Martyn Plummer, Nicky Best, Kate Cowles, and Karen Vines. CODA: Convergence Diagnosis and Output Analysis for MCMC. *R News*, 6(1):7–11, 2006.
38. Andrew Rambaut, Alexei J Drummond, Dong Xie, Guy Baele, and Marc A Suchard. Posterior Summarization in Bayesian Phylogenetics Using Tracer 1.7. *Systematic Biology*, 67(5):901–904, 2018. [doi:10.1093/sysbio/syy032](https://doi.org/10.1093/sysbio/syy032).
39. Fredrik Ronquist, Maxim Teslenko, Paul van der Mark, Daniel L. Ayres, Aaron Darling, Sebastian Höhna, Bret Larget, Liang Liu, Marc A. Suchard, and John P. Huelsenbeck. MrBayes 3.2: efficient Bayesian phylogenetic inference and model choice across a large model space. *Systematic Biology*, 61(3):539–542, 2012. [doi:10.1093/sysbio/sys029](https://doi.org/10.1093/sysbio/sys029).
40. Amy Y. Rossman, John M. McKemy, Rebecca A. Pardo-Schultheiss, and Hans-Josef Schroers. Molecular studies of the Bionectriaceae using large subunit rDNA sequences. *Mycologia*, 93(1):100–110, 2001. [doi:10.1080/00275514.2001.12061283](https://doi.org/10.1080/00275514.2001.12061283).
41. Mike A. Steel and David Penny. Distributions of tree comparison metrics—some new results. *Systematic Biology*, 42(2):126–141, 1993. [doi:10.1093/sysbio/42.2.126](https://doi.org/10.1093/sysbio/42.2.126).
42. Marc A Suchard, Philippe Lemey, Guy Baele, Daniel L Ayres, Alexei J Drummond, and Andrew Rambaut. Bayesian phylogenetic and phylodynamic data integration using BEAST 1.10. *Virus Evolution*, 4(1):vey016, 2018. [doi:10.1093/ve/vey016](https://doi.org/10.1093/ve/vey016).
43. Sung-Oui Suh and Meredith Blackwell. Molecular phylogeny of the cleistothecial fungi placed in Cephalothecaceae and Pseudeurotiaceae. *Mycologia*, 91(5):836–848, 1999. [doi:10.1080/00275514.1999.12061089](https://doi.org/10.1080/00275514.1999.12061089).

44. Gergely J. Szöllösi, Wojciech Rosikiewicz, Bastien Boussau, Eric Tannier, and Vincent Daubin. Efficient exploration of the space of reconciled gene trees. *Systematic Biology*, 62(6):901–912, 2013. doi:10.1093/sysbio/syt054.
45. H.J.C. Berendsen T.P. Straatsma and A.J. Stam. Estimation of statistical errors in molecular simulation calculations. *Molecular Physics*, 57(1):89–95, 1986. doi:10.1080/00268978600100071.
46. Laurens Van der Maaten and Geoffrey Hinton. Visualizing data using t-sne. *Journal of Machine Learning Research*, 9(11), 2008.
47. Dootika Vats and Christina Knudson. Revisiting the Gelman–Rubin Diagnostic. *Statistical Science*, 36(4):518–529, 2021. doi:10.1214/20-STS812.
48. Larry Wasserman. Bayesian model selection and model averaging. *Journal of mathematical psychology*, 44(1):92–107, 2000. doi:10.1006/jmps.1999.1278.
49. Ziheng Yang and Carlos E Rodríguez. Searching for efficient markov chain monte carlo proposal kernels. *Proceedings of the National Academy of Sciences*, 110(48):19307–19312, 2013. doi:10.1073/pnas.1311790110.
50. Ziheng Yang and Anne D. Yoder. Comparison of likelihood and Bayesian methods for estimating divergence times using multiple gene loci and calibration points, with application to a radiation of cute-looking mouse lemur species. *Systematic Biology*, 52(5):705–716, 2003. doi:10.1080/10635150390235557.
51. Anne D. Yoder and Ziheng Yang. Divergence dates for Malagasy lemurs estimated from multiple gene loci: geological and evolutionary context. *Molecular Ecology*, 13(4):757–773, 2004. doi:10.1046/j.1365-294X.2004.02106.x.
52. Cheng Zhang and Frederick A Matsen IV. Generalizing tree probability estimation via Bayesian networks. In S. Bengio, H. Wallach, H. Larochelle, K. Grauman, N. Cesa-Bianchi, and R. Garnett, editors, *Advances in Neural Information Processing Systems*, volume 31, pages 1444–1453, 2018.
53. Cheng Zhang and Frederick A Matsen IV. Variational Bayesian phylogenetic inference. In *International Conference on Learning Representations (ICLR)*, 2018.
54. Ning Zhang and Meredith Blackwell. Molecular phylogeny of dogwood anthracnose fungus (*Discula destructiva*) and the Diaporthales. *Mycologia*, 93(2):355–365, 2001. doi:10.1080/00275514.2001.12063167.

Supplementary Material

We provide additional results on the autocorrelation signatures in [Section A](#), on estimator accuracy in [Section B](#), on their stability in [Section C](#), and on their robustness in [Section D](#) as well as on the modality analysis ([Section E](#)) and trace plots ([Section F](#)).

A Autocorrelation Signature

In addition to the autocorrelation signature plot for DS4 with a target ACT of 25 shown in [Fig. 2](#), we include the corresponding autocorrelation signature plots for all datasets DS1–11 in [Figs. 11 to 21](#).

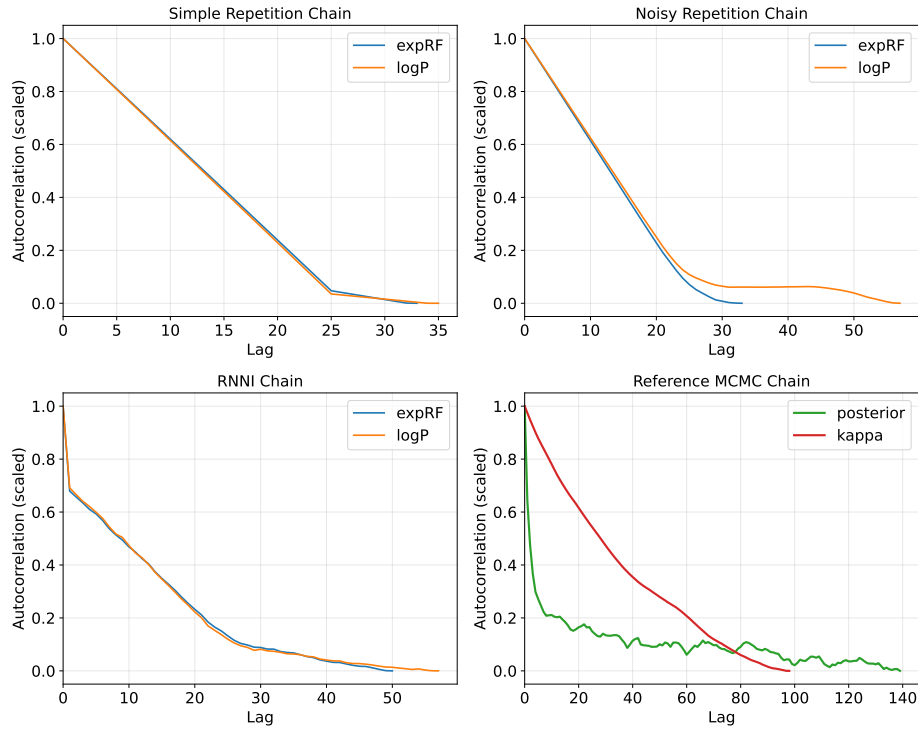


Fig. 11: For DS1, scaled autocorrelation signatures of `logP1` and `expRF1` traces for the three chain simulation methods with a target ACT= 25 and of the posterior (density) and κ (transition/transversion rate ratio) for the corresponding MCMC chain.

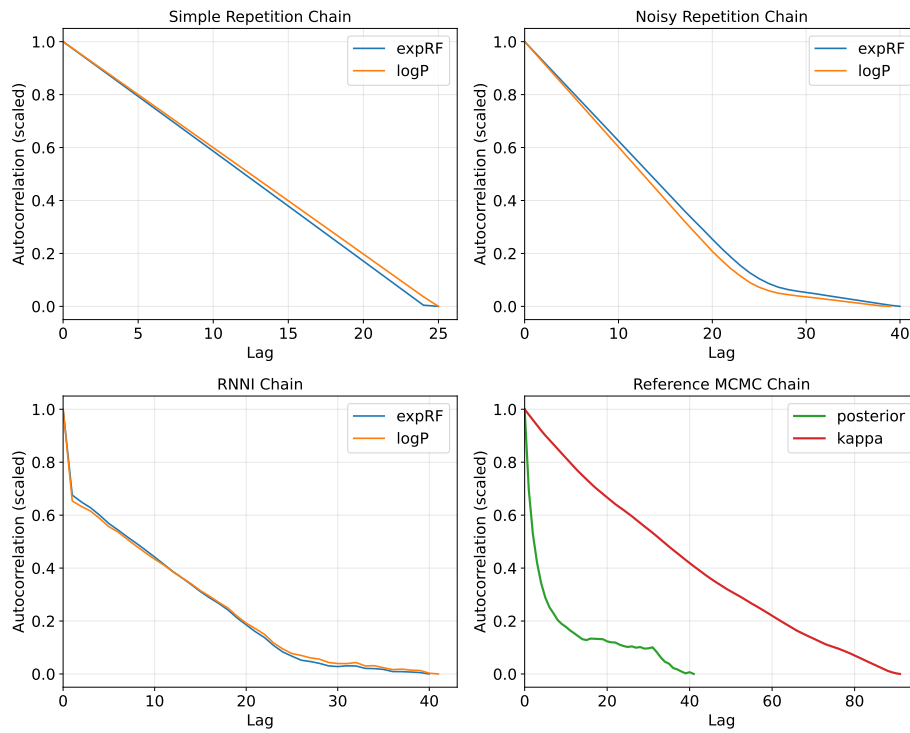


Fig. 12: For DS2, scaled autocorrelation signatures of `logP1` and `expRF1` traces for the three chain simulation methods with a target ACT= 25 and of the posterior (density) and κ (transition/transversion rate ratio) for the corresponding MCMC chain.

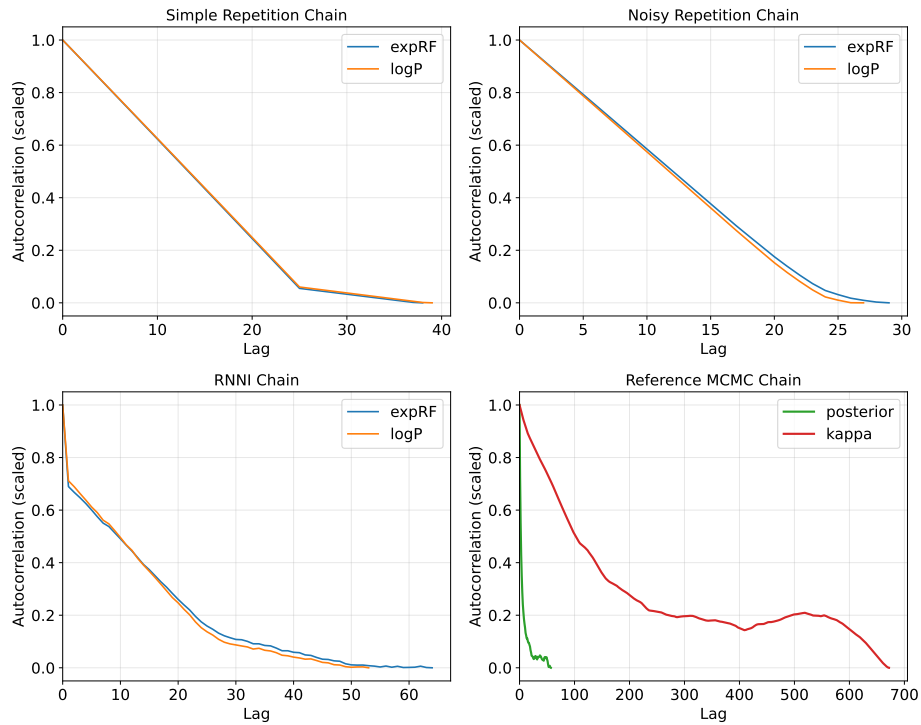


Fig. 13: For DS3, scaled autocorrelation signatures of $\log P_1$ and expRF_1 traces for the three chain simulation methods with a target $\text{ACT} = 25$ and of the posterior (density) and κ (transition/transversion rate ratio) for the corresponding MCMC chain.

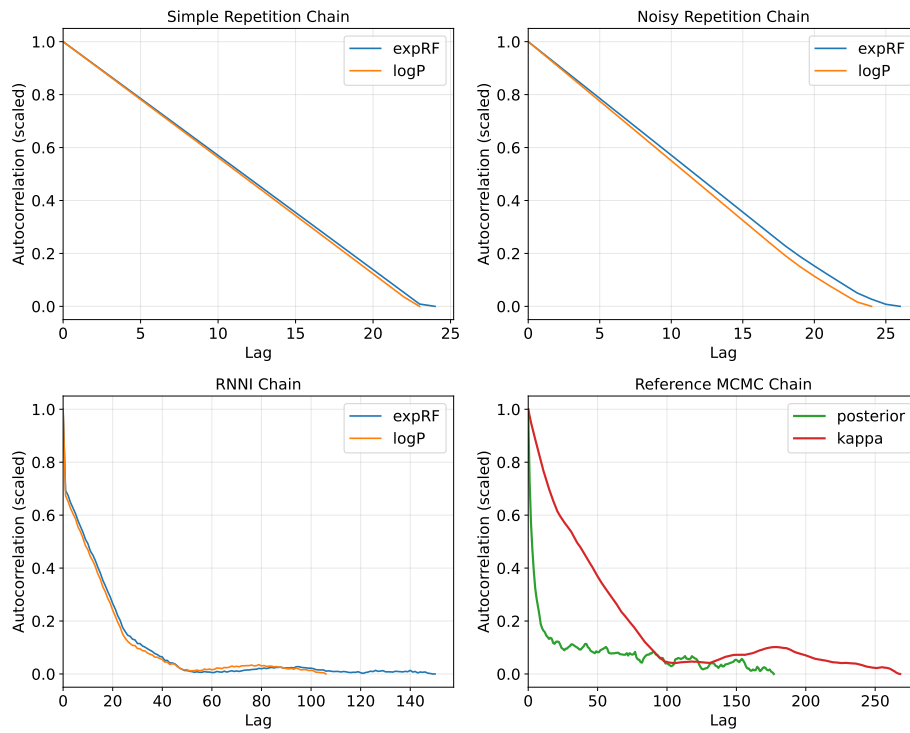


Fig. 14: For DS4, scaled autocorrelation signatures of $\log P_1$ and expRF_1 traces for the three chain simulation methods with a target $\text{ACT} = 25$ and of the posterior (density) and κ (transition/transversion rate ratio) for the corresponding MCMC chain.

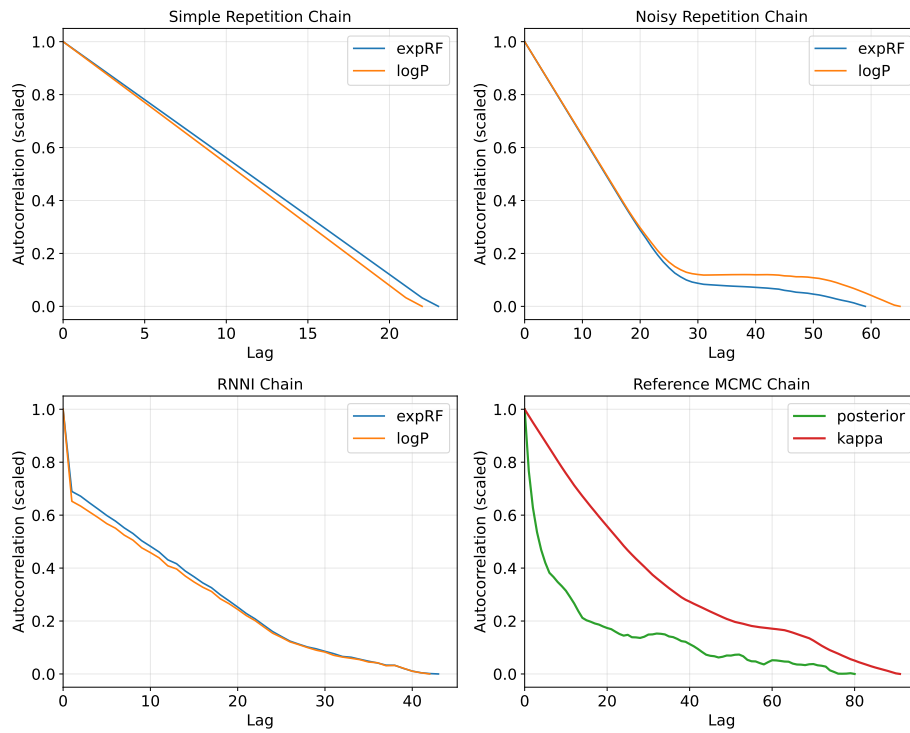


Fig. 15: For DS5, scaled autocorrelation signatures of $\log P_1$ and expRF_1 traces for the three chain simulation methods with a target $\text{ACT} = 25$ and of the posterior (density) and κ (transition/transversion rate ratio) for the corresponding MCMC chain.

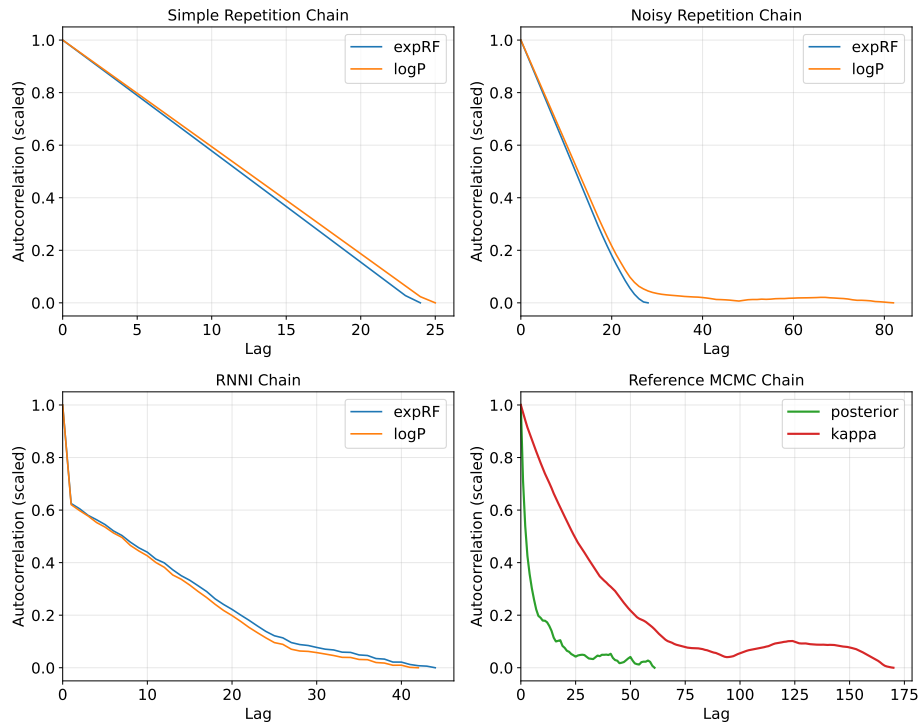


Fig. 16: For DS6, scaled autocorrelation signatures of $\log P_1$ and expRF_1 traces for the three chain simulation methods with a target $\text{ACT} = 25$ and of the posterior (density) and κ (transition/transversion rate ratio) for the corresponding MCMC chain.

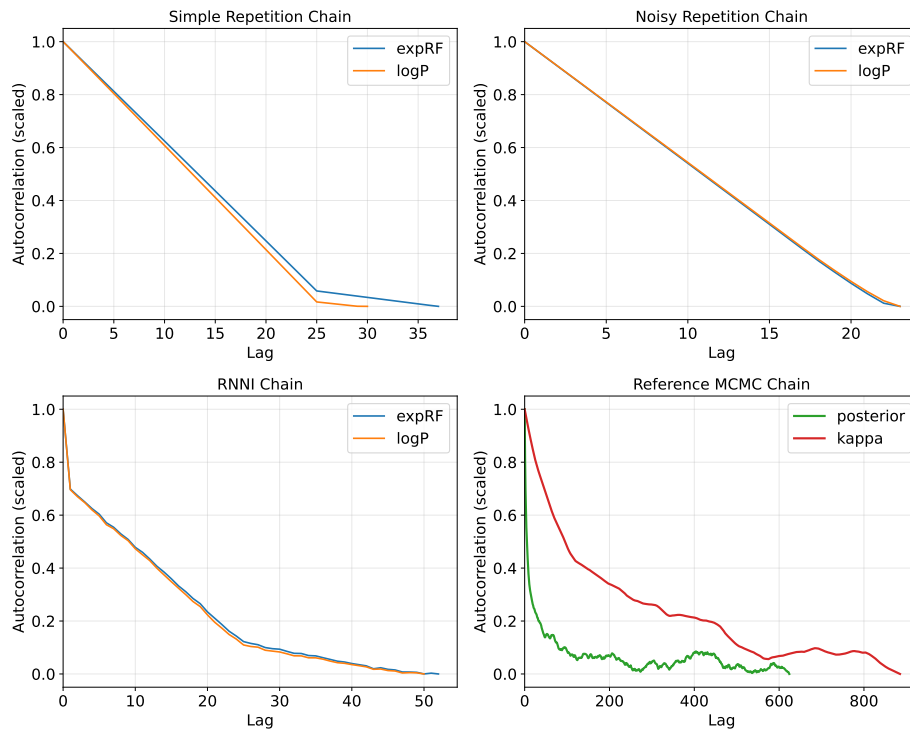


Fig. 17: For DS7, scaled autocorrelation signatures of `logP1` and `expRF1` traces for the three chain simulation methods with a target $ACT=25$ and of the posterior (density) and κ (transition/transversion rate ratio) for the corresponding MCMC chain.

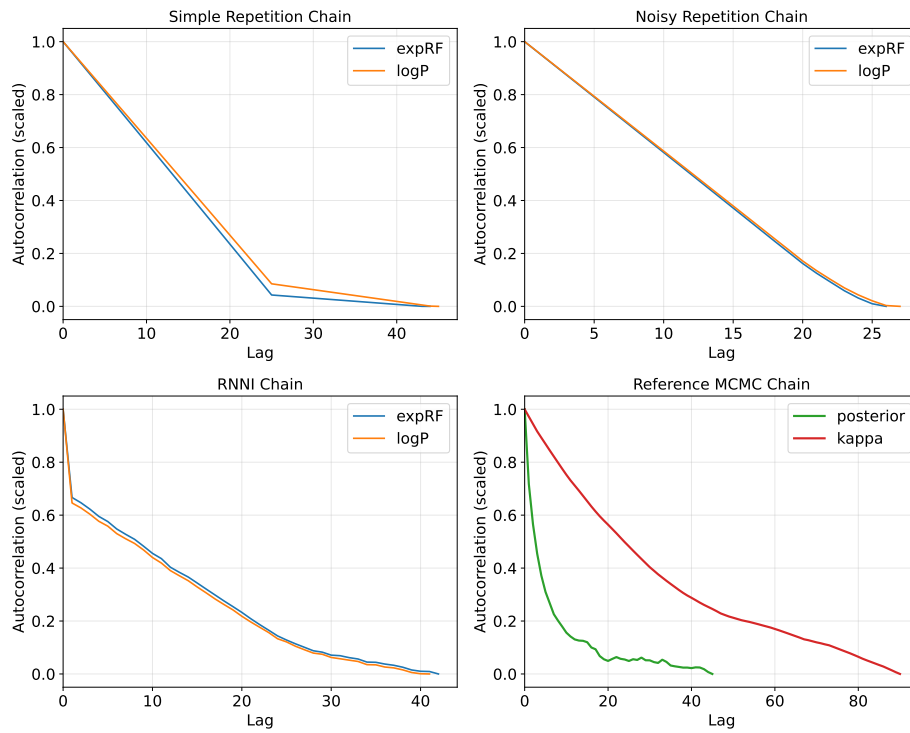


Fig. 18: For DS8, scaled autocorrelation signatures of `logP1` and `expRF1` traces for the three chain simulation methods with a target ACT= 25 and of the posterior (density) and κ (transition/transversion rate ratio) for the corresponding MCMC chain.

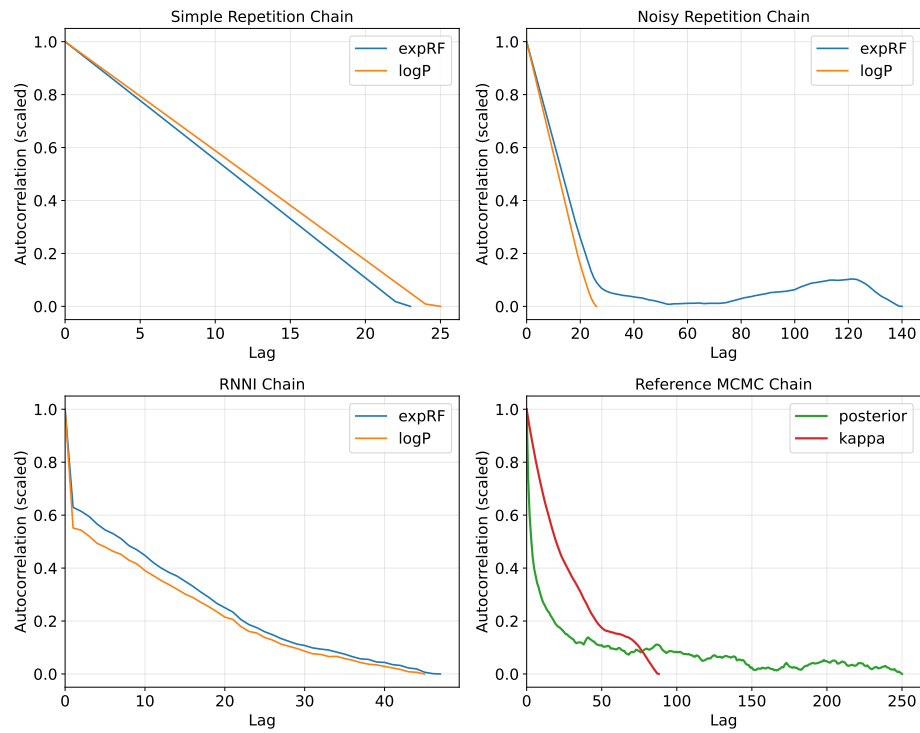


Fig. 19: For DS9, scaled autocorrelation signatures of `logP1` and `expRF1` traces for the three chain simulation methods with a target $ACT=25$ and of the posterior (density) and κ (transition/transversion rate ratio) for the corresponding MCMC chain.

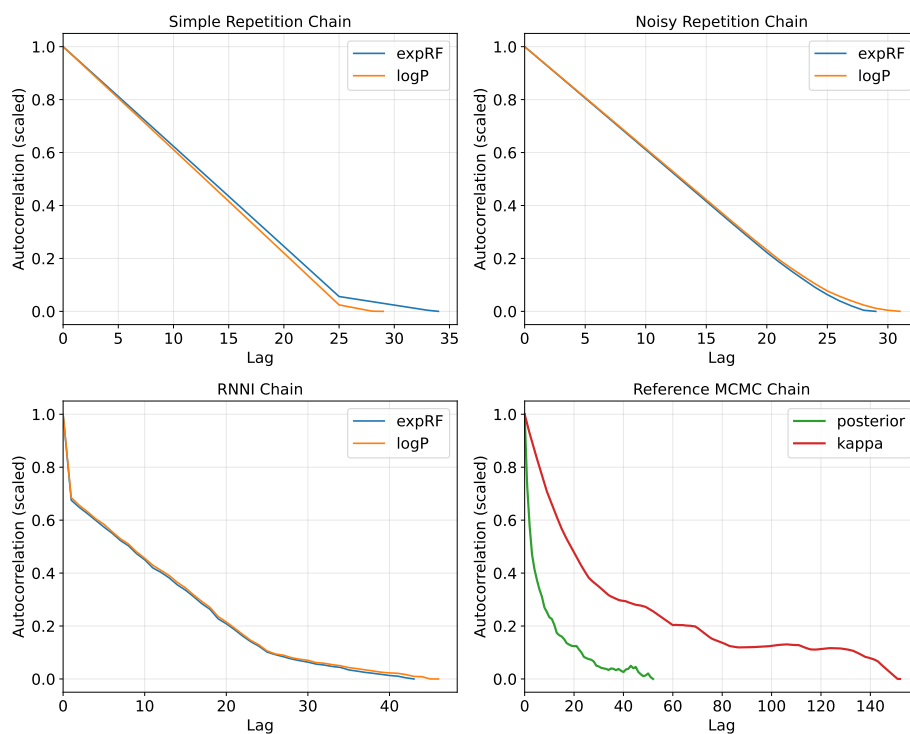


Fig. 20: For DS10, scaled autocorrelation signatures of `logP1` and `expRF1` traces for the three chain simulation methods with a target ACT= 25 and of the posterior (density) and κ (transition/transversion rate ratio) for the corresponding MCMC chain.

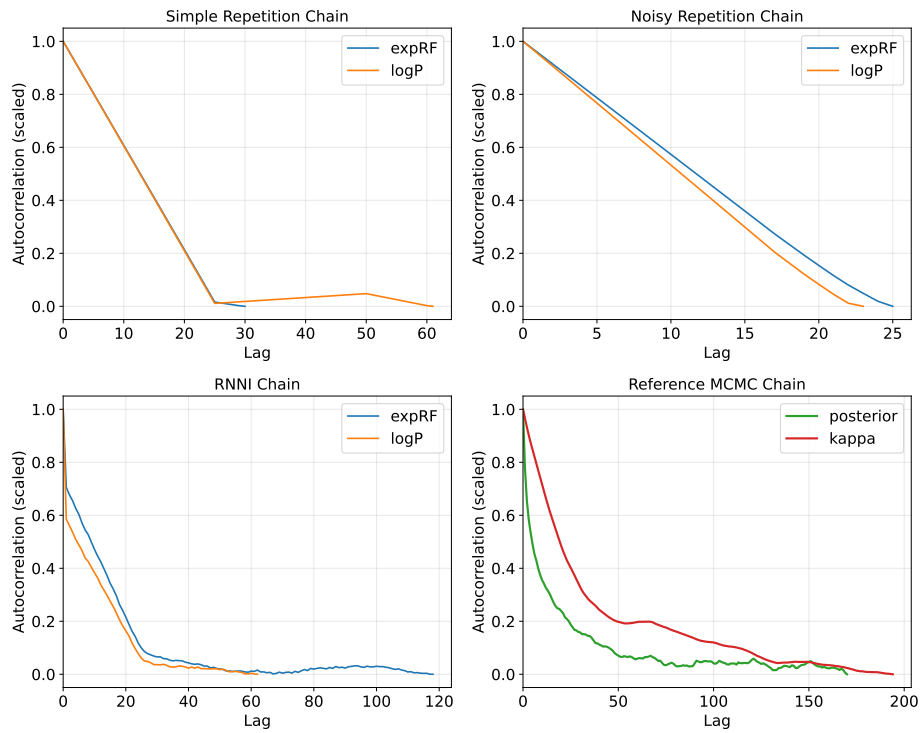


Fig. 21: For DS11, scaled autocorrelation signatures of $\log P_1$ and expRF_1 traces for the three chain simulation methods with a target $\text{ACT} = 25$ and of the posterior (density) and κ (transition/transversion rate ratio) for the corresponding MCMC chain.

B Accuracy

Here we provide additional plots on the accuracy experiments in Section 3.2.

B.1 Relative Accuracy

In addition to the plots for DS3 and DS4 in Fig. 4, we show here the relative accuracy plots (including the EDSF estimators) for DS1–11 and a target ACT of 5 in Figs. 22 to 32

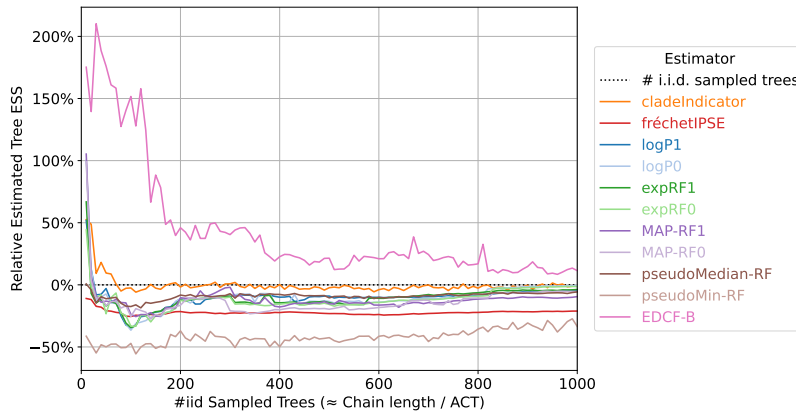


Fig. 22: Relative estimated tree ESS by different estimators for DS1 with respect to lower bound on the ESS of the simulated RNNI chains with target ACT 5.

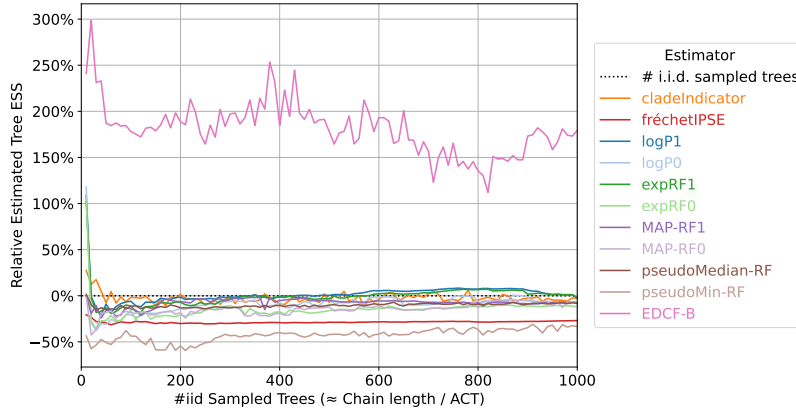


Fig. 23: Relative estimated tree ESS by different estimators for DS2 with respect to lower bound on the ESS of the simulated RNNI chains with target ACT 5.

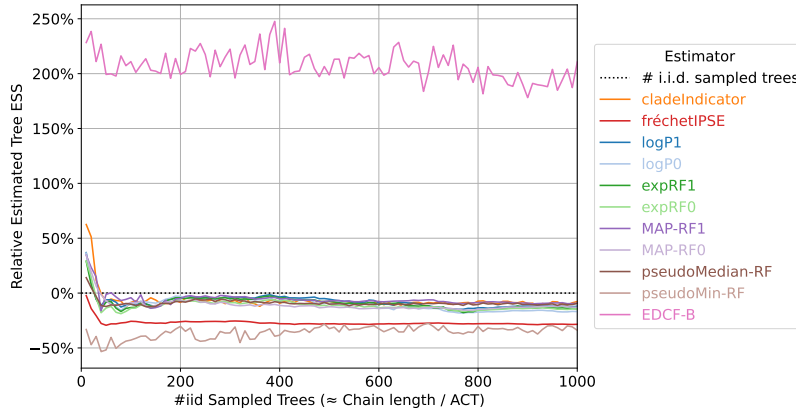


Fig. 24: Relative estimated tree ESS by different estimators for DS3 with respect to lower bound on the ESS of the simulated RNNI chains with target ACT 5.

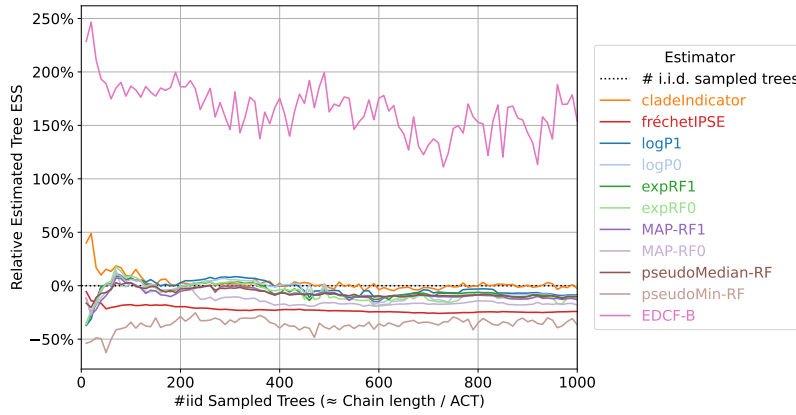


Fig. 25: Relative estimated tree ESS by different estimators for DS4 with respect to lower bound on the ESS of the simulated RNNI chains with target ACT 5.

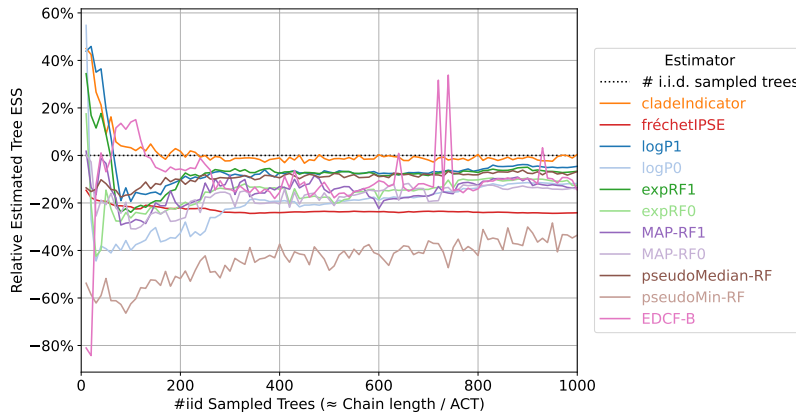


Fig. 26: Relative estimated tree ESS by different estimators for DS5 with respect to lower bound on the ESS of the simulated RNNI chains with target ACT 5.

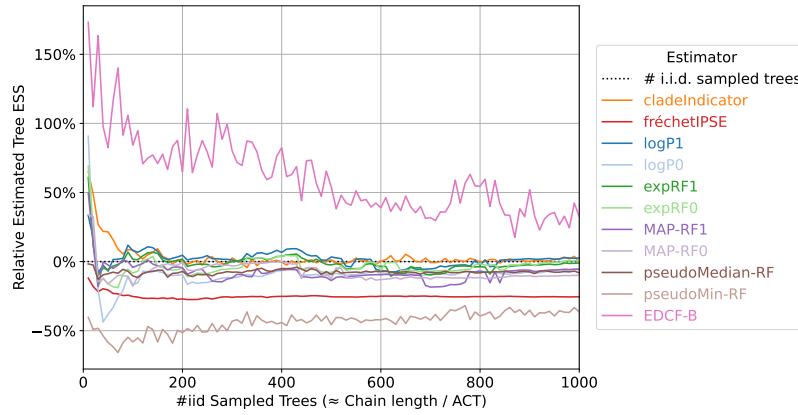


Fig. 27: Relative estimated tree ESS by different estimators for DS6 with respect to lower bound on the ESS of the simulated RNNI chains with target ACT 5.

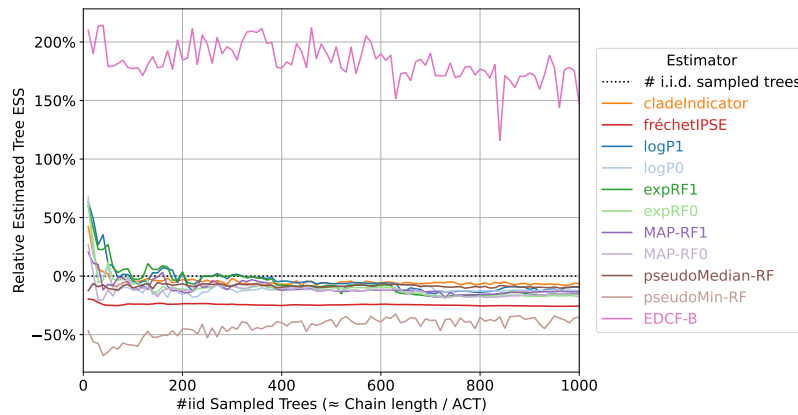


Fig. 28: Relative estimated tree ESS by different estimators for DS7 with respect to lower bound on the ESS of the simulated RNNI chains with target ACT 5.

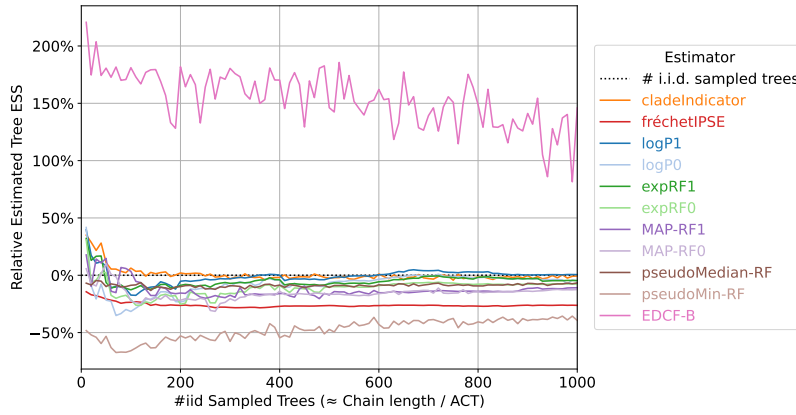


Fig. 29: Relative estimated tree ESS by different estimators for DS8 with respect to lower bound on the ESS of the simulated RNNI chains with target ACT 5.

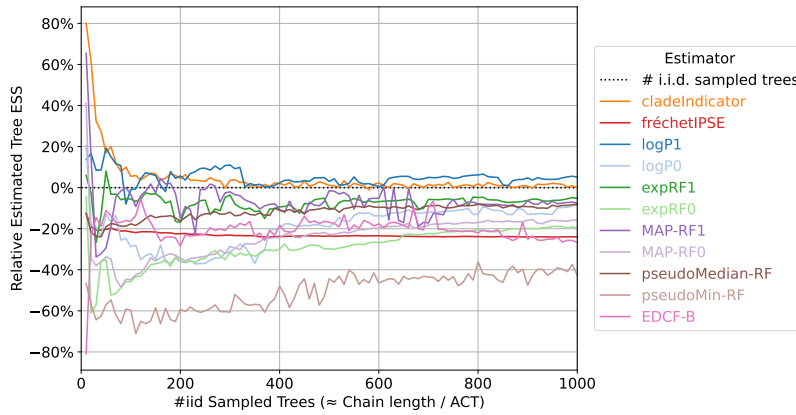


Fig. 30: Relative estimated tree ESS by different estimators for DS9 with respect to lower bound on the ESS of the simulated RNNI chains with target ACT 5.

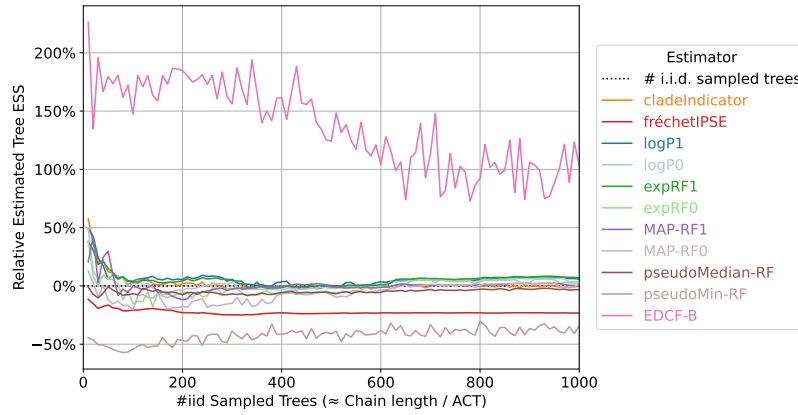


Fig. 31: Relative estimated tree ESS by different estimators for DS10 with respect to lower bound on the ESS of the simulated RNNI chains with target ACT 5.

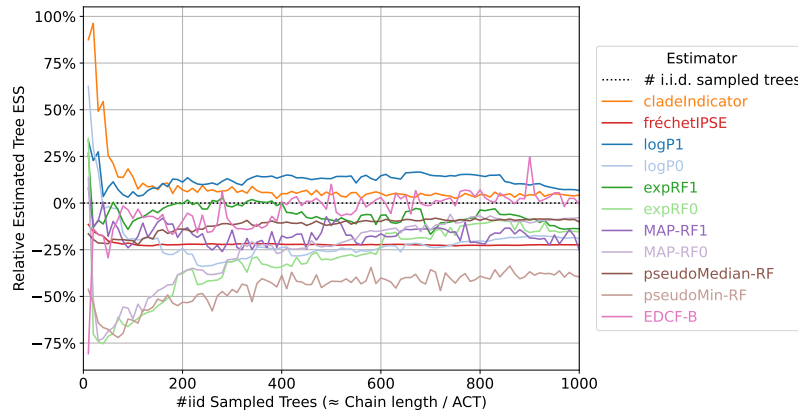


Fig. 32: Relative estimated tree ESS by different estimators for DS11 with respect to lower bound on the ESS of the simulated RNNI chains with target ACT 5.

B.2 Accuracy Summaries

In Figs. 33 and 34 we provide summary plots of the estimator accuracy across different target ACTs and DS1–11 as well as the Yule datasets. Note that some estimators are only shown for small ACTs due to their computational cost.

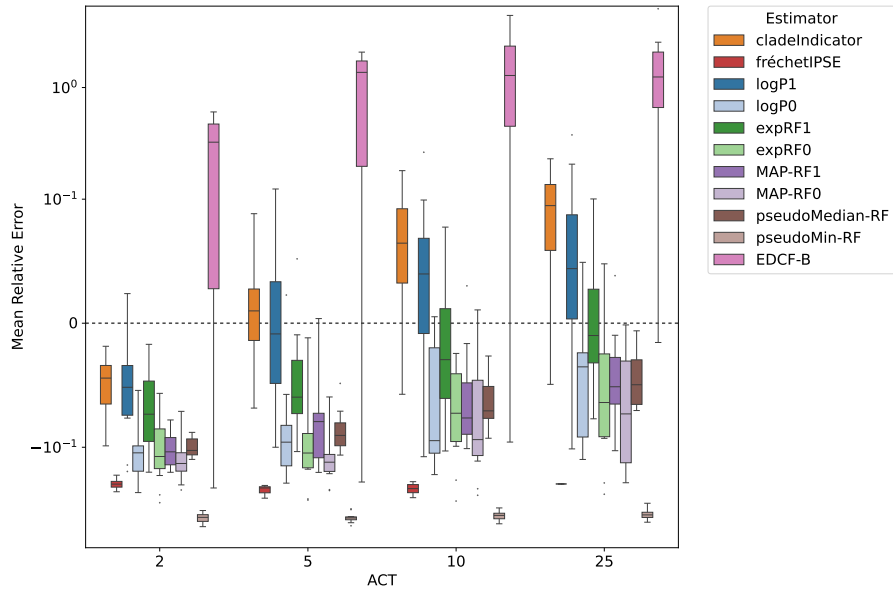


Fig. 33: Summary of estimator accuracy on simulated RNNI chains for the 11 real datasets.

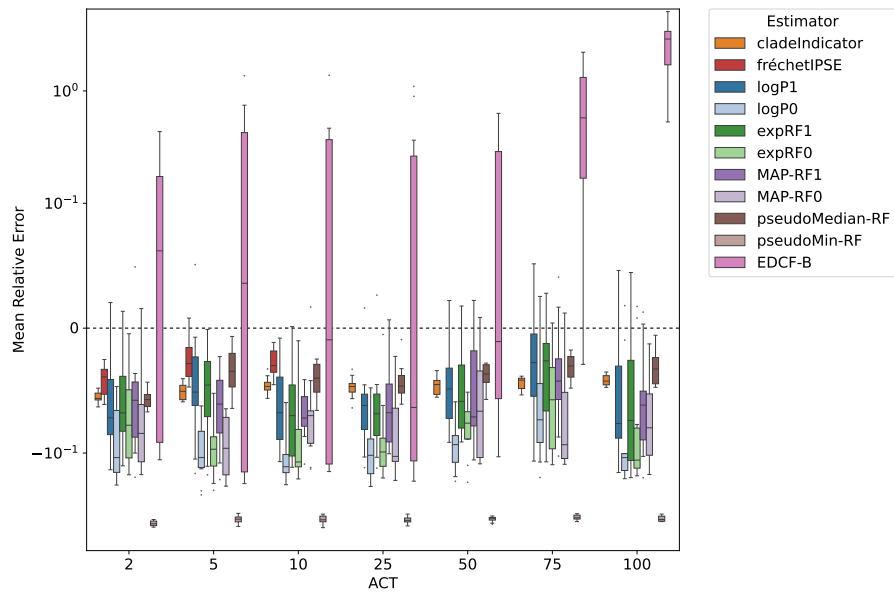


Fig. 34: Summary of estimator accuracy on simulated Noisy chains for the 10 Yule simulations.

C Stability

Here we provide additional plots on the stability experiment in [Section 3.3](#), where we started with oversampled versions of DS1–11 and then sequentially thinned out the tree sets. The plots shown in [Figs. 35 to 45](#) also include additional tree ESS estimators.

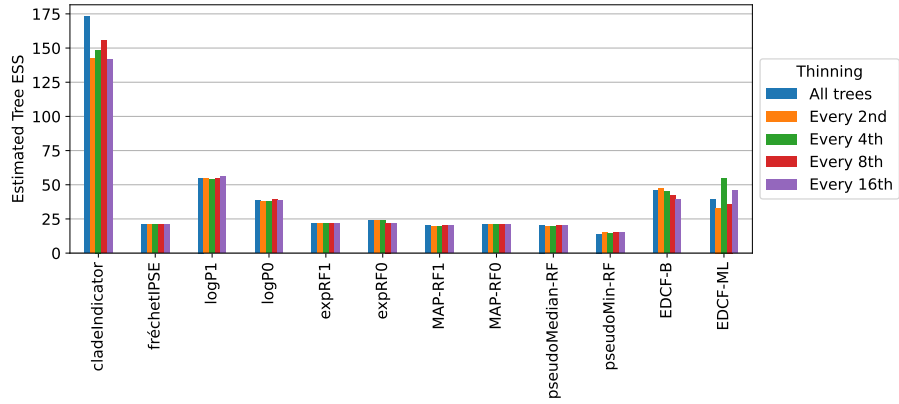


Fig. 35: Tree ESS estimates for the oversampled DS1 under different thinning intervals as per our stability experiment.

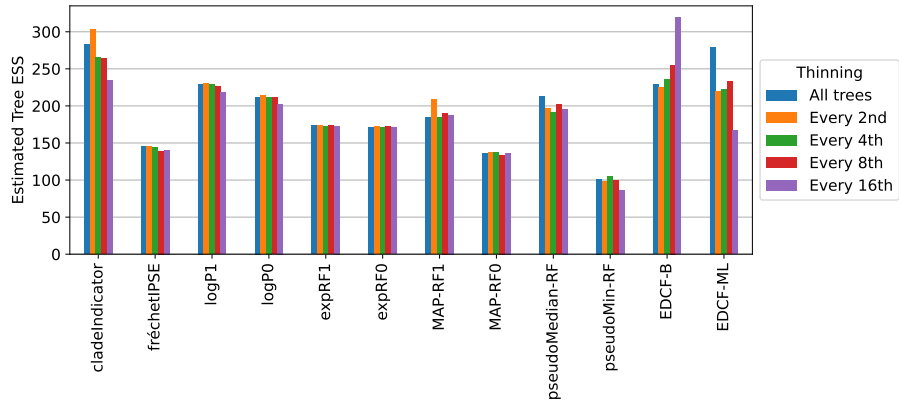


Fig. 36: Tree ESS estimates for the oversampled DS2 under different thinning intervals as per our stability experiment.

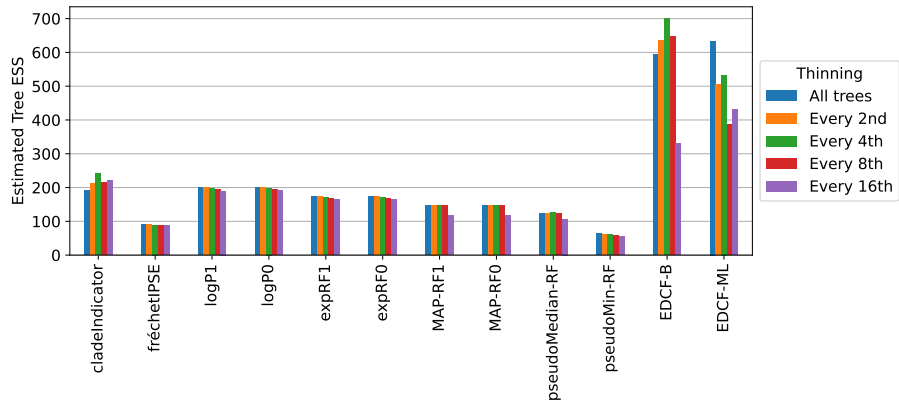


Fig. 37: Tree ESS estimates for the oversampled DS3 under different thinning intervals as per our stability experiment.

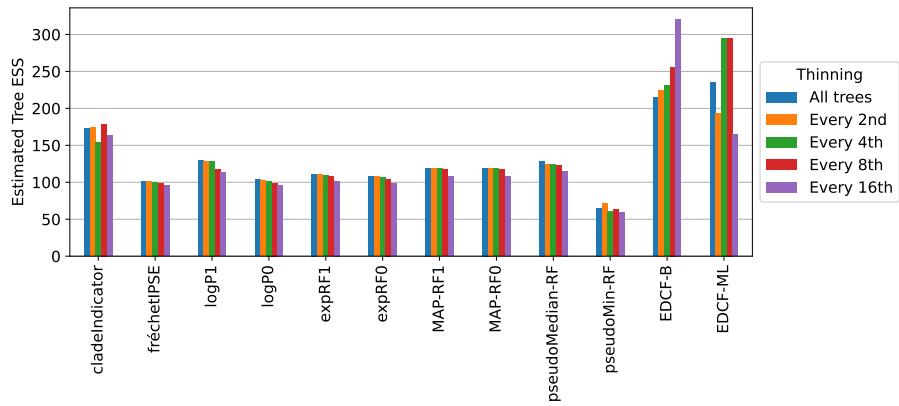


Fig. 38: Tree ESS estimates for the oversampled DS4 under different thinning intervals as per our stability experiment.

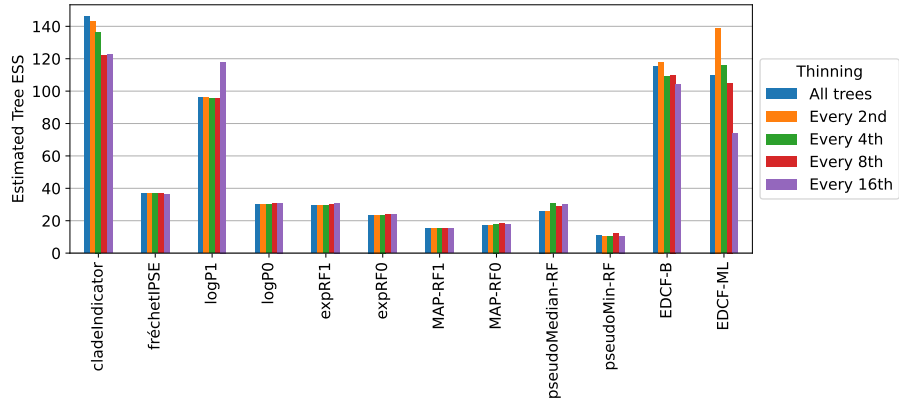


Fig. 39: Tree ESS estimates for the oversampled DS5 under different thinning intervals as per our stability experiment.

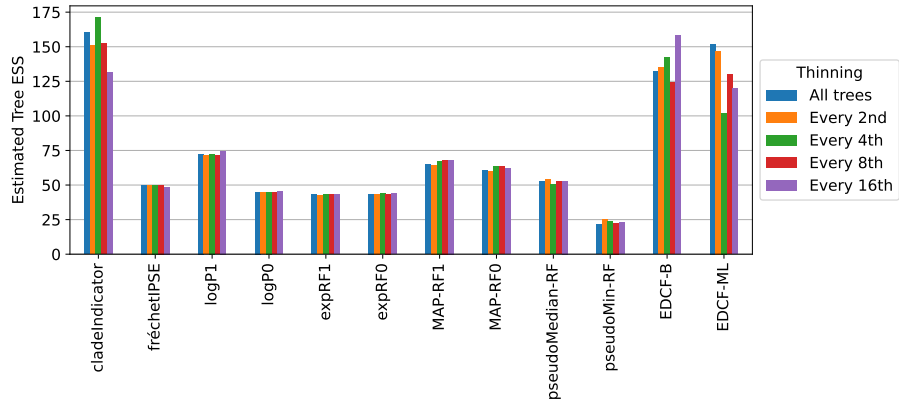


Fig. 40: Tree ESS estimates for the oversampled DS6 under different thinning intervals as per our stability experiment.

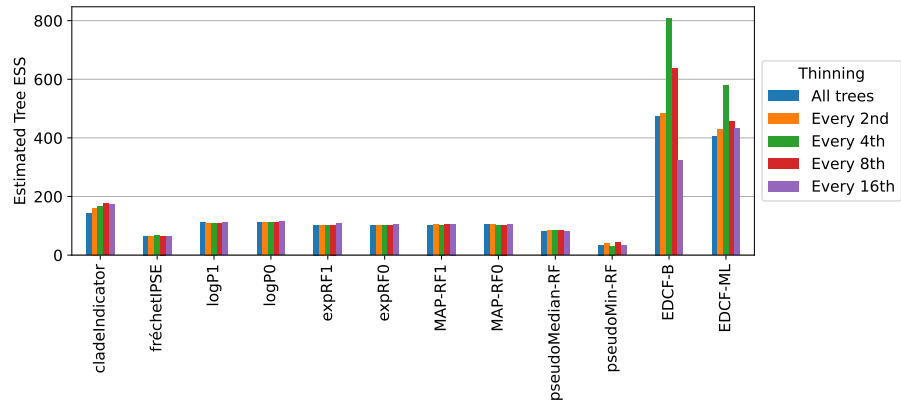


Fig. 41: Tree ESS estimates for the oversampled DS7 under different thinning intervals as per our stability experiment.

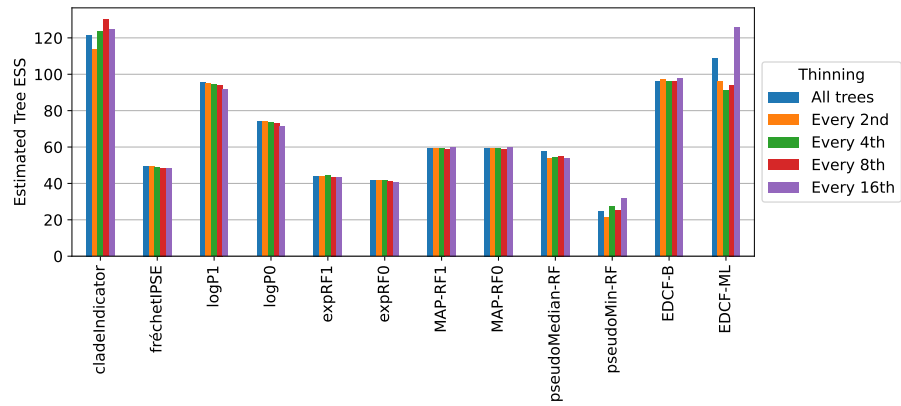


Fig. 42: Tree ESS estimates for the oversampled DS8 under different thinning intervals as per our stability experiment.

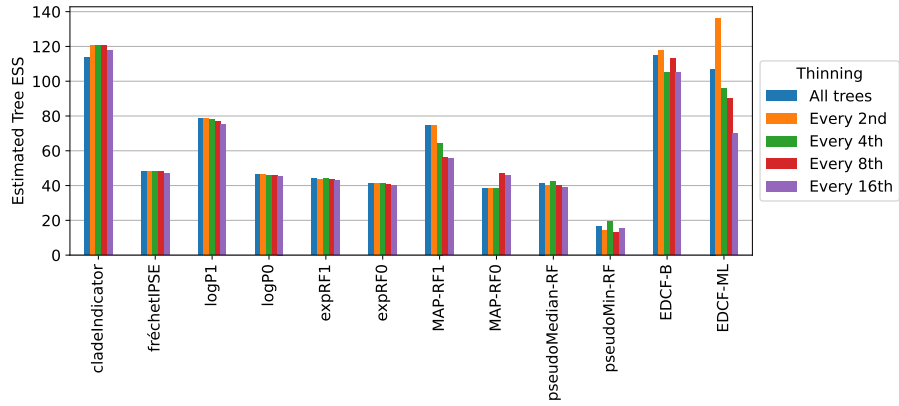


Fig. 43: Tree ESS estimates for the oversampled DS9 under different thinning intervals as per our stability experiment.

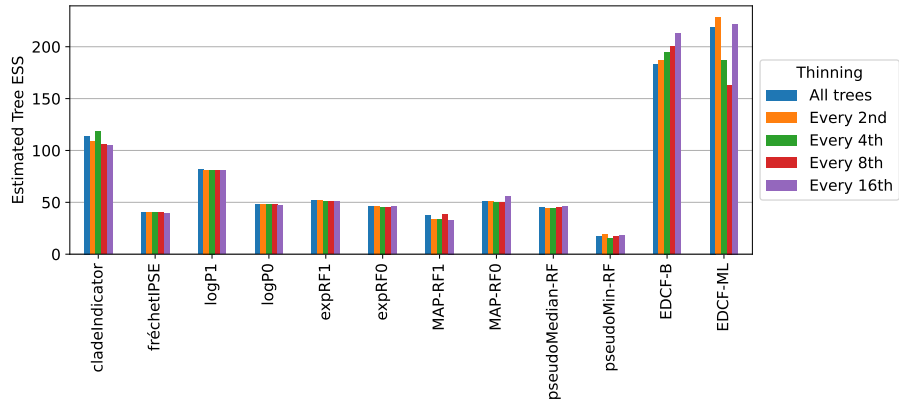


Fig. 44: Tree ESS estimates for the oversampled DS10 under different thinning intervals as per our stability experiment.

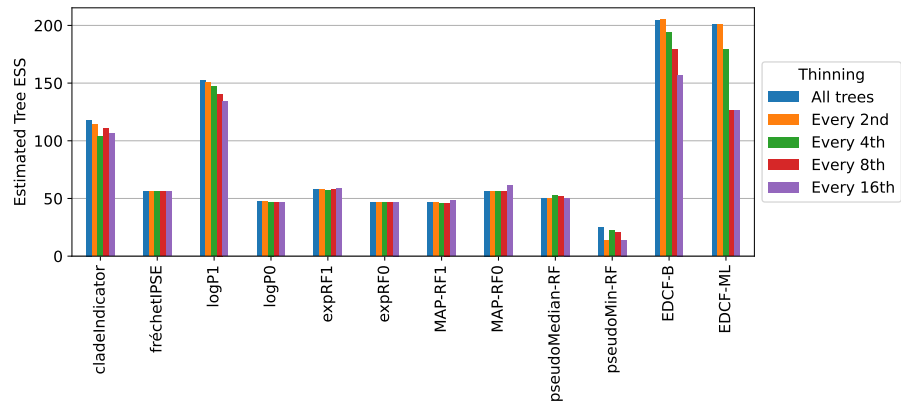


Fig. 45: Tree ESS estimates for the oversampled DS11 under different thinning intervals as per our stability experiment.

D Robustness

In Figs. 46 to 56, we provide additional plots on the robustness experiments in Section 3.4 that include more tree ESS estimators.

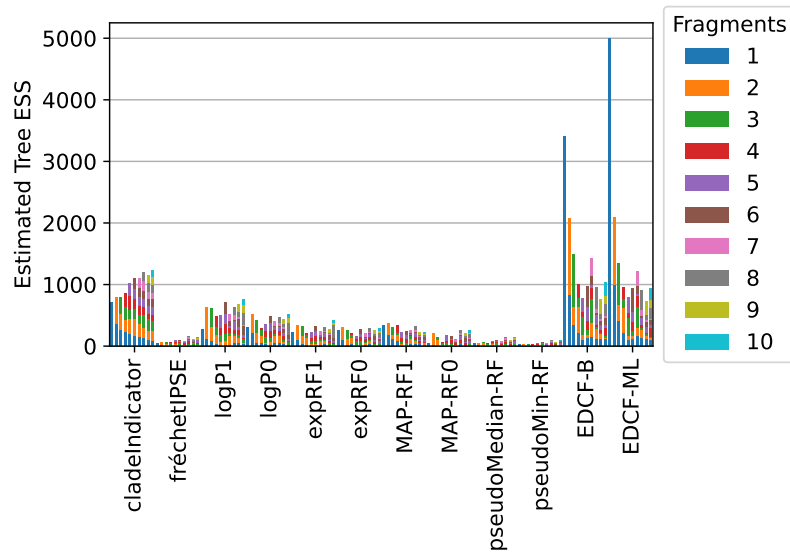


Fig. 46: Robustness of ESS estimators under different chain fragmentations for DS1 with 10k trees.

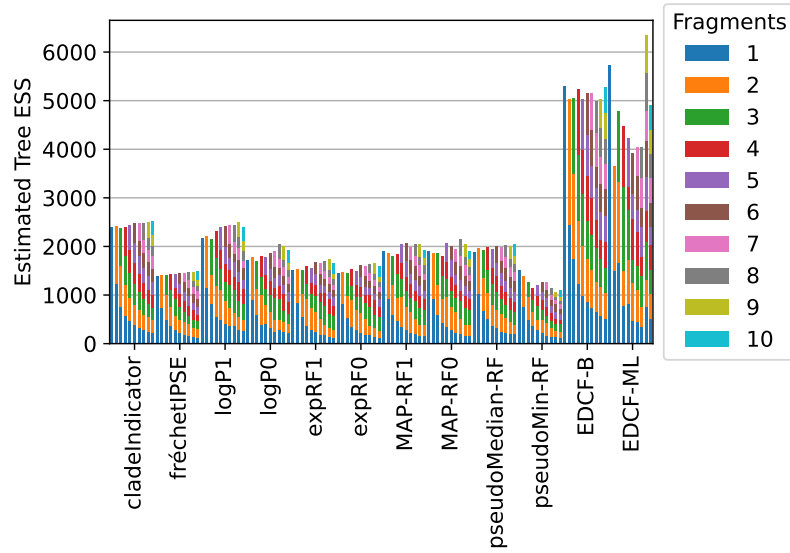


Fig. 47: Robustness of ESS estimators under different chain fragmentations for DS2 with 10k trees.

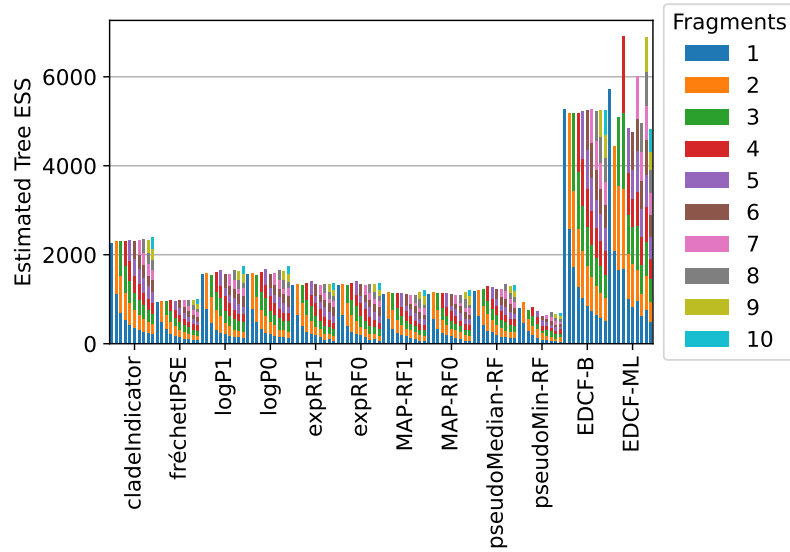


Fig. 48: Robustness of ESS estimators under different chain fragmentations for DS3 with 10k trees.

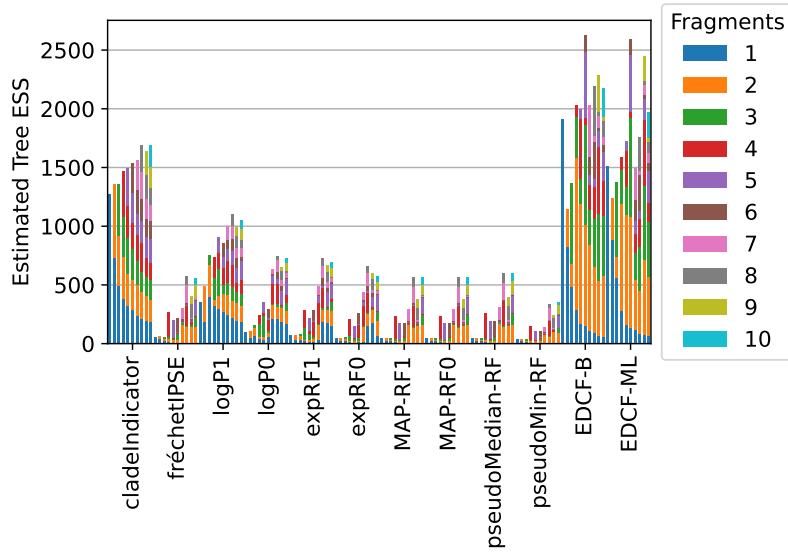


Fig. 49: Robustness of ESS estimators under different chain fragmentations for DS4 with 10k trees.

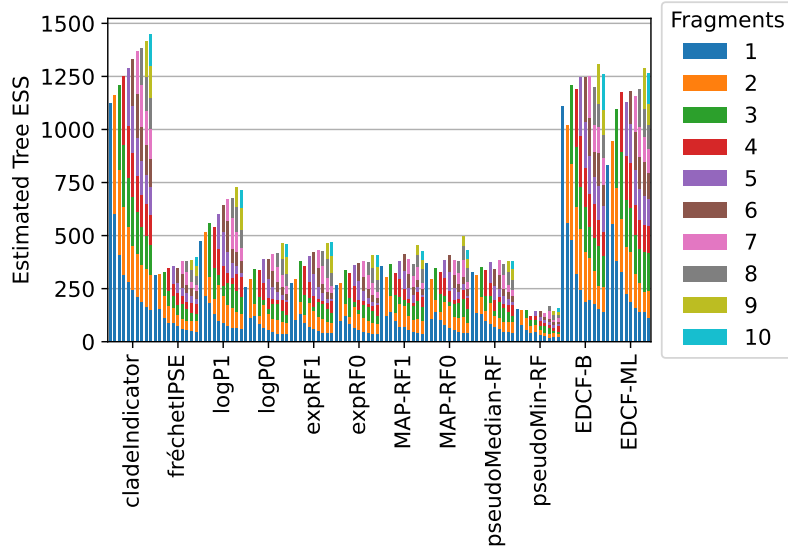


Fig. 50: Robustness of ESS estimators under different chain fragmentations for DS5 with 10k trees.

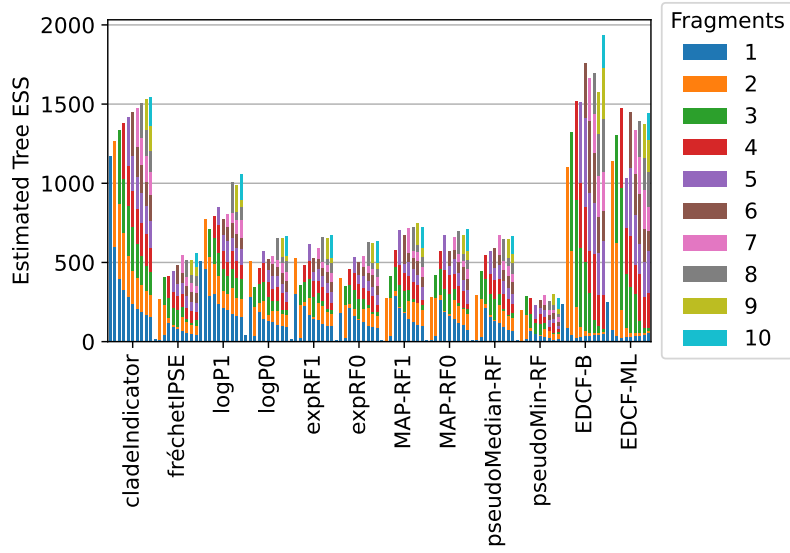


Fig. 51: Robustness of ESS estimators under different chain fragmentations for DS6 with 10k trees.

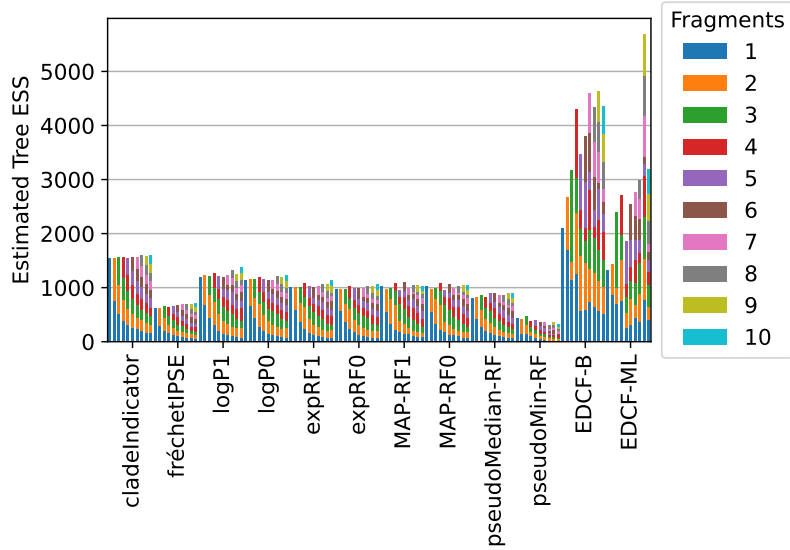


Fig. 52: Robustness of ESS estimators under different chain fragmentations for DS7 with 10k trees.

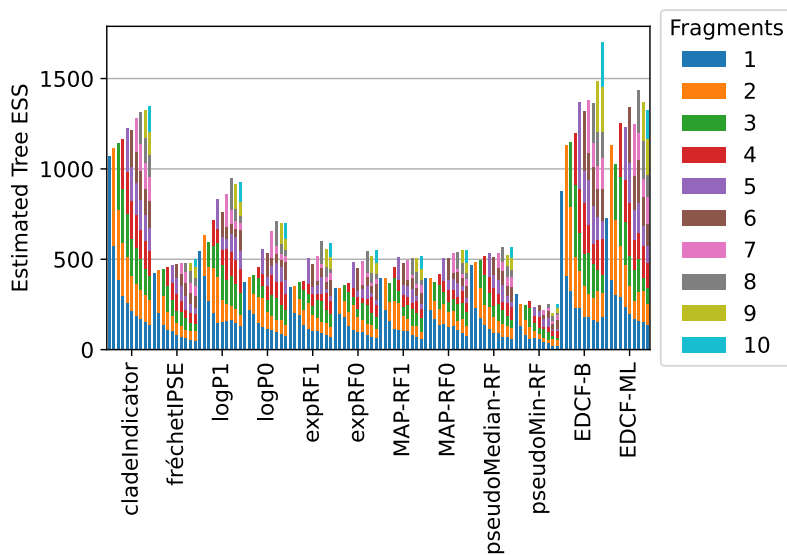


Fig. 53: Robustness of ESS estimators under different chain fragmentations for DS8 with 10k trees.

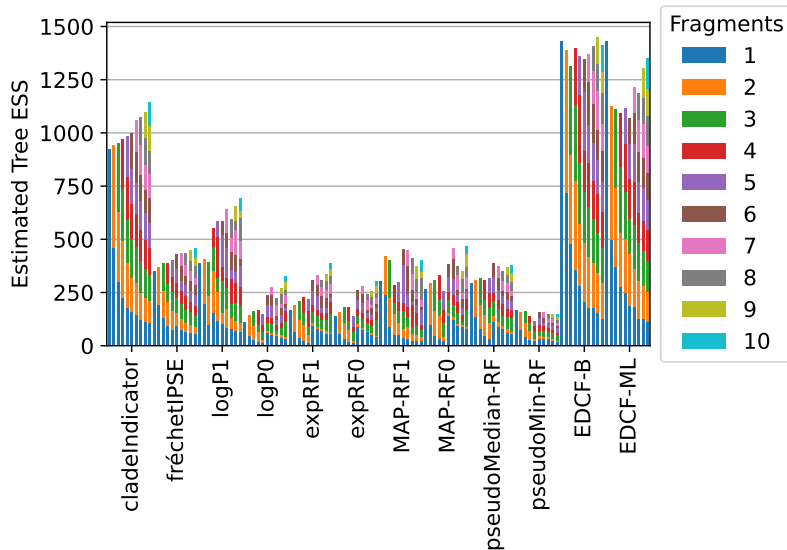


Fig. 54: Robustness of ESS estimators under different chain fragmentations for DS9 with 10k trees.

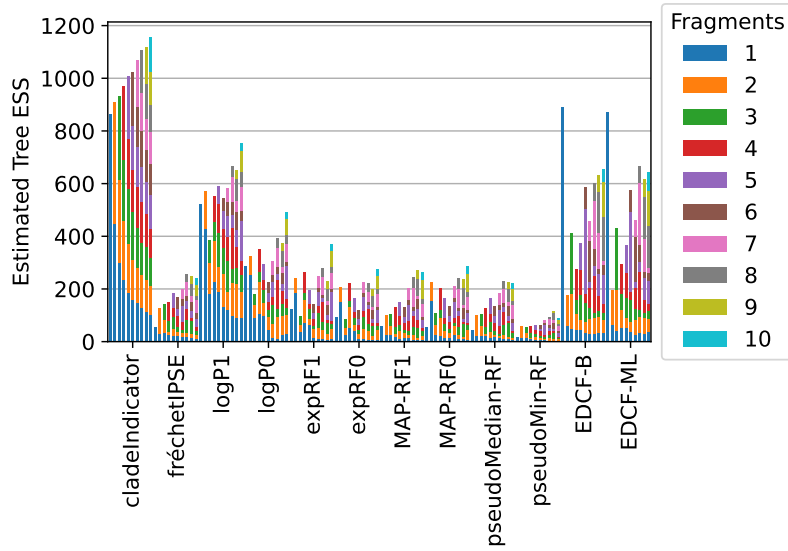


Fig. 55: Robustness of ESS estimators under different chain fragmentations for DS10 with 10k trees.

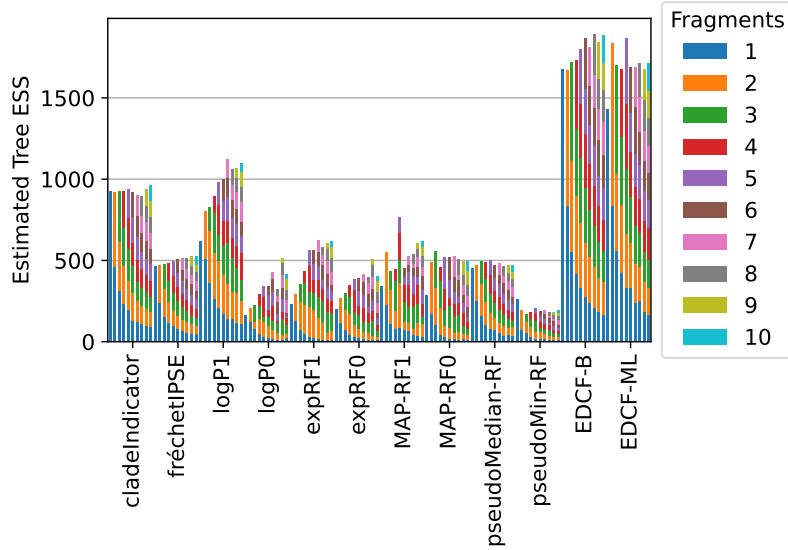


Fig. 56: Robustness of ESS estimators under different chain fragmentations for DS11 with 10k trees.

D.1 Summarizing Robustness

In Tables 4 and 5, we provide summary tables of the robustness experiments that contain all the estimators for the DS1–11 and Yule datasets.

Table 4: Robustness of ESS estimates across 11 datasets (10,000 trees), with lower values indicating more robust performance.

	1	2	3	4	5	6	7	8	9	10	11
cladeIndicator	0.18 ± 0.12	0.02 ± 0.02	0.02 ± 0.01	0.10 ± 0.06	0.09 ± 0.06	0.09 ± 0.06	0.01 ± 0.01	0.08 ± 0.05	0.08 ± 0.05	0.10 ± 0.06	0.02 ± 0.02
fréchetIPSE	0.27 ± 0.19	0.03 ± 0.02	0.02 ± 0.02	0.40 ± 0.27	0.09 ± 0.06	0.31 ± 0.28	0.05 ± 0.04	0.05 ± 0.04	0.09 ± 0.06	0.29 ± 0.19	0.05 ± 0.03
logP1	0.21 ± 0.16	0.06 ± 0.04	0.04 ± 0.03	0.26 ± 0.18	0.14 ± 0.09	0.18 ± 0.13	0.05 ± 0.04	0.19 ± 0.12	0.19 ± 0.13	0.15 ± 0.11	0.17 ± 0.12
logP0	0.18 ± 0.12	0.07 ± 0.04	0.04 ± 0.03	0.42 ± 0.28	0.18 ± 0.11	0.30 ± 0.27	0.03 ± 0.02	0.22 ± 0.14	0.26 ± 0.17	0.21 ± 0.14	0.25 ± 0.16
expRF1	0.19 ± 0.13	0.06 ± 0.04	0.02 ± 0.01	0.43 ± 0.29	0.16 ± 0.11	0.30 ± 0.29	0.04 ± 0.03	0.20 ± 0.13	0.23 ± 0.15	0.26 ± 0.17	0.27 ± 0.20
expRF0	0.18 ± 0.12	0.06 ± 0.04	0.02 ± 0.01	0.43 ± 0.29	0.14 ± 0.10	0.31 ± 0.27	0.03 ± 0.02	0.18 ± 0.12	0.24 ± 0.16	0.27 ± 0.19	0.20 ± 0.14
MAP-RF1	0.18 ± 0.12	0.06 ± 0.04	0.03 ± 0.02	0.41 ± 0.28	0.12 ± 0.08	0.35 ± 0.31	0.05 ± 0.03	0.12 ± 0.09	0.16 ± 0.11	0.33 ± 0.21	0.18 ± 0.13
MAP-RF0	0.33 ± 0.20	0.06 ± 0.04	0.03 ± 0.02	0.41 ± 0.28	0.13 ± 0.09	0.34 ± 0.30	0.05 ± 0.03	0.15 ± 0.11	0.19 ± 0.12	0.29 ± 0.20	0.12 ± 0.14
pseudoMedian-RF	0.28 ± 0.20	0.03 ± 0.02	0.04 ± 0.03	0.41 ± 0.28	0.08 ± 0.05	0.33 ± 0.30	0.04 ± 0.03	0.07 ± 0.04	0.11 ± 0.07	0.32 ± 0.21	0.03 ± 0.02
pseudoMin-RF	0.28 ± 0.23	0.10 ± 0.08	0.12 ± 0.08	0.39 ± 0.28	0.08 ± 0.06	0.27 ± 0.31	0.13 ± 0.09	0.10 ± 0.08	0.10 ± 0.08	0.27 ± 0.20	0.09 ± 0.10
EDCF-B	0.24 ± 0.24	0.03 ± 0.02	0.01 ± 0.00	0.18 ± 0.14	0.07 ± 0.06	0.26 ± 0.24	0.22 ± 0.15	0.15 ± 0.11	0.03 ± 0.02	0.28 ± 0.18	0.05 ± 0.03
EDCF-ML	0.22 ± 0.29	0.15 ± 0.11	0.15 ± 0.11	0.20 ± 0.14	0.12 ± 0.09	0.24 ± 0.26	0.23 ± 0.20	0.16 ± 0.13	0.10 ± 0.07	0.27 ± 0.18	0.06 ± 0.06

Table 5: Robustness of ESS estimates across 10 Yule datasets (10,000 trees), with lower values indicating more stable performance.

	1	2	3	4	5	6	7	8	9	10
cladeIndicator	0.00 ± 0.00	0.01 ± 0.00	0.01 ± 0.01	0.00 ± 0.00	0.00 ± 0.00	0.01 ± 0.01	0.01 ± 0.00	0.00 ± 0.00	0.00 ± 0.00	0.01 ± 0.00
fréchetIPSE	0.00 ± 0.00	0.00 ± 0.00	0.00 ± 0.00	0.00 ± 0.00	0.00 ± 0.00	0.02 ± 0.01	0.00 ± 0.00	0.00 ± 0.00	0.00 ± 0.00	0.01 ± 0.00
logP1	0.04 ± 0.03	0.02 ± 0.01	0.02 ± 0.01	0.01 ± 0.01	0.01 ± 0.01	0.02 ± 0.02	0.04 ± 0.03	0.02 ± 0.01	0.01 ± 0.01	0.04 ± 0.02
logP0	0.02 ± 0.02	0.01 ± 0.01	0.02 ± 0.01	0.01 ± 0.01	0.01 ± 0.01	0.03 ± 0.02	0.02 ± 0.01	0.03 ± 0.02	0.01 ± 0.01	0.02 ± 0.01
expRF1	0.02 ± 0.01	0.01 ± 0.01	0.02 ± 0.01	0.01 ± 0.01	0.01 ± 0.01	0.02 ± 0.02	0.04 ± 0.04	0.03 ± 0.02	0.01 ± 0.00	0.02 ± 0.02
expRF0	0.02 ± 0.01	0.01 ± 0.01	0.01 ± 0.01	0.01 ± 0.01	0.01 ± 0.01	0.03 ± 0.02	0.06 ± 0.05	0.02 ± 0.02	0.01 ± 0.01	0.01 ± 0.01
MAP-RF1	0.02 ± 0.01	0.01 ± 0.01	0.02 ± 0.02	0.04 ± 0.02	0.03 ± 0.02	0.02 ± 0.02	0.04 ± 0.03	0.04 ± 0.03	0.02 ± 0.02	0.02 ± 0.01
MAP-RF0	0.03 ± 0.02	0.03 ± 0.02	0.02 ± 0.02	0.03 ± 0.02	0.04 ± 0.03	0.04 ± 0.03	0.04 ± 0.03	0.04 ± 0.03	0.01 ± 0.01	0.02 ± 0.02
pseudoMedian-RF	0.01 ± 0.01	0.01 ± 0.01	0.01 ± 0.01	0.01 ± 0.01	0.01 ± 0.01	0.01 ± 0.01	0.01 ± 0.01	0.01 ± 0.00	0.01 ± 0.01	0.01 ± 0.01
pseudoMin-RF	0.10 ± 0.07	0.11 ± 0.08	0.10 ± 0.08	0.10 ± 0.06	0.07 ± 0.05	0.08 ± 0.05	0.09 ± 0.07	0.10 ± 0.07	0.10 ± 0.08	0.11 ± 0.07
EDCF-B	0.01 ± 0.01	0.06 ± 0.06	0.03 ± 0.04	0.09 ± 0.16	0.02 ± 0.02	0.03 ± 0.03	0.00 ± 0.00	0.11 ± 0.13	0.00 ± 0.00	0.10 ± 0.07
EDCF-ML	0.00 ± 0.00	0.03 ± 0.03	0.04 ± 0.04	0.03 ± 0.03	0.06 ± 0.05	0.11 ± 0.11	0.07 ± 0.07	0.04 ± 0.03	0.00 ± 0.01	0.11 ± 0.12

E MDS and Clustering

For both multidimensional scaling and clustering of posterior tree sets, we use methods implemented in scikit-learn [36].

To obtain low-dimensional embeddings, we apply t-distributed Stochastic Neighbour Embedding (t-SNE) to pairwise tree distance matrices. This method constructs a two-dimensional representation that preserves local neighbourhood structure, making it suitable for visualizing clustering and potential multimodality in treespace. As with all t-SNE embeddings, global geometric relationships should not be over-interpreted.

To cluster posterior tree sets, we employ spectral clustering. Distances are first converted into affinities using a heat kernel, after which clustering is performed on a low-dimensional embedding of the resulting graph Laplacian. This approach allows us to identify groups of similar trees based on their pairwise tree distances.

E.1 Figures

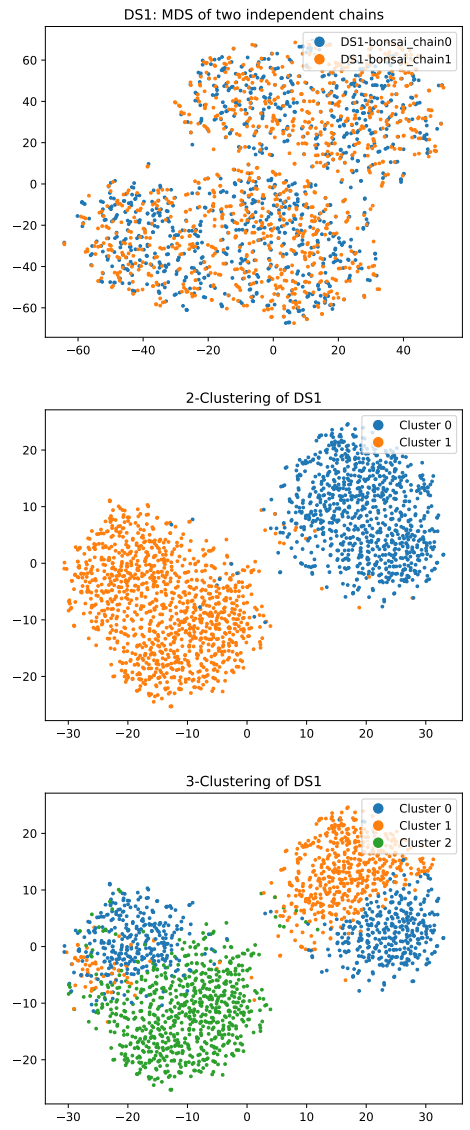


Fig. 57: MDS and clustering for dataset DS1.

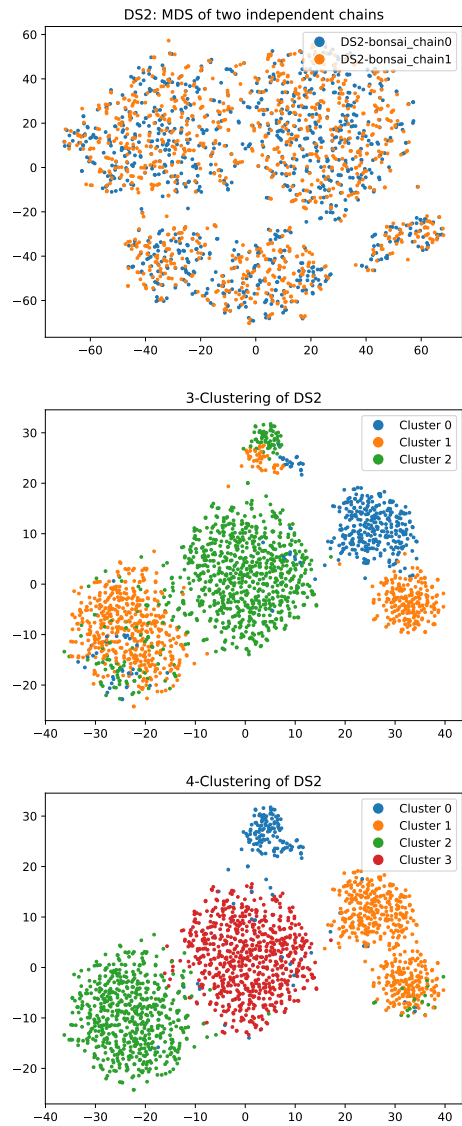


Fig. 58: MDS and clustering for dataset DS2.

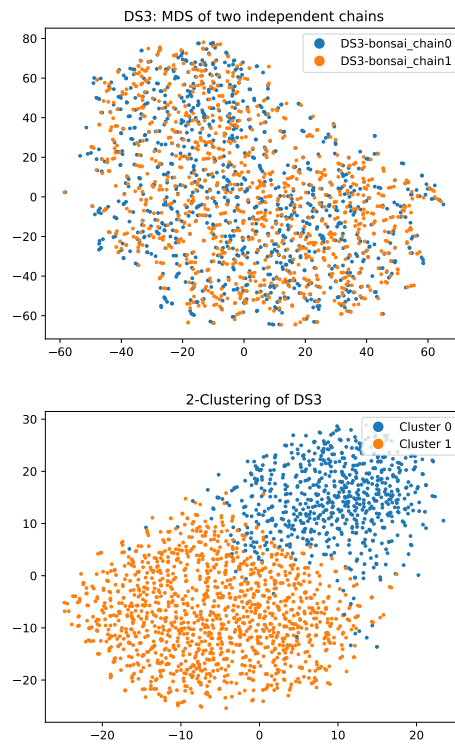


Fig. 59: MDS and clustering for dataset DS3.

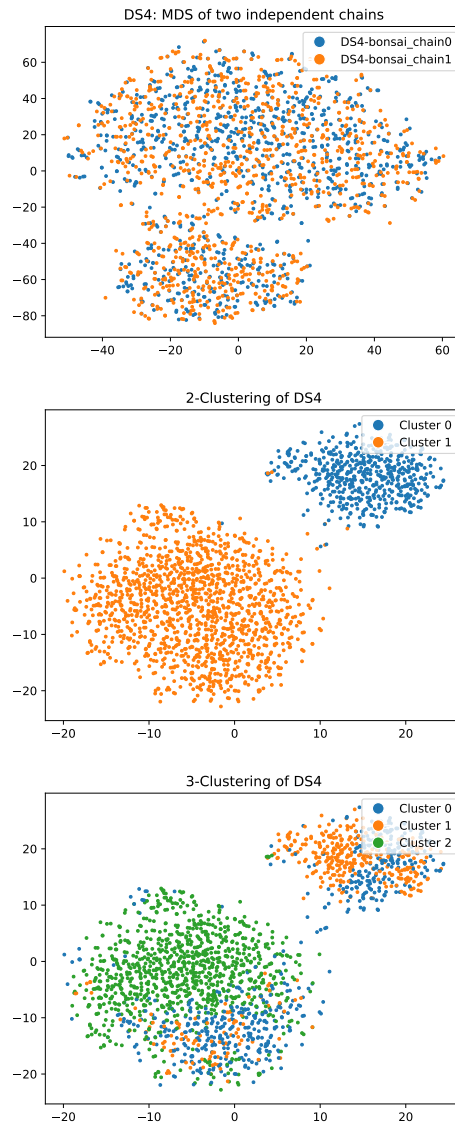


Fig. 60: MDS and clustering for dataset DS4.

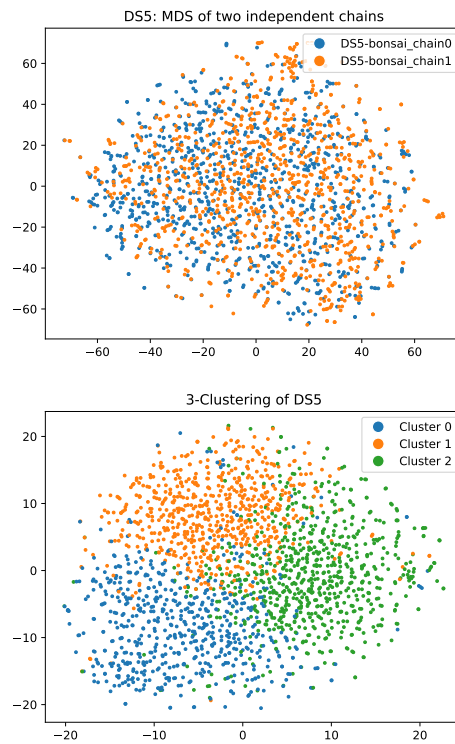


Fig. 61: MDS and clustering for dataset DS5.

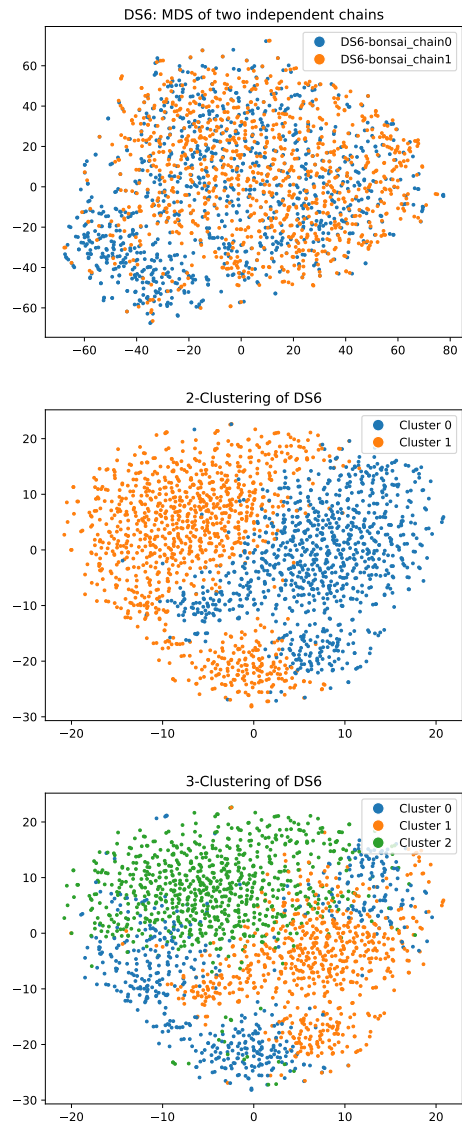


Fig. 62: MDS and clustering for dataset DS6.

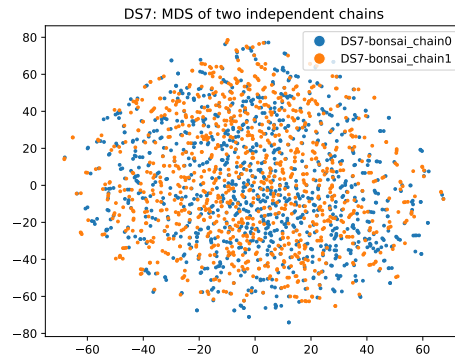


Fig. 63: MDS and clustering for dataset DS7.

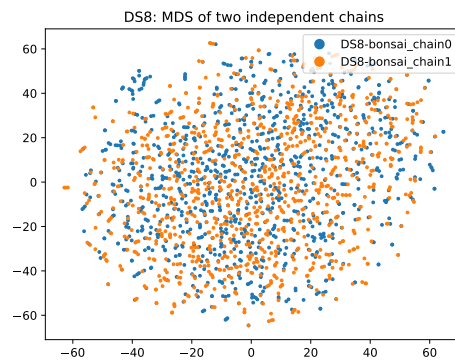


Fig. 64: MDS and clustering for dataset DS8.

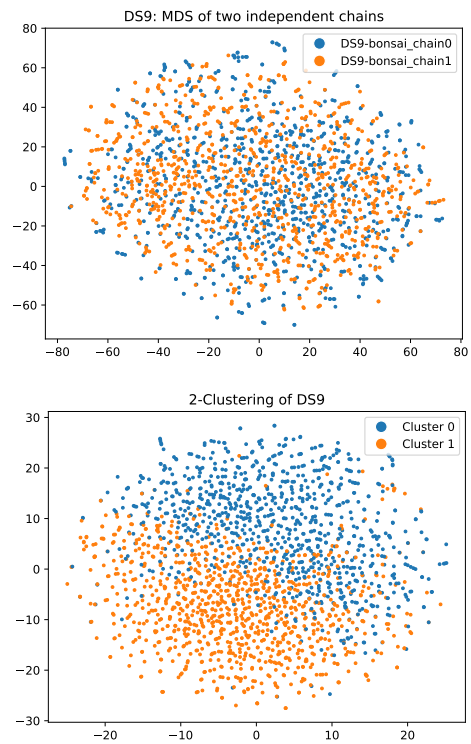


Fig. 65: MDS and clustering for dataset DS9.

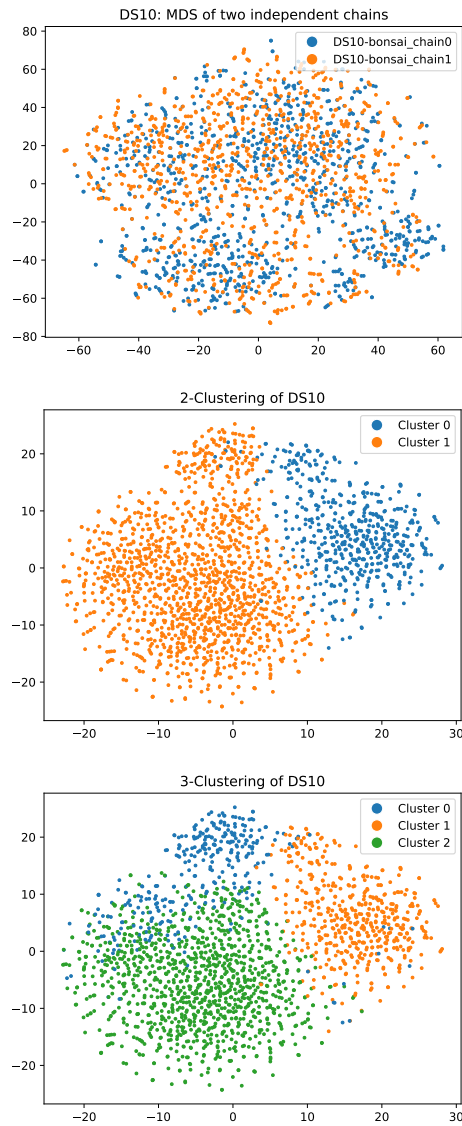


Fig. 66: MDS and clustering for dataset DS10.

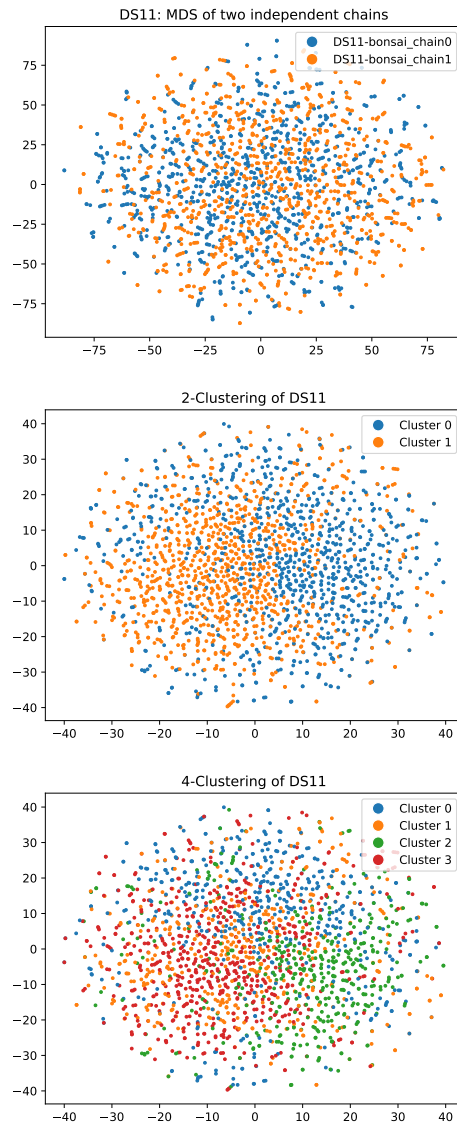


Fig. 67: MDS and clustering for dataset DS11.

F Trace Plots

In [Figs. 68 to 78](#), we provide trace plots for DS1–11 and various traces.

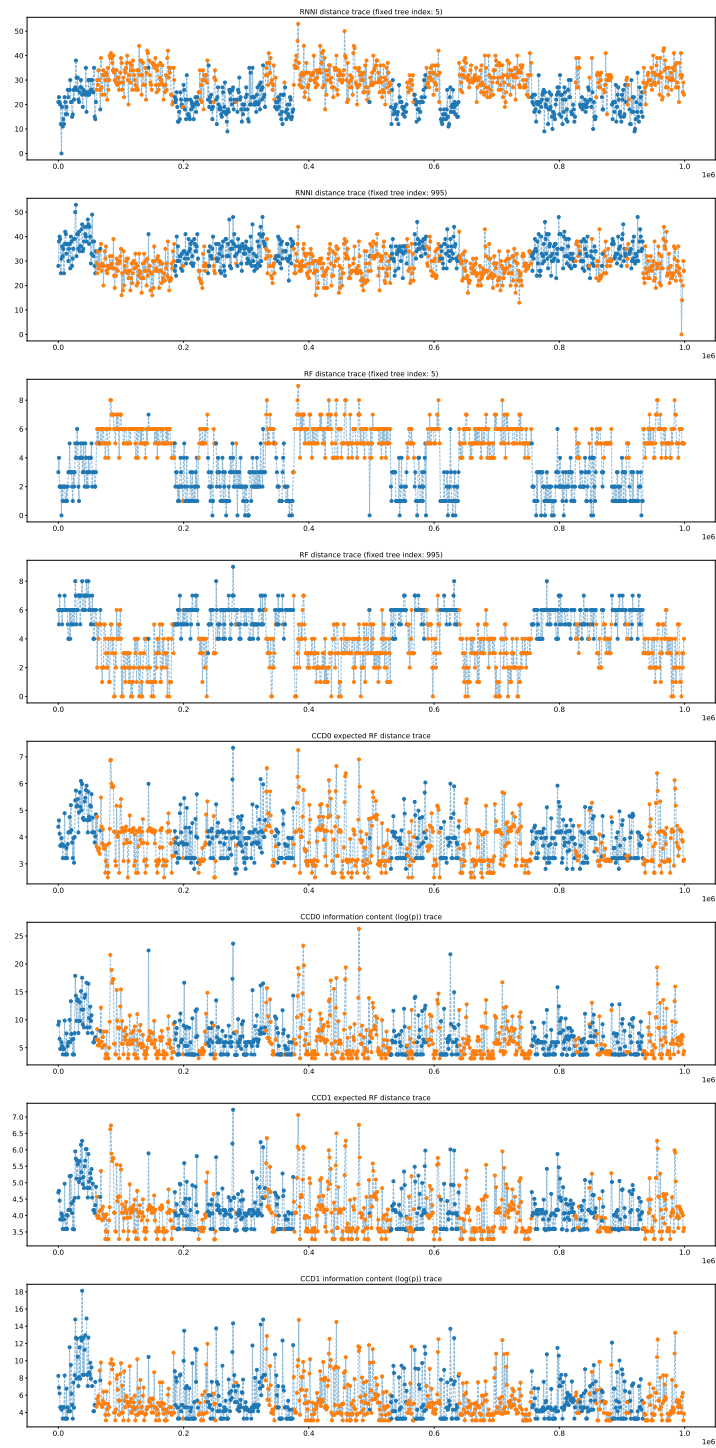


Fig. 68: Tree trace plots for different ESS statistics for DS1, colored according to a 2-clustering.

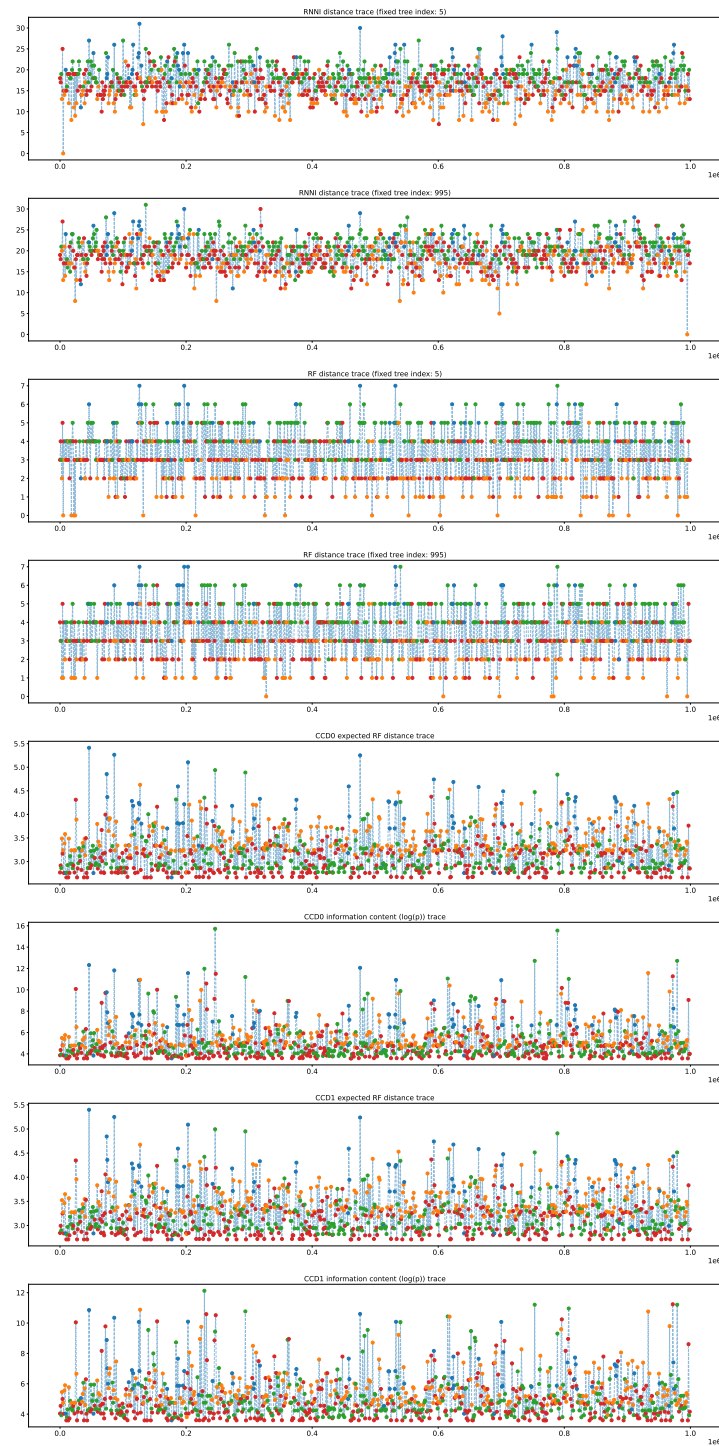


Fig. 69: Tree trace plots for different ESS statistics for DS2, colored according to a 4-clustering.

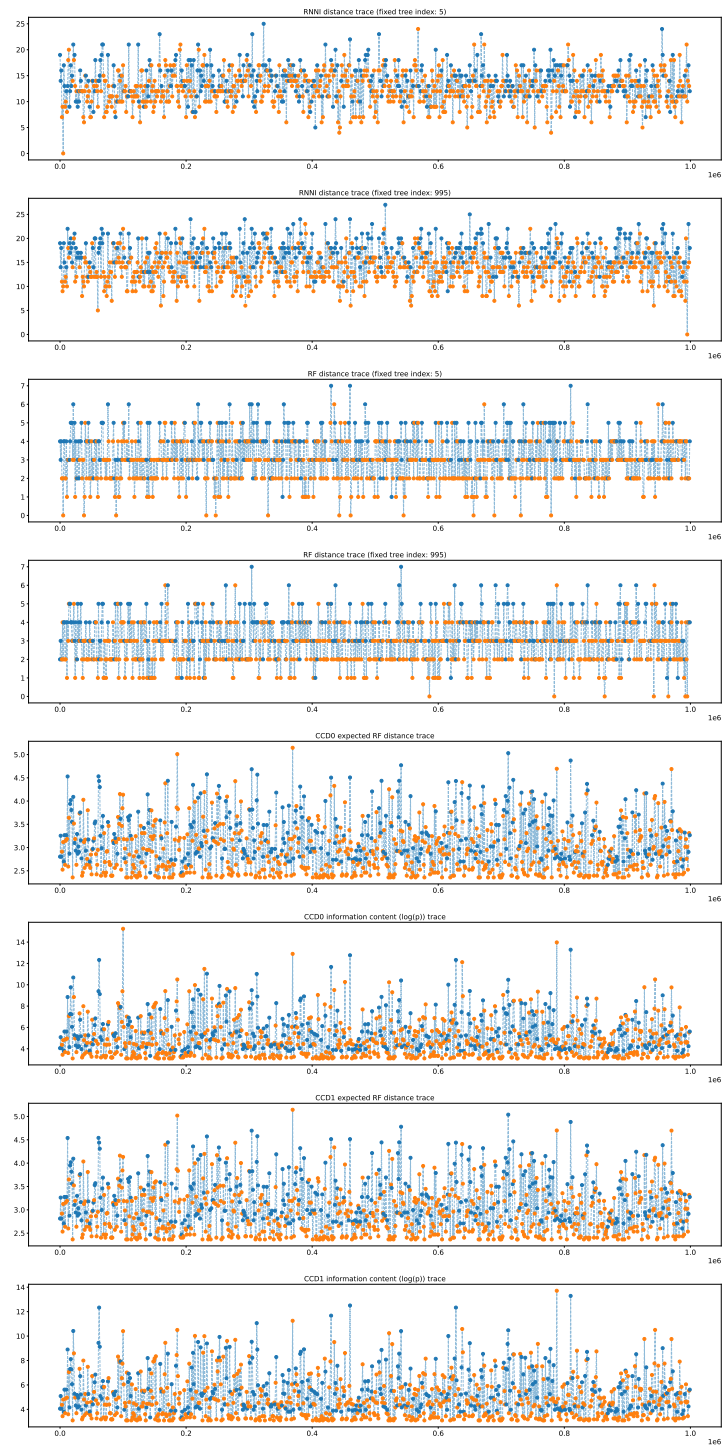


Fig. 70: Tree trace plots for different ESS statistics for DS3, colored according to a 2-clustering.

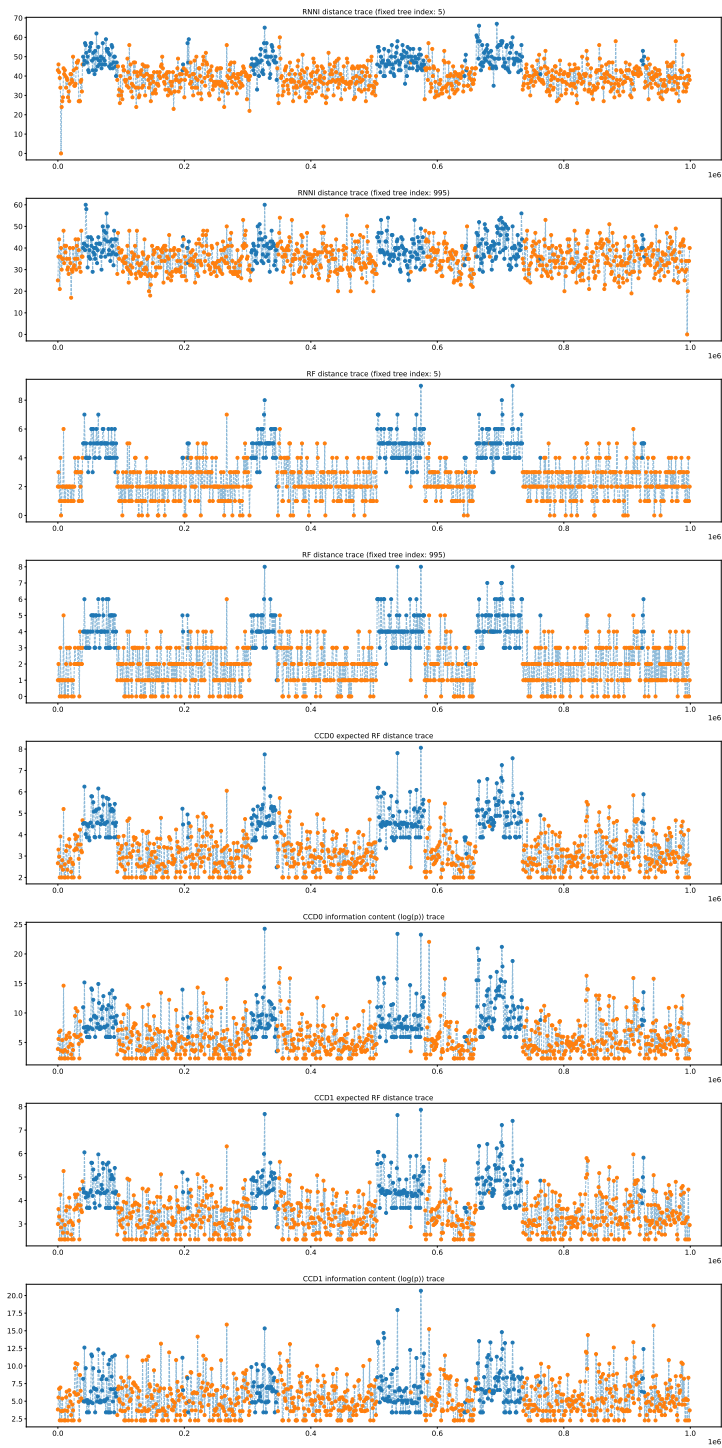


Fig. 71: Tree trace plots for different ESS statistics for DS4, colored according to a 2-clustering.

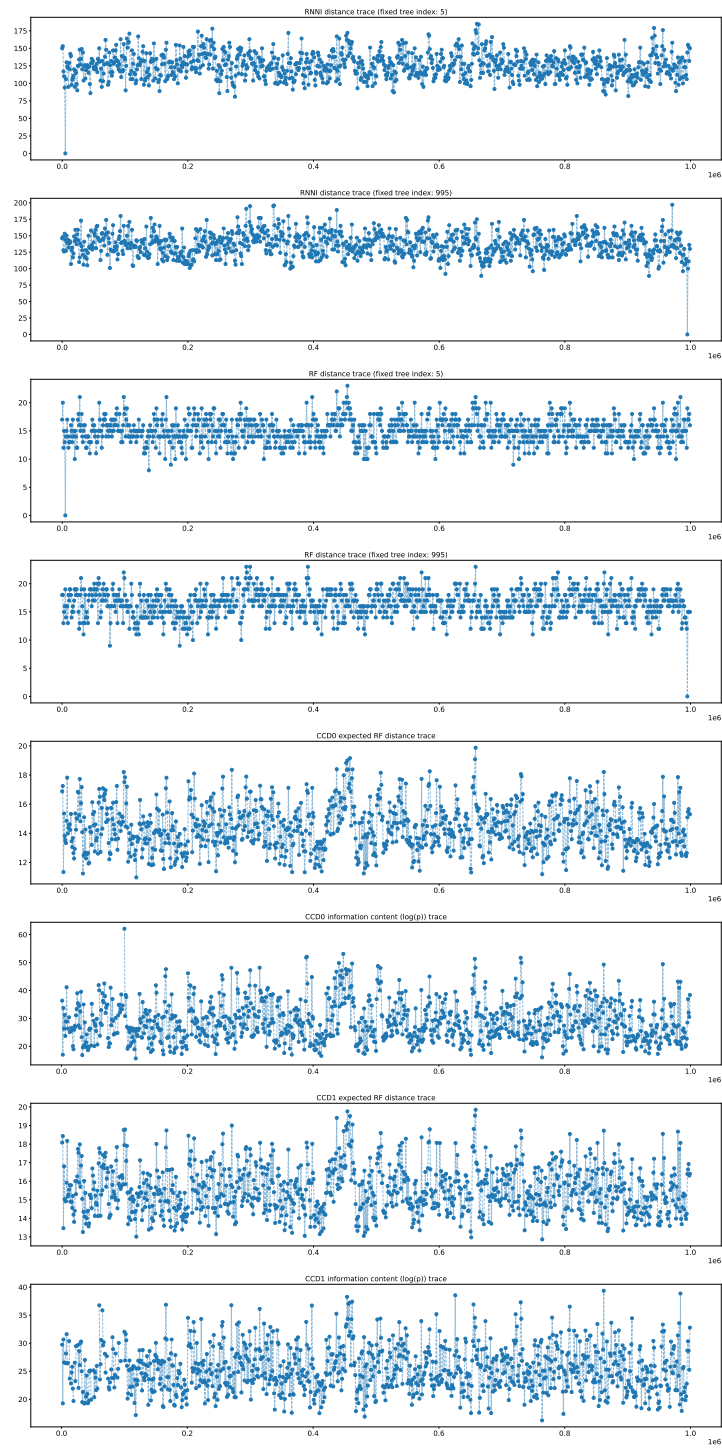


Fig. 72: Tree trace plots for different ESS statistics for DS5, colored according to a 1-clustering.

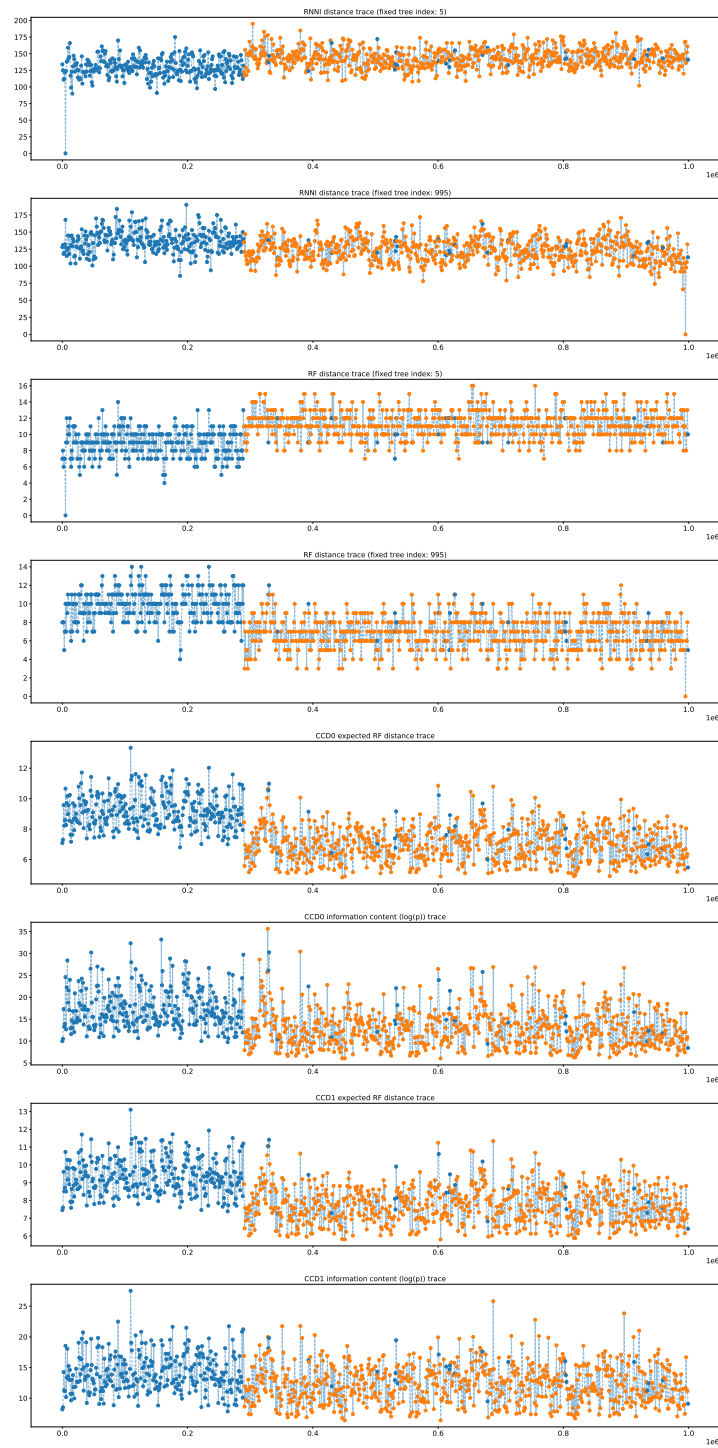


Fig. 73: Tree trace plots for different ESS statistics for DS6, colored according to a 2-clustering.

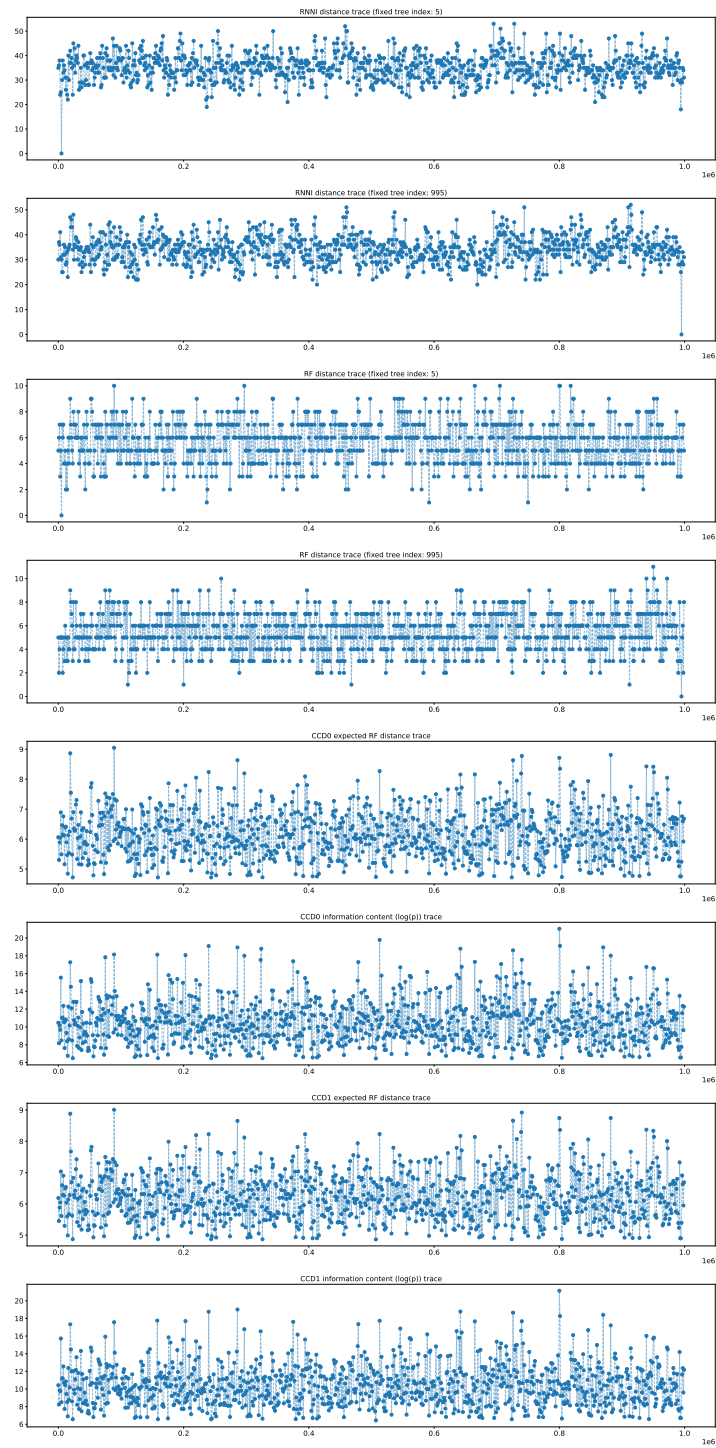


Fig. 74: Tree trace plots for different ESS statistics for DS7, colored according to a 1-clustering.

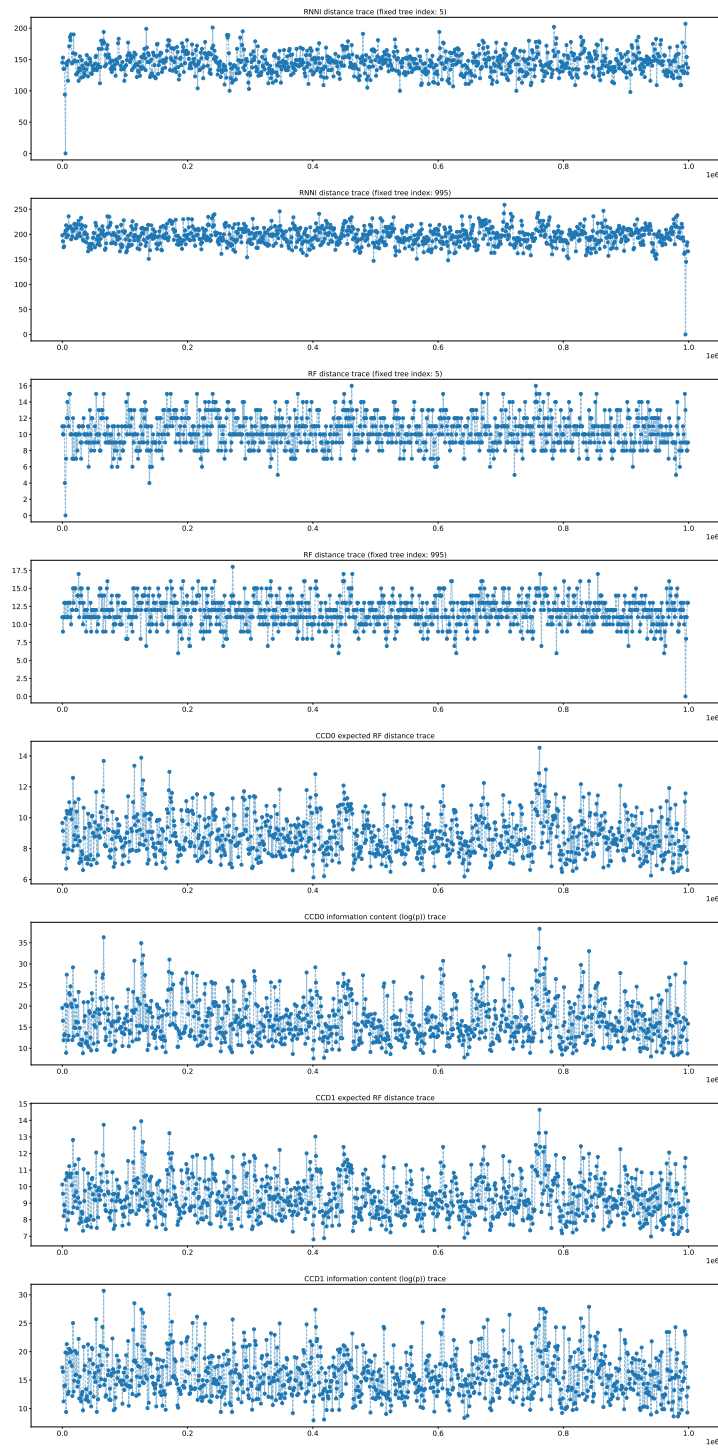


Fig. 75: Tree trace plots for different ESS statistics for DS8, colored according to a 1-clustering.

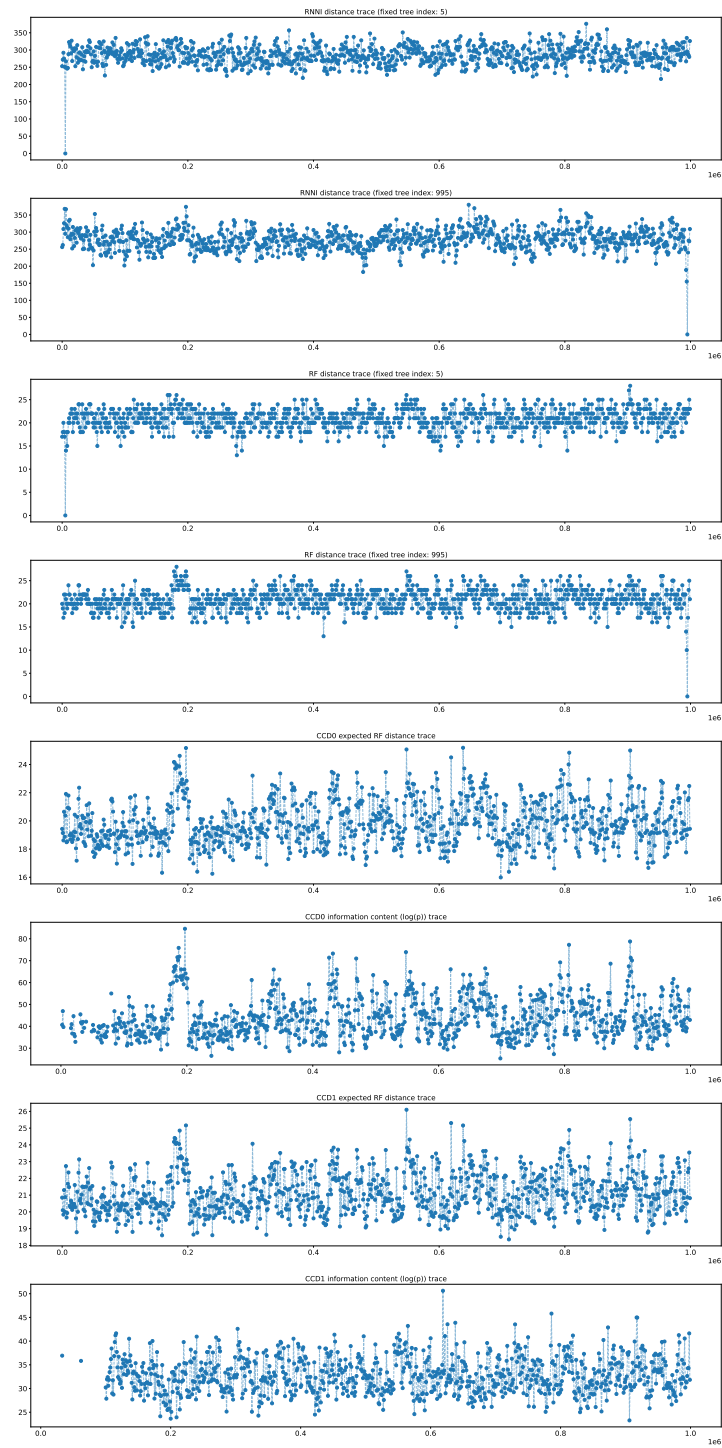


Fig. 76: Tree trace plots for different ESS statistics for DS9, colored according to a 1-clustering.

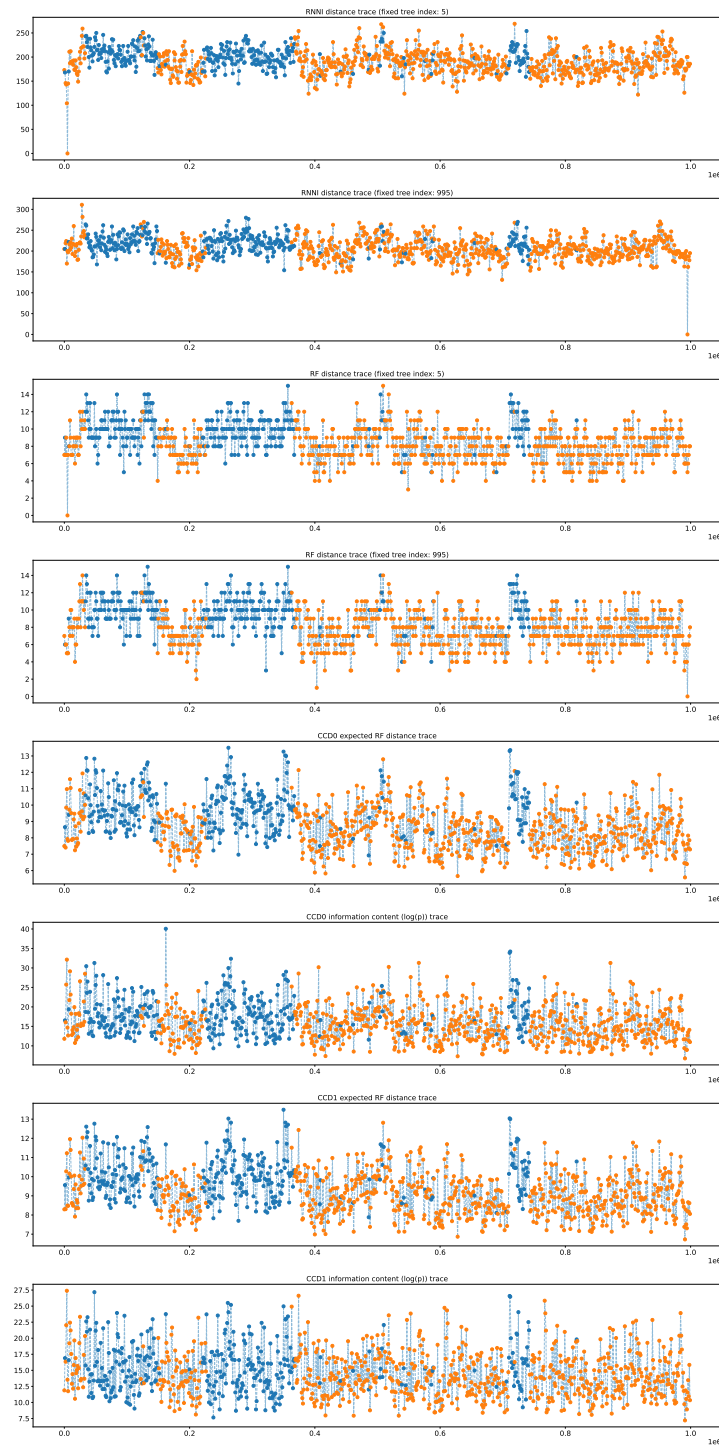


Fig. 77: Tree trace plots for different ESS statistics for DS10, colored according to a 2-clustering.

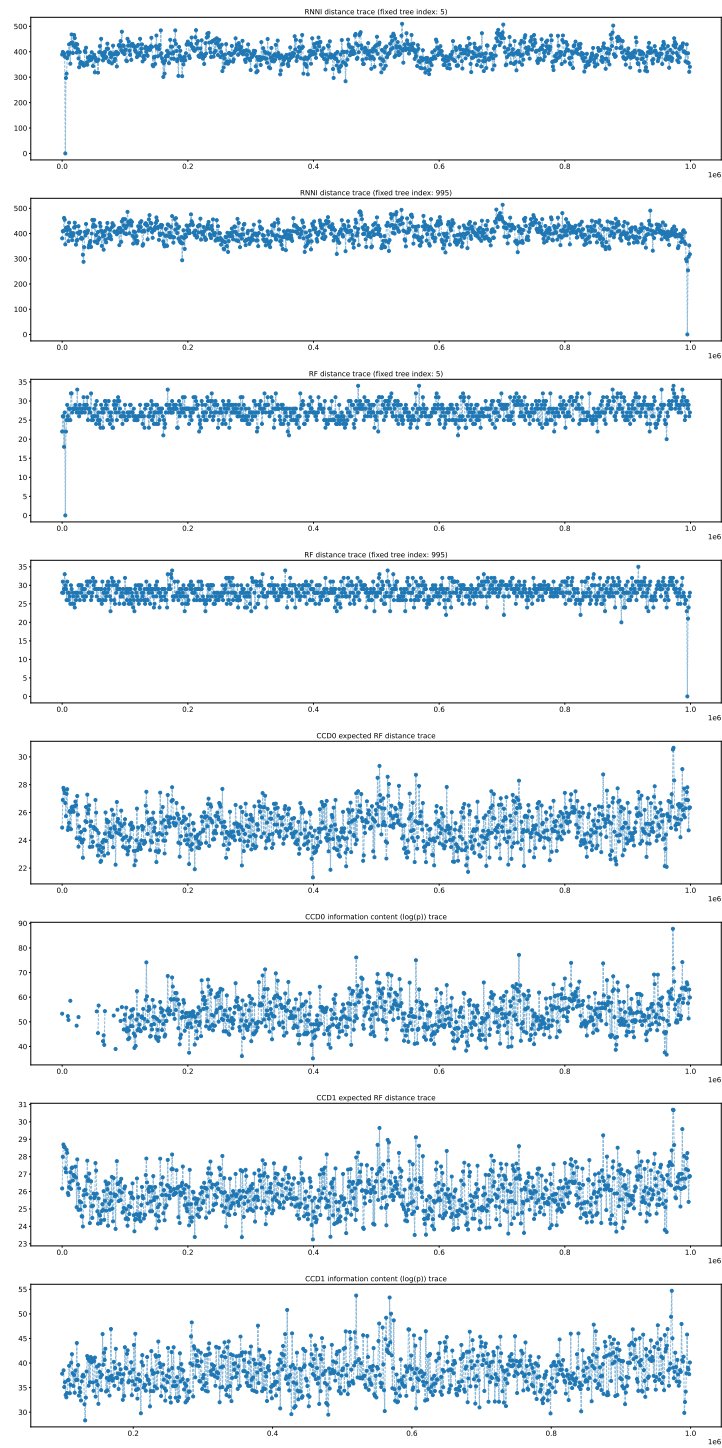


Fig. 78: Tree trace plots for different ESS statistics for DS11, colored according to a 1-clustering.